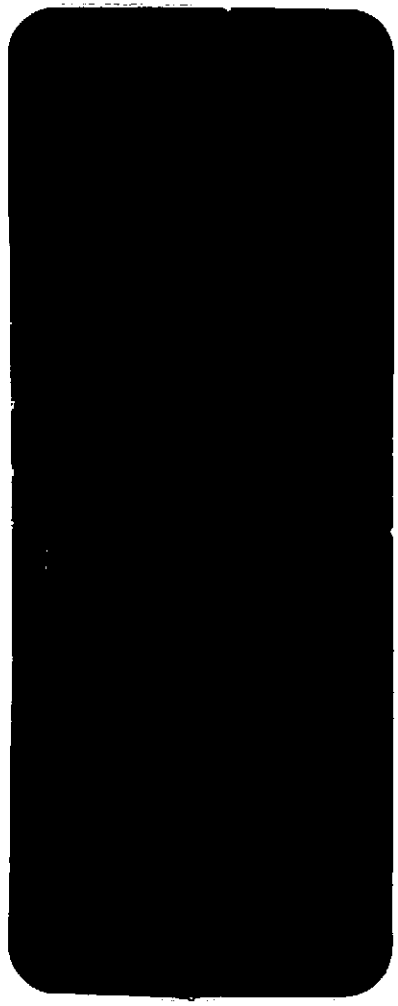

NOVEMBER 1972

ATL TR 169

ANALYSIS OF SUPERSONIC COMBUSTION FLOW FIELDS WITH EMBEDDED SUBSONIC REGIONS

By

S. Dash & P. Del Guidice

PREPARED FOR

NASA
LANGLEY, VIRGINIA

UNDER

CONTRACT NO. NAS1-10948

BY

ADVANCED TECHNOLOGY LABORATORIES, INC.
400 Jericho Turnpike
Jericho, N. Y. 11753

I

INDEX

FOREWORD

This work was carried out under the supervision of Dr. Antonio Ferri who provided valuable guidance in all phases of this work. The authors acknowledge the programming assistance of Mr. Paul Kalben. A description and listing of the numerical program based on the method described in this report may be found in the report entitled "A FORTRAN Program for the Analysis of Supersonic Combustion Flow Fields with Embedded Subsonic Regions", ATL TM 167. The technical aspects of this program were monitored by Dr. Harry L. Beech of NASA Langley.

ABSTRACT

The viscous characteristic analysis for supersonic chemically reacting flows as reported in NASA CR 111783, has been extended to include provisions for analyzing embedded subsonic regions. This report describes the numerical method developed to analyze this mixed subsonic-supersonic flow fields. A discussion of the boundary conditions related to the supersonic-subsonic and subsonic-supersonic transition as well as a heuristic description of several other numerical schemes for analyzing this problem is included. An analysis of shock waves generated either by pressure mismatch between the injected fluid and surrounding flow or by chemical heat release is described.

LIST OF SYMBOLS

C_p	=	C_p^*/C_{p_∞} specific heat
J	=	0 for two dimensional flow, 1 for axisymmetric flow
L^*	=	reference length
L_e	=	Lewis number
M	=	Mach number
m_i	=	molecular weight of ith specie
n	=	distance normal to streamline
P	=	$P^*/\rho_\infty u_\infty^2$ pressure
P_r	=	Prandtl number
q	=	q^*/u_∞ velocity
R	=	mixture gas constant
R_e	=	free stream Reynolds number $\frac{\rho_\infty u_\infty L^*}{\mu_\infty}$
R_0	=	universal gas constant
$S_{1,2,3_i}$	=	forcing function terms
T	=	T^*/T_∞ temperature
W	=	average molecular weight of mixture
w_i	=	chemical production terms
x	=	x^*/L^* axial distance
y	=	y^*/L^* radial distance
α_i	=	mass fraction of ith specie
γ	=	ratio of specific heats
θ	=	flow inclination relative to axis

LIST OF SYMBOLS (Continued)

ρ	=	ρ^*/ρ_∞ density
μ_f	=	Mach angle
μ	=	viscosity
ψ	=	stream function
$*$	=	dimensional variables
∞	=	free stream conditions (dimensional)
f	=	frozen state

I. INTRODUCTION

One of the interesting phenomena produced by combustion in a supersonic flow is the possibility of producing transition from supersonic to subsonic flow due to the heat addition. This transition has been analyzed in the past for the case of one dimensional flow, however, a more complex flow field is usually generated in a supersonic combustion process controlled by mixing. In the flame zone of this flow, where the static temperature of the gas increases, the local Mach number can decrease, even if the static pressure decreases, because the value of the local speed of sound increases. Therefore, a transition from supersonic to subsonic flow can take place in a localized region of the flow where the pressure changes slowly and the region can be completely surrounded by supersonic flow.

The transition from subsonic to supersonic flow can occur through several mechanisms; when the flow surrounding the subsonic region is cooler than the flow in this region (because combustion takes place only in a limited region of the flow), then, because of mixing of the combusted gases with the surrounding air, the temperature of the gas in the subsonic region gradually decreases and the flow can become supersonic without pressure variation, or even with a small static pressure raise. The second possibility is that the stagnation temperature remains roughly constant but the pressure decreases, the flow accelerates and again becomes supersonic. The subsonic flow field region is essentially the opposite of the classical transonic region about airfoils, where the flow becomes locally supersonic, because the pressure decreases and then again becomes subsonic downstream, usually through a shock, and a localized region of supersonic flow is embedded in a subsonic stream. Extensive discussions on the existence of transonic flows without shocks have taken place in the past for this type of flow. It is now well recognized that smooth solutions (without shocks) are special solutions of this transonic problem and require special boundary conditions.

The possibility of transition from supersonic to subsonic flow due to combustion has been recognized in the past. In Reference (1) this possibility

was discussed qualitatively and some of the important aspects of the presence of such subsonic regions were described, however, a detailed treatment of this problem is still lacking. A quantitative understanding of the physical aspects of such a transition are of primary importance for the development of a practical scramjet engine, in view of the fact that the efficiency of the engine, at flight Mach numbers of the order of 6 to 8, depends strongly on the value of the static pressure and local Mach number at which the heat addition takes place. High efficiency and high specific impulse requires a low local Mach number where heat is released due to chemical reaction. If the Mach number before combustion is low, during the combustion process subsonic regions are formed, even if the pressure locally does not change because of the increase of the local speed of sound. In addition, the scramjet must be able to operate at lower flight Mach number than design. For these conditions, large regions of the burner have subsonic flow.

ATL has developed for NASA in the past, methods where the flow fields of supersonic streams with chemical reactions can be analyzed (Reference 2). Such numerical methods permit analyzing the flow between discontinuities, provided that the entire flow remains supersonic, in view of the fact that such a method uses "viscous characteristics" as first described in References (3) and (4). In the present phase of the work, a numerical method capable of determining the formation of combustion shocks has been developed. In addition, the possibility of numerically determining the region of transition from supersonic to subsonic flow, and then subsonic to supersonic as can occur in the flame has been investigated.

The numerical investigation of a transonic problem, as described requires the development of a numerical scheme, valid in the transonic region, that can be coupled with the "viscous characteristic program". In addition, it requires a clear understanding of appropriate boundary conditions for the subsonic regions. A problem similar to the problem related to the existence of smooth subsonic-supersonic transition over a two dimensional profile near M=1, exists for this flow; therefore, the first step in this effort is to generate a clear understanding of the boundary conditions related to the transition problem.

II. BOUNDARY CONDITIONS RELATED TO THE TRANSITION FROM SUBSONIC TO SUPERSONIC FLOW AND FROM SUPERSONIC TO SUBSONIC FLOW

In the combustor of a scramjet engine, the flow downstream of the burner is supersonic, and the flow reaching the burner is also supersonic, therefore, any subsonic region generated locally by combustion is contained between these two supersonic regions. Consider first the case in which the subsonic region is completely imbedded in a supersonic stream, as shown in Figure (1).

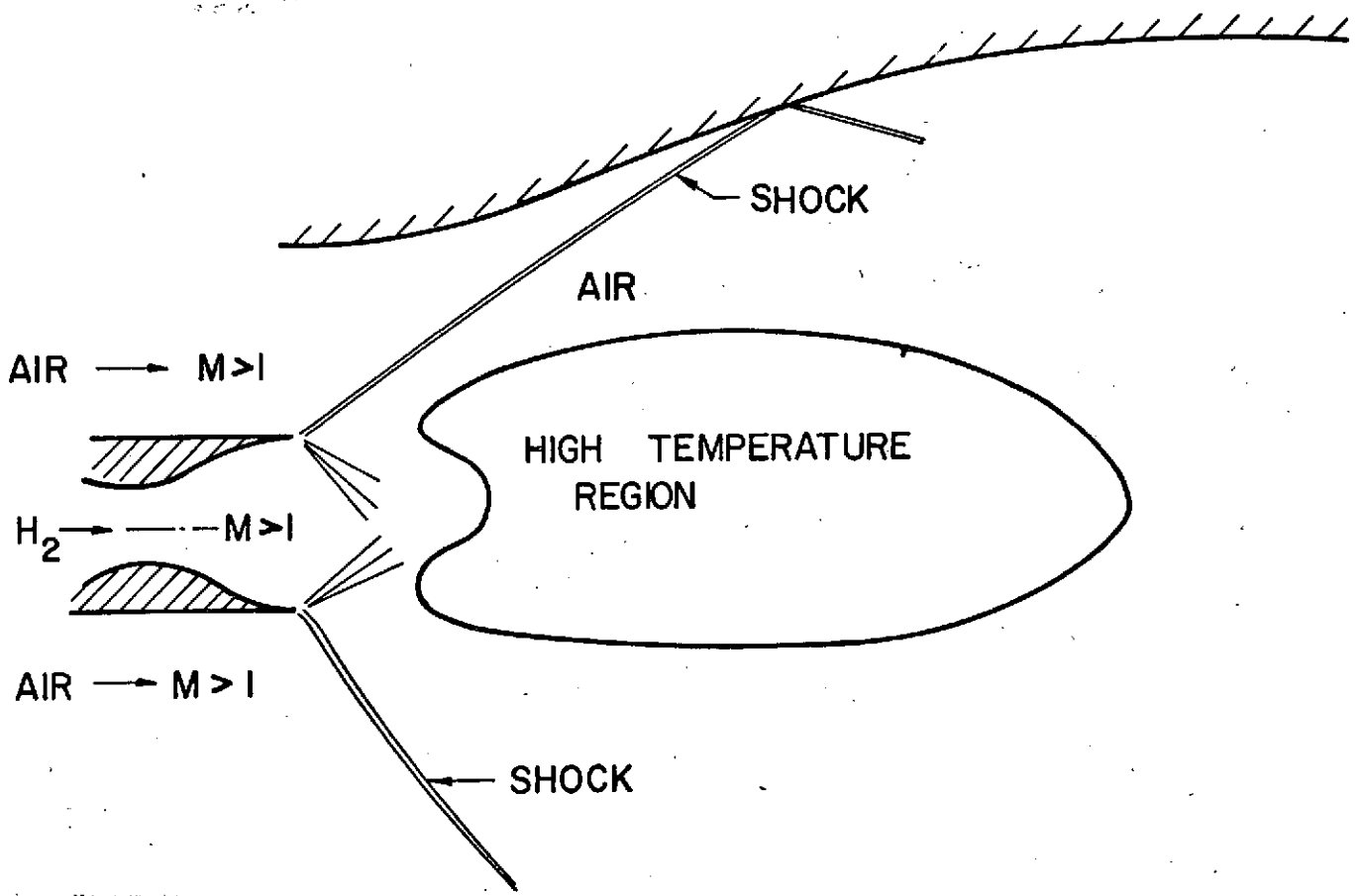

FIGURE 1.

The hydrogen from the injector mixes with the air outside and combustion takes place; the pressure rises because of the decrease in density of the stream due to combustion; the speed of sound increases, and in this high

temperature region the flow can become subsonic. Since the duct in which burning occurs diverges and the downstream pressure is much lower than the pressure at the injector face, the flow must again cross a sonic line.

If the temperature in the high temperature zone is higher than the average temperature after combustion (case of $\phi<1$), the flow outside the high temperature region will remain supersonic. Therefore, the shape of the sonic line is as shown in Figures (1) and (2). The static pressure distribution between A and B does not uniquely define the flow and the line M=1 is not a line of constant static pressure temperature, and velocity as in the case of the wing, because the stagnation temperature changes from point to point. Hence, several different pressure distributions are possible depending on the amount of diffusion and chemical reaction taking place between A and B. The pressure can first increase and then decrease, can remain approximately constant, can continuously decrease, or can slowly increase. In this last case, the variation of the speed of sound due to diffusion must be larger than in the other cases.

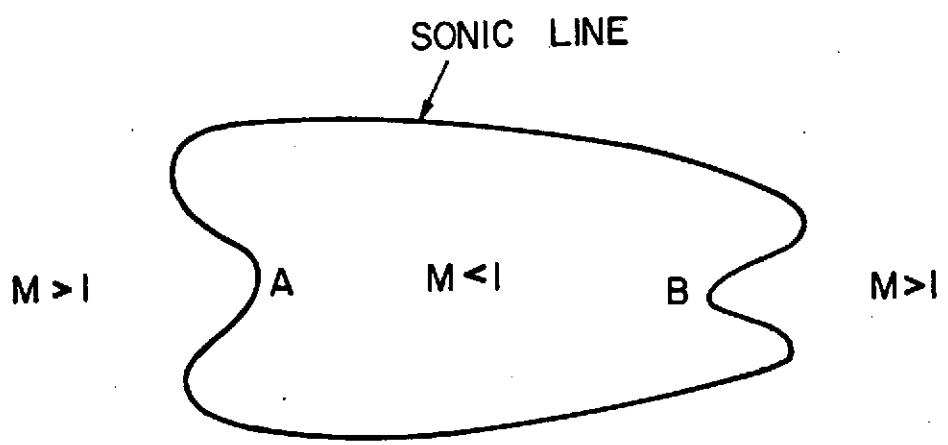

FIGURE 2.

It is not clear á priori, if the presence of a closed sonic line in the flow, as shown in Figure (2) is physically possible. The boundary conditions required in order to obtain such smooth conditions must be investigated first.

In order to understand the physics of the problem it is convenient to analyze the problem in two steps. The first step is related to the transition from subsonic to supersonic velocity. Then we can transform the problem in such a way that the properties of the subsonic region can be controlled independently of the supersonic region, as shown in Figure (3). We assume that flow 1 can be controlled independently of flow 2 and that flow 1 is initially subsonic.

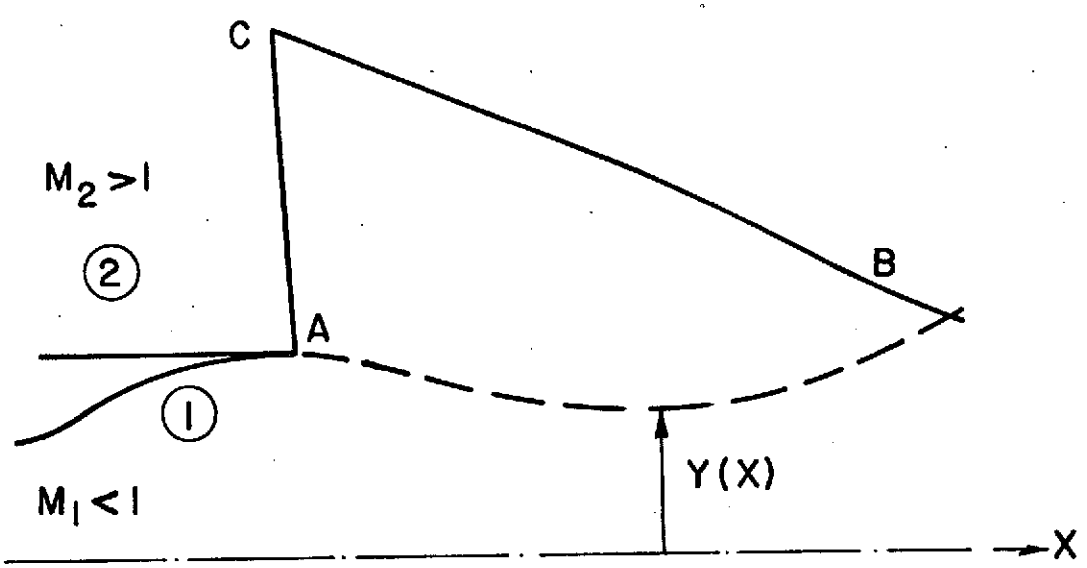

FIGURE 3.

The simplest case of such a flow occurs when stream 1 is uniform and initially subsonic (one dimensional) at the exit of the jet and stream 2 is supersonic. If we neglect transport properties and assume both flows to be inviscid, the flow properties as specified along the line, AC yield a unique relation between the pressure and the angle of the streamline AB, where CB is a characteristic line emenating from C. The unique relation between p and θ corresponds to a unique relation between p(x) and y(x) since

$$y = \int_0^x \tan\theta \, dx$$

A similar relation can be determined for streamline AB. For example, if we assume that the pressure in region 1 is independent of y (one dimensional flow), we have a simple relation between y and p given by the continuity equation. Thus, a step by step calculation can be performed where at each step Δx between A and B, the variation Δp in the step can be assumed as a parameter and a single calculation can be performed (Figure 4). The equa-

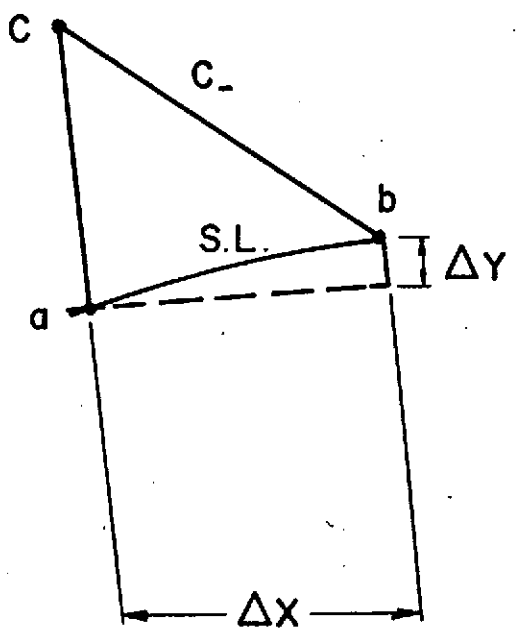

FIGURE 4.

tion of characteristics applied along Cb yields a relation between p_b and θ_b.

For a two dimensional flow

$$\frac{2}{\gamma}\frac{(p_b-p_c)}{(p_b+p_c)} - \frac{(\theta_b - \theta_c)}{\cos\mu \sin\mu} = 0 \qquad (1)$$

where

$$\tan\mu = \frac{1}{2}(\tan\mu_b + \tan\mu_c)$$

Then, for a given value of Δp (i.e., p_b-p_a), p_b is given and θ_b is calculated. Then, Δy is determined from

$$\frac{1}{2}(\tan\theta_a + \tan\theta_b)\,\Delta x \qquad (2)$$

The one dimensional relation yields

$$\frac{y_b}{y_a} = \left(\frac{p_a}{p_b}\right)^{1/\gamma} \left(\frac{1 - \left(\frac{p_a}{p_o}\right)^{\frac{\gamma-1}{\gamma}}}{1 - \left(\frac{p_b}{p_o}\right)^{\frac{\gamma-1}{\gamma}}}\right)^{1/2} \qquad (3)$$

where p_o is the stagnation pressure of stream 1.

Only one value of Δp satisfies Equations (1), (2) and (3). Then, the variation of y as a function of x can be obtained. However, in the region where M_1 becomes equal to one $\left.\frac{dy}{dp}\right|_{M=1} = 0$. Then, a solution can not be found unless $\theta \to 0$ and $\frac{\partial\theta}{\partial x}$ tends to zero for the external flow in the region where $M_1 \to 1$. If this does not occur, we have a "choking" condition and the initial subsonic flow distribution assumed in Figure (3) is not physical.

A "choking" condition can be found independently of the approximation used in the analysis of the subsonic flow. The physics of the simple case shown in Figure (3) is clear. The pressure at station A has been assumed arbitrarily. If choking occurs, this implies that an incorrect value of the pressure at A has been assumed. If we change the value of M_1 at A and, therefore, the corresponding value of p_A, the shape of the streamline AB changes. If the value of θ of the streamline AB at the choking point is negative, then the mass flow of stream 1 must be decreased; hence p_A for a given p_o must increase. This change tends to increase the value of θ at the choking region. Therefore, by an iterative process the value of p_A that gives a physical solution can be determined. The problem is substantially more complex if flow 1 is not assumed to be one dimensional, and transport properties and chemistry are included in the analysis, as will be discussed later on. However, the controlling mechanism is the same. For any given initial flow distribution in the supersonic region, and given stagnation conditions and channel shape of the subsonic flow, a single solution can always be found that permits the subsonic flow to cross the M=1 line, which corresponds to a given value of the static pressure at A. Therefore, the correct boundary conditions for the problem requires a selection of the pressure at A that avoids "choking", and the assumption that the downstream pressure is sufficiently low. Then, the initial flow properties along AC and the geometry defines the problem.

Let us now consider the case depicted in Figures (1) and (2). In this case the flow is initially supersonic, therefore, the flow field in front of the sonic line is completely determined by the initial conditions. In Figure (5) the flow along the line a is given. Then, the flow along line b is uniquely determined. If the flow becomes subsonic due to chemical reaction, the flow properties along the sonic line S are completely determined; therefore, only one solution can be found that gives a smooth transition from supersonic to subsonic flow and a unique flow can be determined along line S where M=1 having an embedded smooth subsonic region. Hence, the possibility of changing a parameter, equivalent to changing the value of the pressure p_A of Figure

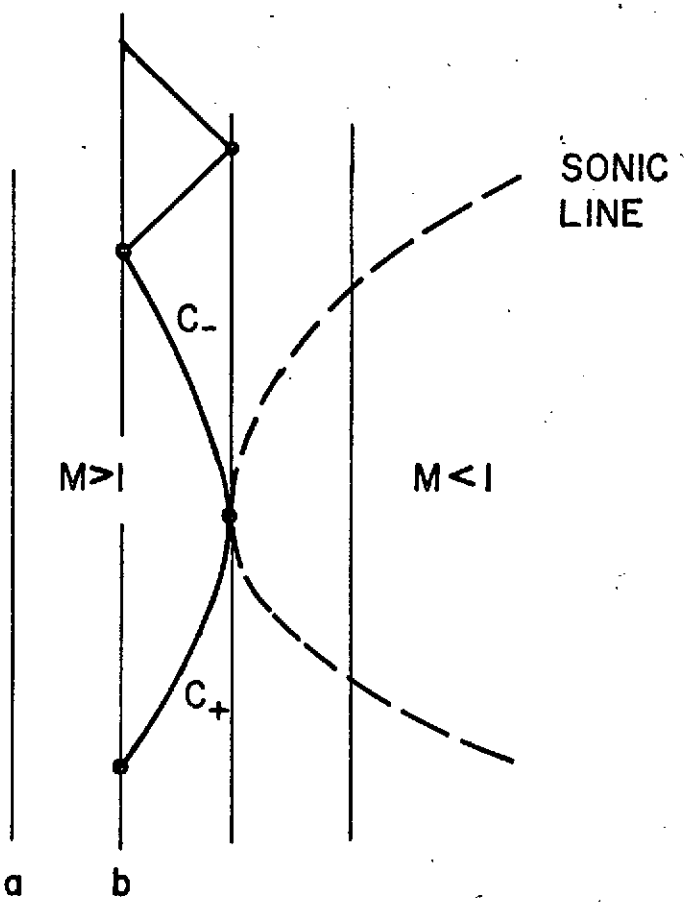

FIGURE 5.

(3),(in the case that choking occurs because of the downstream conditions) is not available for this flow. However, if downstream, the flow Mach number tends to increase and the subsonic region tends to decrease, then the sonic line crosses all the streamlines and closes as shown in Figure (6),

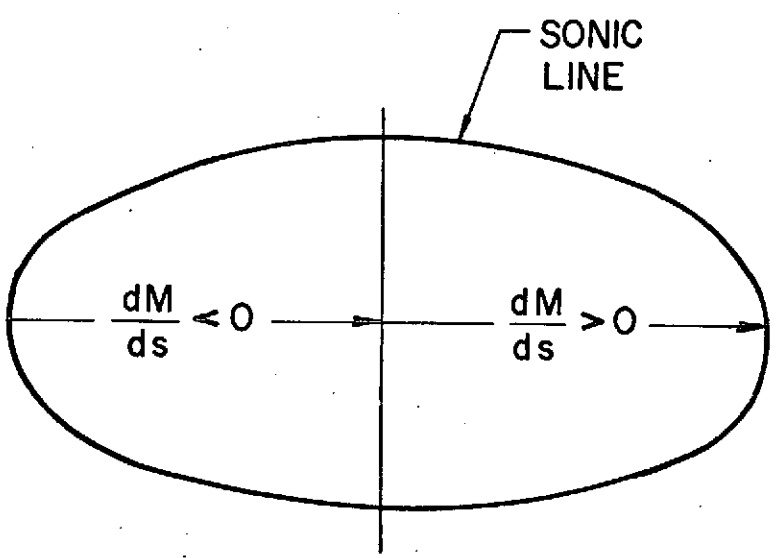

FIGURE 6.

Therefore, the possibility of having the choking condition described before, still exists. For some conditions, the flow cannot undergo transition from subsonic to supersonic because the flow is choked; therefore, some modifications must be introduced upstream to change the initial conditons of the subsonic flow. The only existing mechanism for this adjustment is the formation of a shock. The choking condition produces a disturbance that moves upstream of the sonic line (Figure 7) forming a shock. The transition from supersonic to subsonic then occurs by means of this discontinuity as shown in Figure (7).

The position and shape of the shock depends on the choking conditions, which are dependent on the flow properties along AB. Then, in the general case, for any given flow distribution along AB, the transition from supersonic to subsonic occurs through a strong shock (subsonic flow behind), the position of this shock being highly dependent on the flow properties in the supersonic region outside the choking region (region CC of Figure 7).

Similarly to the transonic case, a smooth transition can exist for specially selected boundary conditions and can be calculated by specifying only a part of the flow properties along the initial station AB, for example, along AD of Figure (7). Then, the flow properties along DB can be determined by an inverse process where the transonic region CC is determined first and the region DCCB is determined later on.

The determination of the shock cannot be obtained by a direct (marching) calculation as it depends on the downstream flow conditions; it should be obtained by a procedure similar to that used for transonic flow analysis. The procedure that appears the most feasible for this problem is an iteration procedure where a smooth transition from supersonic to subsonic is assumed first and a "choking" error is determined at the subsonic to supersonic transition in terms of the amount of mass flow that cannot cross the region of M=1. Then, a shock position, s, is assumed ahead of the first transition. This position, s, defines a new flow field . Such a flow field defines a new error associated with choking at the second transition.

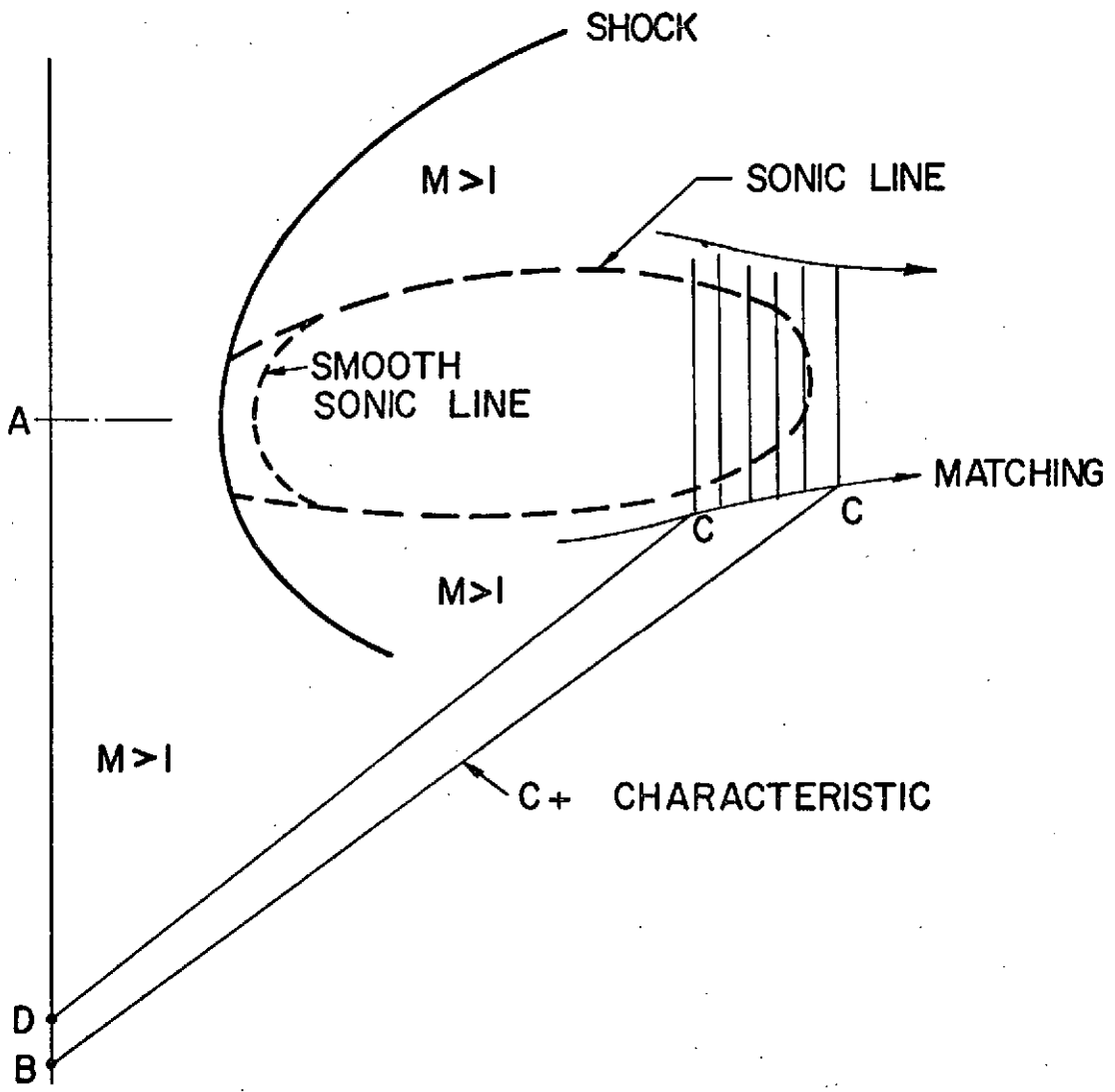
SHOCK
M>I
SONIC LINE
SMOOTH
SONIC LINE
A
MATCHING
C
C
M>I
M>I
C+ CHARACTERISTIC
D
B

FIGURE 7.

The error obtained is smaller than the previous error. A program that can perform this type of analysis and perform these iterations can be developed, however, it is not part of this effort. The effort supported by NASA in the mentioned contract is limited to the development of a program that analyzes only the inverse problem. This analysis is described in detail in the following sections.

III. GOVERNING EQUATIONS

The analysis developed for calculating the subsonic region of the flow must be consistent with the "viscous characteristic" method employed in the supersonic region and must be capable of analyzing a viscous, reacting flow with both lateral and transverse pressure gradients. The pressure p and flow inclination θ have been selected as independent variables since the equations written in terms of p and θ do not explicitly contain the entropy as a flow variable, which can have extremely large gradients in the combustion region. Use of equations written in terms of velocity components, could lead to numerical difficulties regarding mesh size in the combustion zone since the entropy gradients would have to be evaluated by means of finite difference formulas.

The governing equations are the well known "viscous-inviscid" equations employed in higher order boundary layer and viscous flow field analyses (References 5 and 6) with the finite rate chemistry terms included. The equations are as follows:

Global Continuity:

$$\frac{\partial(\rho q)}{\partial s} + \rho q \frac{\partial \theta}{\partial n} + \frac{J \rho q}{y} \sin \theta = 0 \tag{4}$$

(J=0 for two dimensional fow and J=1 for axisymmetric flow)

S-Momentum:

$$\rho q \frac{\partial q}{\partial s} + \frac{\partial p}{\partial s} = \frac{1}{Re}\left[\frac{\partial}{\partial n}(\mu \frac{\partial q}{\partial n}) + \frac{J}{y} \cos \theta \, \mu \frac{\partial q}{\partial n}\right] = S_1 \tag{5}$$

N-Momentum:

$$\rho q^2 \frac{\partial \theta}{\partial s} + \frac{\partial p}{\partial n} = 0 \tag{6}$$

Energy:

$$C_p \rho q \frac{\partial T}{\partial s} - q \frac{\partial p}{\partial s} = \frac{1}{Re(\gamma_\infty - 1)M_\infty^2}$$

$$\left[\frac{\partial}{\partial n} \frac{\mu C_p}{Pr} \frac{\partial T}{\partial n} + \frac{J}{y} \cos\theta \frac{C_p \mu}{Pr} \frac{\partial T}{\partial n} + \frac{\mu L_e}{Pr} \frac{\partial T}{\partial n} \Sigma C_{p_i} \frac{\partial \alpha_i}{\partial n}\right. \tag{7}$$

$$\left. + (\gamma_\infty - 1)M_\infty^2 \mu \left(\frac{\partial q}{\partial n}\right)^2\right] - \Sigma \dot{w}_i h_i = S_2 - \Sigma \dot{w}_i h_i$$

Species Conservation:

$$\rho q \frac{\partial \alpha_i}{\partial s} = \frac{1}{Re}\left[\frac{\partial}{\partial n} \frac{L_e \mu}{Pr} \frac{\partial \alpha_i}{\partial n} + \frac{J}{y} \frac{L_e}{Pr} \cos\theta \, \mu \frac{\partial \alpha_i}{\partial n}\right] \tag{8}$$

$$+ \dot{w}_i = S_{3_i} + \dot{w}_i$$

State:

$$p = \frac{W_\infty \rho T}{\gamma_\infty M_\infty^2 W} \tag{9}$$

where

$$W = \Sigma \frac{\alpha_i}{m_i}^{-1}$$

These equations are written in an intrinsic coordinate system with s along and n normal to the streamlines. We have assumed that transport effects are produced only by gradients normal to streamlines.

IV. HEURISTIC DESCRIPTION OF SEVERAL NUMERICAL SCHEMES FOR ANALYZING SUBSONIC ZONES

A marching technique (as described in Section II) may be developed using a one dimensional approximation for the subsonic stream. Such an analysis is described in Reference (7) for analyzing supersonic air-ejector flow fields. In using a two dimensional description of the subsonic stream, the mathematical nature of the problem changes. In this representation, the normal momentum is introduced, an equation not accounted for in the one dimensional approximation. The governing flow equations in the supersonic region of the flow field are hyperbolic-parabolic in nature and hence may be solved by a marching technique; but, in the subsonic portion of the flow field, the flow equations are elliptic. This situation presents significant difficulties in attempting to analyze viscous, combusting flow fields, since both mixing and chemistry are analyzed numerically by marching along the flow streamlines.

While a marching scheme for an elliptic system yields an improperly posed problem mathematically, it has provided solutions of the inverse blunt body problem. Hence, a marching type numerical method was envisioned as a possible approach to the solution of this problem. Regarding such a numerical approach, (Reference 8), "fundamental questions arise with respect to the uniqueness and existence of a solution and with respect to stability and convergence of calculated procedures." Then, the possibility of obtaining physical solutions to elliptic problems by a marching scheme is highly dependent on the scheme utilized.

A marching scheme was developed employing the governing equations in finite difference and using the numerical scheme described in Appendix I. This scheme for analyzing the subsonic region was incorporated into the "viscous-characteristic" program and test cases were performed to analyze mixed subsonic-supersonic flow fields. Both "direct" problems (where an upper subsonic boundary shape was iterated upon to yield a lower subsonic boundary that satisfies either a wall, axis or characteristic compatibility constraint)

and "inverse" problems (where the upper subsonic boundary shape is prescribed, yielding a wall shape at the lower subsonic boundary) were attempted. In all cases that were run (both of the "direct" and "inverse" type) oscillations developed in both the pressure and flow deflection profiles after marching several axial stations which grew in magnitude and caused the program to terminate. It was felt that a polynomial representations for the pressure and flow deflection in the subsonic region might alleviate the instabilities obtained with the finite difference approach. This polynomial scheme is described in Appendix II. This method permits the calculation of a mixed subsonic-supersonic flow fields by a marching technique employing "viscous-characteristics" in the supersonic portion of the flow field and a multi-strip integral technique for the subsonic portion. A simple two dimensional test case was run employing the initial profiles shown in Figure (8), with a wall producing a rapid expansion imposed as an upper boundary, as sketched in this figure. A solution was sought that would accelerate the flow producing an all supersonic flow field downstream of the initial station.

For this test case, the medium was air, and the viscosity was set to zero, to simplify understanding the elemental physics involved. The flow is, however, rotational and non-homentropic. The matching point selected on the initial profile was at a Mach number of 1.03.

The marching scheme, as described in Appendix II, entails an iteration for the pressure at the matching point, the correct pressure being the one that passes the appropriate value of mass flow. Cases 1, 2 and 3 are distinguished only by the differences in the initial flow deflection (θ) profiles. As indicated by streamwise pressure and Mach number variations at the axis Figure (9), the flow solutions differed substantially for these cases. In case (1), the flow accelerated to a local minimum section which was apparently larger than the critical area required to accelerate the flow to the supersonic branch, hence the flow decelerated downstream of this station. In case (2), the flow smoothly accelerated from subsonic to supersonic, while in case (3) the flow reached a station where local choking occurred. Hence,

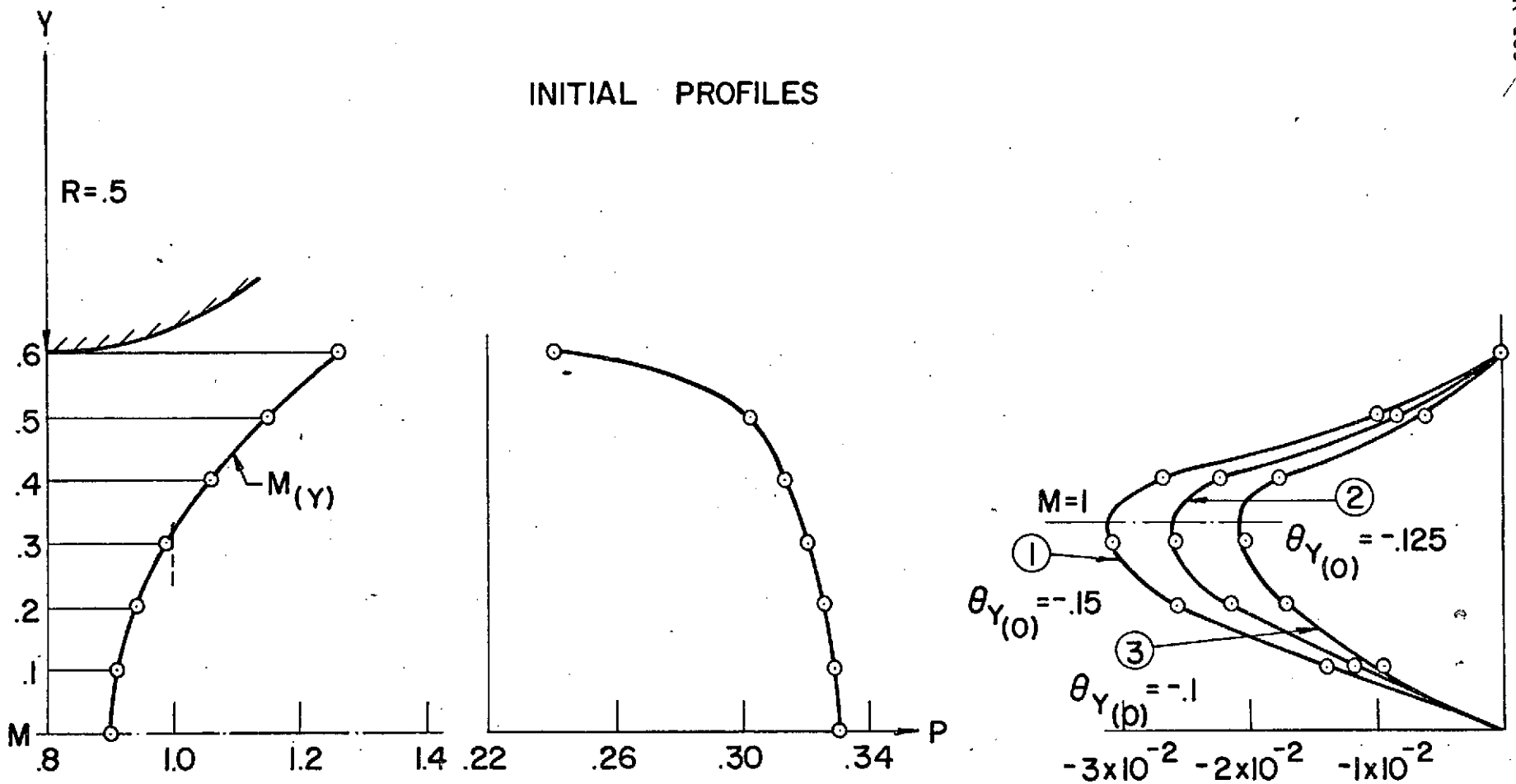
INITIAL PROFILES
Y
R=.5
.6
.5
.4
.3
.2
.1
M
.8
1.0
1.2
1.4
M(Y)
.22
.26
.30
.34
P
M=1
1
2
3
θY(0) =-.15
θY(0) =-.125
θY(0) =-.1
-3x10-2
-2x10-2
-1x10-2

FIGURE 8.

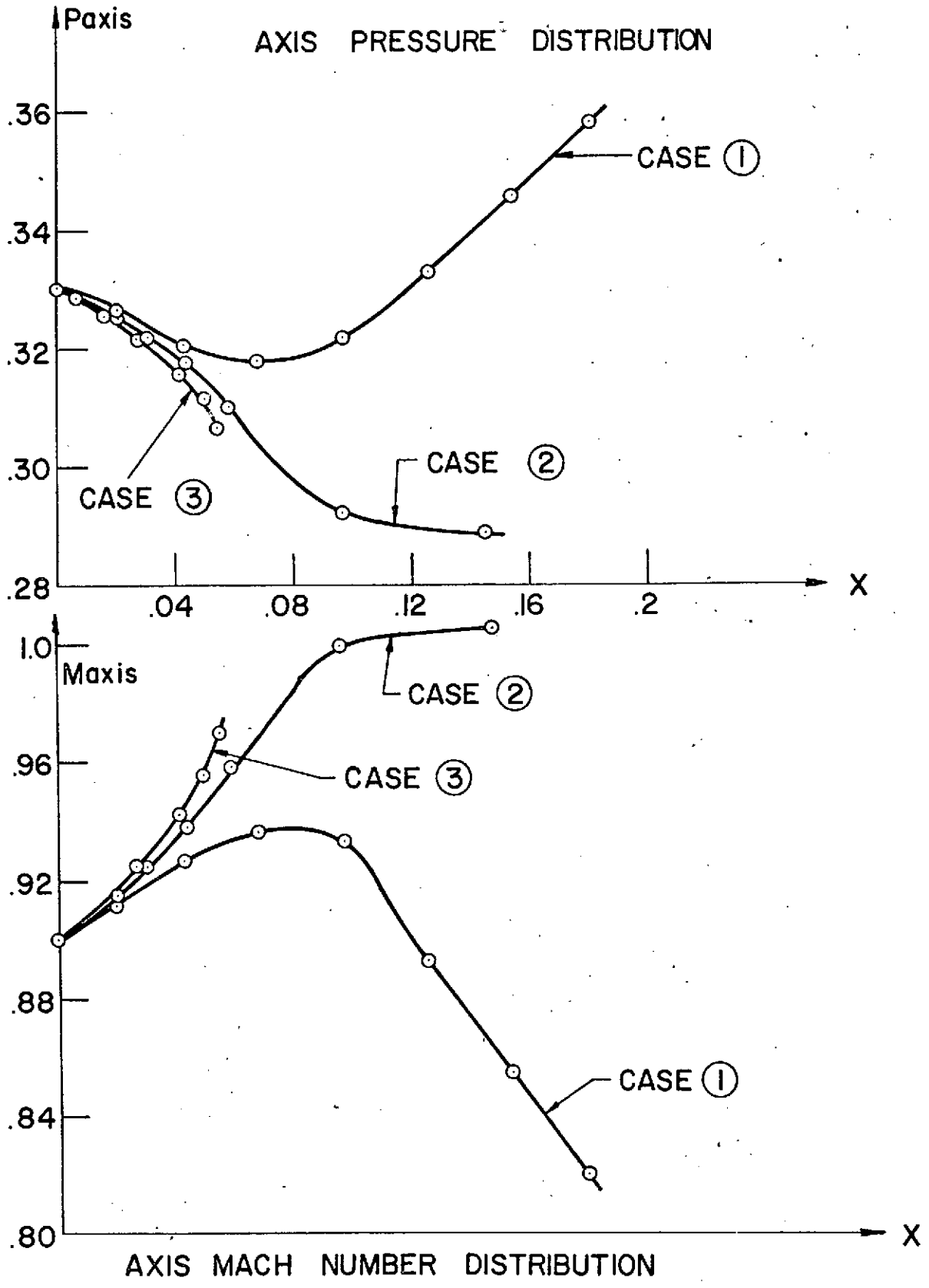
Paxis
AXIS PRESSURE DISTRIBUTION
.36
.34
.32
.30
.28
CASE (1)
CASE (2)
CASE (3)
.04
.08
.12
.16
.2
X
1.0
Maxis
.96
.92
.88
.84
.80
CASE (2)
CASE (3)
CASE (1)
X
AXIS MACH NUMBER DISTRIBUTION

FIGURE 9.

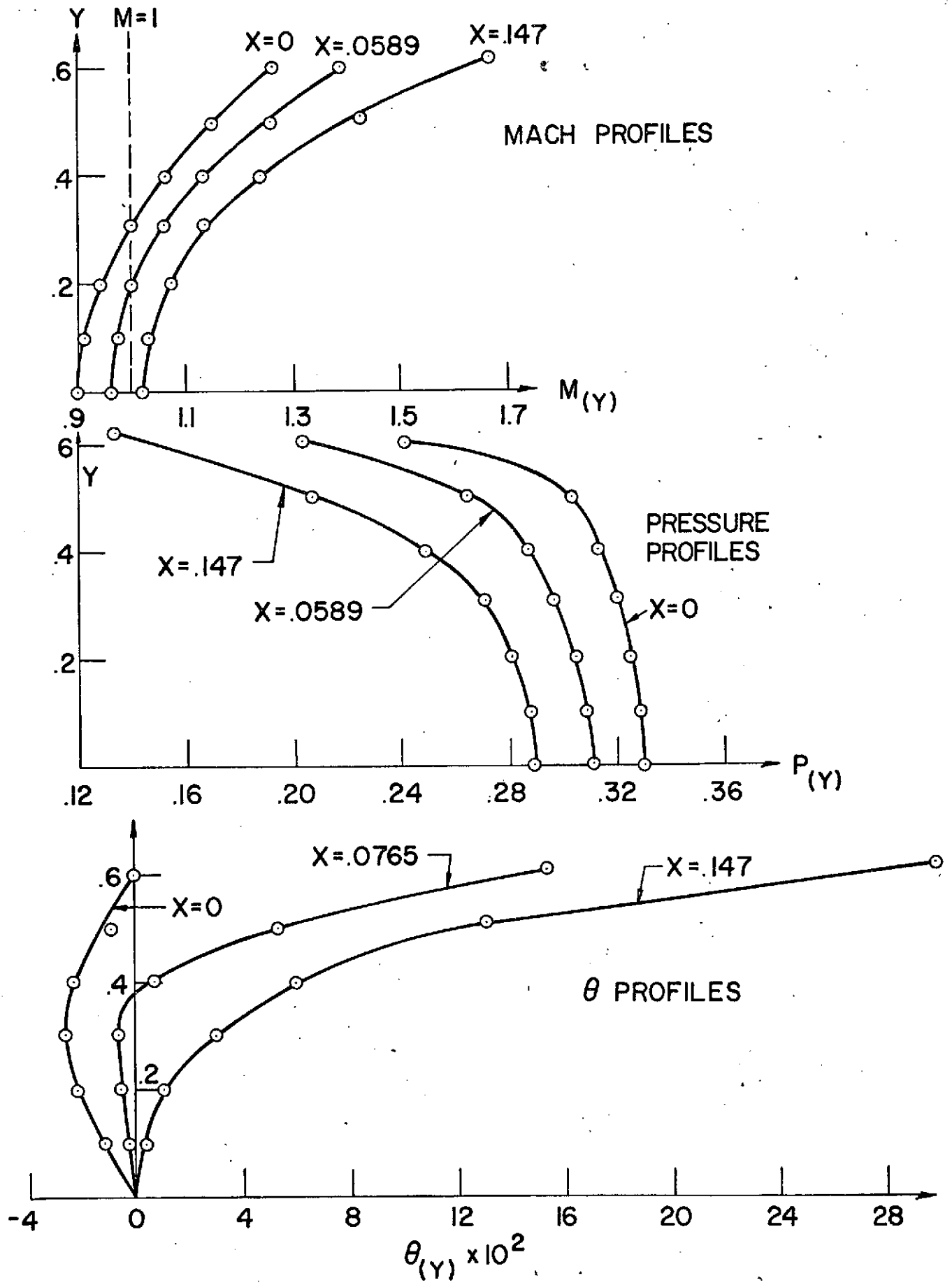
Y
M=1
X=0
X=.0589
X=.147
.6
.4
.2
MACH PROFILES
.9
1.1
1.3
1.5
1.7
M(Y)
6
Y
.4
X=.147
X=.0589
PRESSURE
PROFILES
X=0
.2
.12
.16
.20
.24
.28
.32
.36
P(Y)
X=.0765
X=.147
.6
X=0
.4
θ PROFILES
.2
-4
0
4
8
12
16
20
24
28
θ(Y) x 10²

FIGURE 10.

only case (2) could be analyzed by a direct marching approach. Case (1) cannot be handled by a direct marching technique since the downstream conditions are not known á priori while case (3) requires the addition of shock waves to adjust the incoming mass flow. Figure (10) indicates M, P and θ profiles at several axial stations for case (2).

When the polynomial method was applied to the analysis of viscous-combusting flow fields the following difficulties were encountered:

(1) Both the pressure and flow deflections exhibited oscillations at the upper and lower bounding subsonic streamlines which tended to rapidly grow in magnitude. It was found that these oscillations were strongly a function of the size of the marching step in the streamwise direction; the larger the axial step size, the smaller the amplitude of the oscillation. This is analogous to the numerical difficulties encountered in the blunt body problem, but cannot be simply resolved since both the chemistry and the mixing impose limitations on the allowing axial step size.

(2) When one of the bounding streamlines was a wall, it was found that the flow deflection polynomial θ(y) could not physically describe a subsonic-supersonic or supersonic to subsonic transition at this wall.

(3) In attempting to run problems of the "direct" type, local choking consistently occurred causing the program to terminate.

On the basis of the results obtained with both numerical schemes developed the following conclusions were reached:

(a) A marching scheme employing a finite difference approximation of the governing equations (Equations 4 - 9) of

all grid points appears to be unstable for both direct and indirect problems.

(b) A marching scheme employing polynomial expressions for the pressure and flow deflection yields oscillations at the bounding streamlines; cannot represent bounded flow fields with subsonic flow adjacent to one of the boundaries and yields local choking for direct problems.

The numerical scheme described in the following section yields a workable method for problems of the inverse type, for embedded subsonic regions adjacent to walls.

V. NUMERICAL PROCEDURE FOR THE ANALYSIS OF EMBEDDED SUBSONIC REGIONS

A numerical method of the inverse type has been developed for the analysis of embedded subsonic regions adjacent to walls. A typical flow field is depicted in Figure (11).

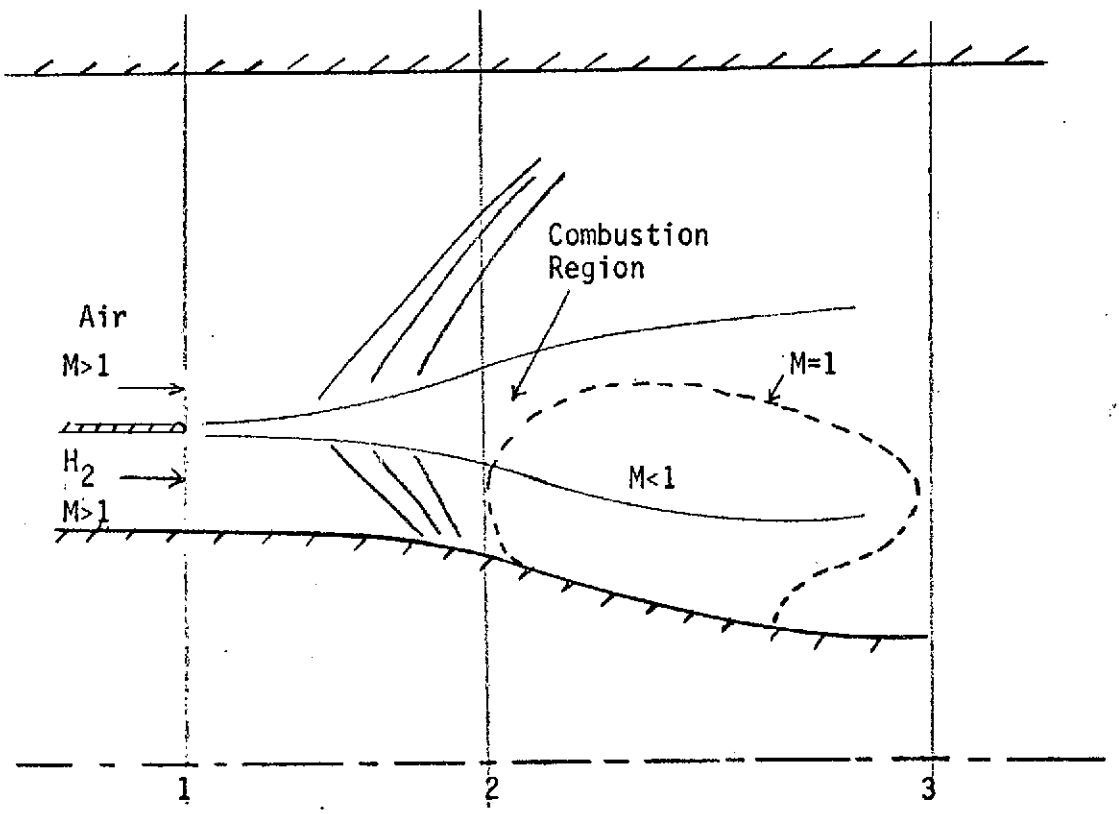

FIGURE 11.

The flow field contained between Station (1) (initial profile) and Station (2) is entirely supersonic and hence may be analyzed by "viscous-characteristics" as described in Reference (2). It should be pointed out that the "viscous-characteristic" program as described in Reference (2) was catered to analyzing expanding supersonic nozzle flow fields. In this current effort, combustion generated compression fields are being analyzed, hence major changes have been incorporated into the basic "viscous-characteristic program. These changes include the capability of calculating the initial mixing region including the determination of an initial underexpansion shock; carrying shocks as discrete discontinuities in the flow field; the detection and calculation of envelope shocks produced by the coalescence of compression waves; and grid spacing logic for analyzing a mixing region of small transverse extent in a nonuniform supersonic flow field. These revisions will be described in later sections of this report.

Consider the flow field at Station (2), where the program has first encountered a grid point with a Mach number $M \leq 1.01$. At this station, the lower wall (AB) becomes the lower subsonic boundary and a slightly supersonic streamline (FG with $M \sim 1.1$ to 1.2) becomes the upper subsonic boundary, as depicted in Figure (12)

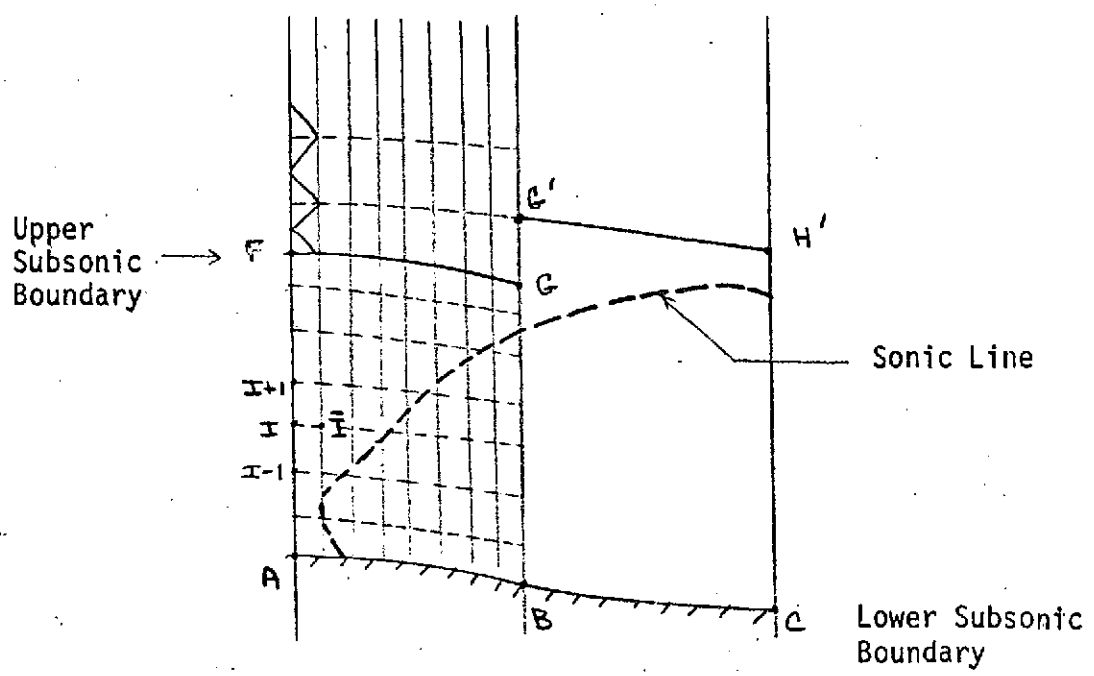

FIGURE 12.

The shape of the upper subsonic bounding streamline (F-G) is specified as the polynomial

$$Y_{FG} = A + B\,\bar{X} + C\,\frac{\bar{X}^2}{2} + D\,\frac{\bar{X}^3}{6} + \text{-----} \tag{10}$$

where $\bar{X} = X - X_F$

The first four coefficients in this polynomial are related to the streamline shape at F as follows:

$$A = Y_F \tag{11a}$$

$$B = \left(\frac{dy}{dx}\right)_F = \tan\theta_F \tag{11b}$$

$$C = \left(\frac{d^2y}{dx^2}\right)_F = \left(\frac{\theta_s}{\cos^3\theta}\right)_F \tag{11c}$$

$$D = \left(\frac{d^3y}{dx^2}\right)_F = \left(\frac{\theta_{ss} + 3\tan\theta\,(\theta_s)^2}{\cos^4\theta}\right)_F \tag{11d}$$

The quantities θ_s and θ_{ss} can be obtained from the y derivatives of flow quantities at F. Consider the following system of equations;

$$\begin{pmatrix} (M^2-1) & 0 & 0 & (\gamma PM^2) \\ 0 & 1 & (\gamma PM^2) & 0 \\ \sin\theta & \cos\theta & 0 & 0 \\ 0 & 0 & \sin\theta & \cos\theta \end{pmatrix} \begin{pmatrix} P_s \\ P_n \\ \theta_s \\ \theta_n \end{pmatrix} = \begin{pmatrix} A \\ 0 \\ P_y \\ \theta_y \end{pmatrix} \tag{12}$$

which are modified continuity equation, normal momentum equation and the geometric relation $\partial/\partial y = \cos\theta\,\partial/\partial n + \sin\theta\,\partial/\partial s$ applied to both P and θ. The righthand side terms may be evaluated at F since they consist of differentiation in the y direction only. (A is related to the mixing and

chemistry terms as described by Equation (AI-3). A derivation of the modified continuity equation may be found in Reference 2). Solution of this system of equations then yields θ_s, P_s, θ_n and P_n at point F. Expressions for θ_s and P_s are given by Equations (AI-1) and (AI-2) in Appendix I. Then,

$$\theta_n = \frac{A - (M^2-1)\, P_s}{\gamma P M^2} \tag{13}$$

and

$$P_n = - \gamma P M^2 \theta_s \tag{14}$$

Consider $\partial/\partial n$ of the modified continuity equation, $\partial/\partial s$ of the normal momentum equation and $\partial/\partial y$ by both θ_s and θ_n. This yields the following system of equations:

$$\begin{pmatrix} (M^2-1) & 0 & 0 & (\gamma PM^2) \\ 1 & 0 & (\gamma PM^2) & 0 \\ 0 & \cos\theta & \sin\theta & 0 \\ 0 & \sin\theta & 0 & \cos\theta \end{pmatrix} \begin{pmatrix} P_{ns} \\ \theta_{ns} \\ \theta_{ss} \\ \theta_{nn} \end{pmatrix} = \begin{pmatrix} a \\ b \\ c \\ d \end{pmatrix} \tag{15}$$

where

$$a = A_n - 2MM_n\, P_s - (\gamma PM^2)_n\, \theta_n \tag{16a}$$

$$b = - (\gamma PM^2)_s\, \theta_s \tag{16b}$$

$$c = - (\theta_s)_y \tag{16c}$$

$$d = - (\theta_n)_y \tag{16d}$$

This system may be solved for θ_{ss} yielding

$$\theta_{ss} = (-A_n\cos\theta+2\cos\theta MM_nP_s+(\gamma PM^2)_n\cos\theta(\theta_n)$$

$$(-\gamma PM^2)_s\cos^2\theta(M^2-1)\theta_s+(\gamma PM^2)\sin\theta(\theta_{s_y}) \qquad (17)$$

$$(-\gamma PM^2\cos\theta(\theta_n)_y)/(\gamma PM^2[M^2\cos^2\theta-1])$$

Note that $\partial/\partial y$ of θ_s and θ_n are obtained numerically by obtaining these quantities at grid points above and below F, while A_n is approximated by A_y consistent with the assumption in the governing equations that for the transport terms $\partial/\partial n \sim \partial/\partial y$.

With the upper boundary streamline now specified (if we do not impose higher order terms), the pressure distribution could be obtained along this streamline independent of the subsonic flow field, if there were no viscous effects. Due to the presence of viscosity, the following iterative procedure is used to calculate the combined flow fields.

The lower wall is prescribed by the polynomial

$$Y_{AB} = a + b\,\bar{x} + \frac{c\bar{x}^2}{2} + \frac{d\bar{x}^3}{6} \qquad (18)$$

where a, b and c are prescribed by the relations (11a), (11b) and (11c) prescribed at point A. The term d is the parameter iterated upon in the problem; if a value of d is assumed, the lower wall AB is specified. The pressure distribution in the y direction is prescribed by a parabola

$$P_{(y)} = \bar{a} + \bar{b}\,y + \bar{c}\,y \qquad (19)$$

and initially (when first encountering a subsonic zone), the existing pressure distribution must be fit with this parabola to avoid spurious pressure gradients in the subsonic region due to "wiggles" in the actual pressure distribution.

In determining the flow properties at the next axial station, the axial step

Δx taken is governed by the allowable stability criterion described in Appendix III), the supersonic portion of the flow field (points above F') may be calculated by "viscous-characteristics". With the flow deflection known at point F', the pressure is obtained using the compatibility relation

$$B_1 (P_{F'}-P_K) - (\theta_{F'}-\theta_K) + [J \frac{\sin\theta}{y}_{F'K} + B_2 + B_3] B_4 \Delta x=0 \qquad (20)$$

applied along F'K where

$$B_1 = (\frac{\sin\mu\cos\mu}{\gamma P}) \qquad (21)$$

$$B_2 = \frac{S_1}{\rho q^2} - \frac{(\gamma-1)S_2}{\gamma P q} - \frac{W}{\rho q} \sum_i \frac{S_{3_i}}{m_i} \qquad (22)$$

$$B_3 = - [\frac{1}{T} (\frac{\partial T}{\partial s})_{chem} + W \sum_i (\frac{\partial \alpha_i}{\partial s} \frac{1}{m_i})_{chem}] \qquad (23)$$

$$B_4 = \frac{\sin\mu}{\cos(\theta-\mu)} \qquad (24)$$

Note that the chemistry is uncoupled as explained in Reference (2) and the term B_3 may be evaluated along the flow streamlines prior to the computations of the fluid mechanical properties.

With the pressure gradient and streamline location known, the velocity, temperature and species mass fraction may be obtained at F' (or any mesh point $\bar{I}$) by using an explicit finite difference formulation of Equations (5), (7) and (8).

$$q_{\bar{I}} = q_I - \frac{2(P_{\bar{I}} - P_I)}{\rho_1 q_1 + \rho_{\bar{I}} q_{\bar{I}}} + \frac{2S_1 \Delta s}{\rho_I q_I + \rho_{\bar{I}} q_{\bar{I}}} \qquad (25)$$

where S_1 is approximated by derivatives in the y direction

$$S_1 = \mu_T [\frac{\partial^2 q}{\partial y^2} + J \frac{\cos\theta}{y} \frac{\partial q}{\partial y}]/Re \qquad (26)$$

and the derivatives $\frac{\partial q}{\partial y}$ and $\frac{\partial^2 q}{\partial y^2}$ are evaluated at the grid point I by the non-centered finite difference formulas

$$\left(\frac{\partial q}{\partial y}\right)_I = \frac{q_{I+1}\frac{\Delta y_1}{\Delta y_2} - q_I\left(\frac{\Delta y_1}{\Delta y_2} - \frac{\Delta y_2}{\Delta y_1}\right) - q_{I-1}\frac{\Delta y_2}{\Delta y_1}}{\Delta y_1 + \Delta y_2} \tag{27}$$

and

$$\left(\frac{\partial^2 q}{\partial y^2}\right)_I = \frac{2\left[q_{I+1}\frac{\Delta y_1}{\Delta y_1 + \Delta y_2} - q_I + q_{I-1}\frac{\Delta y_2}{\Delta y_1 \Delta y_2}\right]}{\Delta y_1 \Delta y_2} \tag{28}$$

where $\Delta y_1 = y_I - y_{I-1}$

and $\Delta y_2 = y_{I+1} - y_I$

The temperature T is determined by the finite difference relation

$$T_{\bar{I}} = T_I + \left(\frac{\partial T}{\partial s}\right)_{I_{chem}} \Delta s + \frac{2\,(P_{\bar{I}} - P_I)}{C_{p_I}\rho_I + C_{p_{\bar{I}}}\rho_{\bar{I}}} + \frac{2\,S_2\,\Delta s}{(\rho q C_p)_I + (\rho q C_p)_{\bar{I}}} \tag{29}$$

where

$$S_2 = \mu_T\left[\frac{C_p}{Pr}\frac{\partial^2 T}{\partial y^2} + \frac{1}{Pr}\frac{\partial C_p}{\partial T}\left(\frac{\partial T}{\partial y}\right)^2 + J\frac{\cos\theta}{y}\frac{C_p}{Pr}\left(\frac{\partial T}{\partial y}\right) + \frac{L_e}{Pr}\left(\frac{\partial T}{\partial y}\right)\Sigma C_{p_i}\frac{\partial \alpha_i}{\partial y}\right.$$

$$\left. + (\gamma_\infty - 1)\,M_\infty^2\left(\frac{\partial q}{\partial y}\right)^2\right] / [Re\,(\gamma_\infty - 1)\,M_\infty^2] \tag{30}$$

All first and second derivatives are evaluated as described by Equations (27) and (28).

The i^{th} species mass fraction α_i is determined by the finite difference relation

$$\alpha_{i_{\bar{I}}} + \alpha_{i_I}\left(\frac{\partial \alpha_i}{\partial s}\right)_{I_{chem}}\Delta s + \frac{2\,S_{3_i}\,\Delta s}{(\rho_I q_I + \rho_{\bar{I}} q_{\bar{I}})} \tag{31}$$

where

$$S_{3_i} = \mu_T \left[\frac{L_e}{\partial y^2}\frac{\partial^2 \alpha_i}{} + J \frac{\cos\theta}{y}\frac{L_e}{Pr}\frac{\partial \alpha_i}{\partial y}\right]/Re \tag{32}$$

The remaining properties are made as follows. The average molecular weight is obtained from

$$W = \left[\Sigma \left(\frac{\alpha_i}{m_i}\right)\right]^{-1} \tag{33}$$

hence the mixtures gas constant is $R = \frac{R_o}{W}$. From the equation of state, the density is

$$\rho = \frac{W_p}{T}\frac{\gamma_\infty M_\infty^2}{W_\infty} \tag{34}$$

The specific heat (frozen) is expressed by

$$C_p = \Sigma\, C_{p_i}(T)\, \alpha_i = \Sigma \left(\alpha_i \frac{\partial h_i(T)}{\partial T}\right) \tag{35}$$

where $C_{p_i}(T)$ is a specified function of temperature, thermodynamic data being tabulated from Reference (15).

The ratio of specific heats is

$$\gamma_f = \frac{C_p}{C_p - R/C_{p_\infty}} \tag{36}$$

and the Mach number is given by

$$M_f = \frac{M_\infty q}{\sqrt{T}} \left[\frac{\gamma_\infty R_\infty}{\gamma R}\right]^{\frac{1}{2}} \tag{37}$$

The derivative P_y at F' is computed from P_n and P_s, where P_n is evaluated using the normal momentum equation (Equation 14). θ_s at F' is obtained from the relation

$$\theta_{s_{F'}} = \cos^3\theta_F \left[C + D\,(x_{F'} - x_F)\right] \tag{38}$$

while P_s is evaluated by a backward difference.

The $P_{(y)}$ polynomial at the new axial station A'F' is then obtained employing a simple iterative procedure. A value for P_y at A' is assumed (for a first guess, the value at A is used), and the polynomial coefficients $\bar{a}$, $\bar{b}$ and $\bar{c}$ are evaluated using $P_{F'}$, $P_{y_{F'}}$ and $P_{y_{A'}}$. This yields the pressure at A', hence all flow properties can be evaluated using Equations (25) - (37). Then, the normal momentum equation is used to obtain P_n and combining this with P_s an alternate value of P_y is obtained at A'. The value of P_y initially assumed is then perturbed and the process repeated until the two values of P_y agree to within a specified tolerance. Then, employing the polynomials at both stations, the pressure gradient is specified for each streamline in the subsonic region Equations (25) - (37) then yield flow properties at all the grid points. This process is repeated for subsequent axial stations until Station II is reached. Station II is either a specified number of Δx steps from Station I or is the station at which the Mach number along the upper bounding streamline falls below some prescribed value.

At Station II, the mass flow contained between the upper and lower subsonic boundaries (GB) is evaluated as follows:

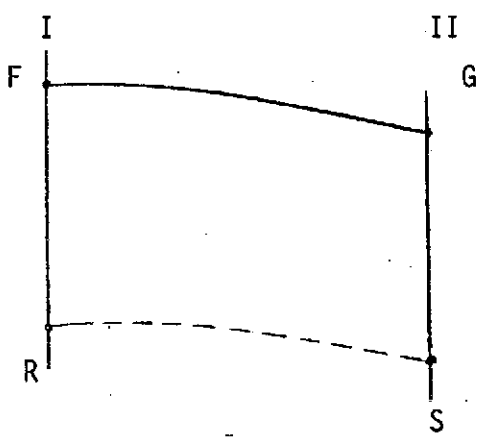

FIGURE 13.

Referring to Figure (13), let RS denote the streamline below FG. Along RS

$$y_S = y_R + (\tan\theta_R)\,(x_S-x_R) + \left(\frac{\theta_s}{\cos^3\theta}\right)_R \left(\frac{x_S-x_R}{2}\right)^2 + \frac{\varepsilon}{6}(x_S-x_R)^3 \qquad (39)$$

$$\tan\theta_s = \tan\theta_R + \left(\frac{\theta_s}{\cos^3\theta}\right)(x_S-x_R) + \frac{\varepsilon}{2}(x_S-x_R)^2 \qquad (40)$$

while between G and S

$$\psi_G = \psi_S + \frac{1}{2}\left((\rho q\cos\theta)_S+(\rho q\cos\theta)_G\right)\frac{y_S^{1+J}-y_G^{1+J}}{1+J} \qquad (41)$$

where $\psi_G = \psi_F$ and $\psi_S = \psi_R$

Equations (39), (40) and (41) may be solved for y_G, θ_G and ε. This process is continued down to the wall (point B of Figure 12) yielding a value of y_B^* different than the value of y_B obtained using Equation (18). A value d^* is obtained from Equation (18), which would adjust the lower wall shape so that $y_B=y_B^*$. The numerical procedure is restarted from Station I with a new value of d' chosen such that $d' = \frac{d+d^*}{2}$. The iteration procedure for d appears to be self converging. Note that in repeating the calculation of the subsonic flow field ABFG with a new lower wall shape, the supersonic portion of the flow is not recalculated. Flow properties along FG are stored so that the derivatives can be made for evaluating the shear terms. It is assumed that the slight perturbations in the wall shape AB occurring in the iteration process do not influence the value of the terms stored along FG. Having converged on the lower wall shape, a new upper matching streamline is determined at Station II based on the Mach number profile. Then, the calculation proceeds from II to III as described above. This process is repeated until the sonic line closes and the entire flow field is again calculable by "viscous-characteristics".

VI. SHOCK PHENOMENA

Numerical techniques have been developed for analyzing shock discontinuities occurring in a viscous combusting flow field. The analysis of higher order shock structure has been discussed extensively in References (16) and (17). For the problem under consideration, it appears that the modifications to the Rankine-Hugoniot relations to include the effects of heat conduction, viscosity and shock structure (which involve the local shock curvature) involve higher order approximations than the inclusion of these terms in the characteristic relations, hence the shock model employed uses the standard Rankine-Hugoniot relations, with the chemistry frozen across the shock. The flow may be nonuniform on both sides of the shock and "viscous-characteristics" are used in performing a shock point calculation, which takes the transport and chemistry terms into account.

A. Shock Point Calculation - Assume a coordinate system oriented along ($\hat{t}$ direction) and normal to the shock surface ($\hat{n}$ direction) as shown in Figure (14). The angle beta (β) is the direction cosine of the shock with respect to the Cartesian direction x, and $\tilde{u}$ and $\tilde{v}$ are the velocity components in the $\hat{n}$ and $\hat{t}$ directions.

$$\hat{n} = -\sin\beta\hat{i}_x + \cos\beta\hat{i}_y \tag{42}$$

$$\hat{t} = \cos\beta\hat{i}_x + \sin\beta\hat{i}_y \tag{43}$$

$$\vec{V} = -\tilde{u}\,\hat{n} + \tilde{v}_t\,\hat{t} = u\hat{i}_x + v\hat{i}_y \tag{44}$$

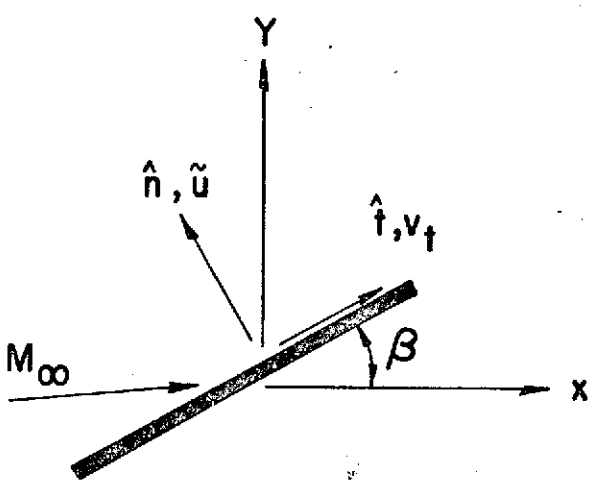

$$\hat{n} = -\sin\beta\,\hat{i}_x + \cos\beta\,\hat{i}_y$$

$$\hat{t} = \cos\beta\,\hat{i}_x + \sin\beta\,\hat{i}_y$$

$$M_\infty = -M_n\,\hat{n} + M_t\,\hat{t}$$

FIGURE 14.

The Rankine Hugoniot relations take the form

$$\text{Continuity:} \qquad \rho_1 \tilde{u}_1 = \rho_2 \tilde{u}_2 \tag{45}$$

$$\text{Normal Momentum:} \qquad P_1 + \rho_1 \tilde{u}_1^2 = P_2 + \rho_2 \tilde{u}_2^2 \tag{46}$$

$$\text{Tangential Momentum:} \qquad \tilde{v}_{t_1} = \tilde{v}_{t_2} \tag{47}$$

$$\text{Energy:} \qquad H = h + \frac{1}{2} V^2 = \text{constant} \tag{48}$$

where

$$h = \sum_{i=1}^{n} \alpha_i h_i(T)$$

$$\text{State:} \qquad \rho = \rho(P, T, \alpha_i) \tag{49}$$

The α_i's are the mass fractions (and remain constant across the shock) and h_i's the enthalpies of the i^{th} chemical species. Employing the jump relations for a given shock angle and upstream conditions requires an iteration process since the mixture is calorically imperfect.

Let 1 designate upstream conditions and 2 downstream conditions. To solve the jump relations knowing conditions at 1, a value for $\tilde{u}_2$ is assumed. The density using Equation (45) ρ_2 is computed; P_2 is computed using Equation (46) and Equation (48) yields a value for h_2 which can be inverted by a local iteration to find T_2, since the composition is assumed frozen. The state Equation (49) then yields an alternate value for the density. If this value for density does not agree with that calculated from continuity to within a specified tolerance, a new value of $\tilde{u}_2$ is assumed and this process is repeated until convergence is achieved.

Referring to Figure (15), a typical shock wave calculation is performed as follows. A value of the shock angle β_C is assumed, which locates the point C. Since properties are nonuniform on the upstream side of the shock, a

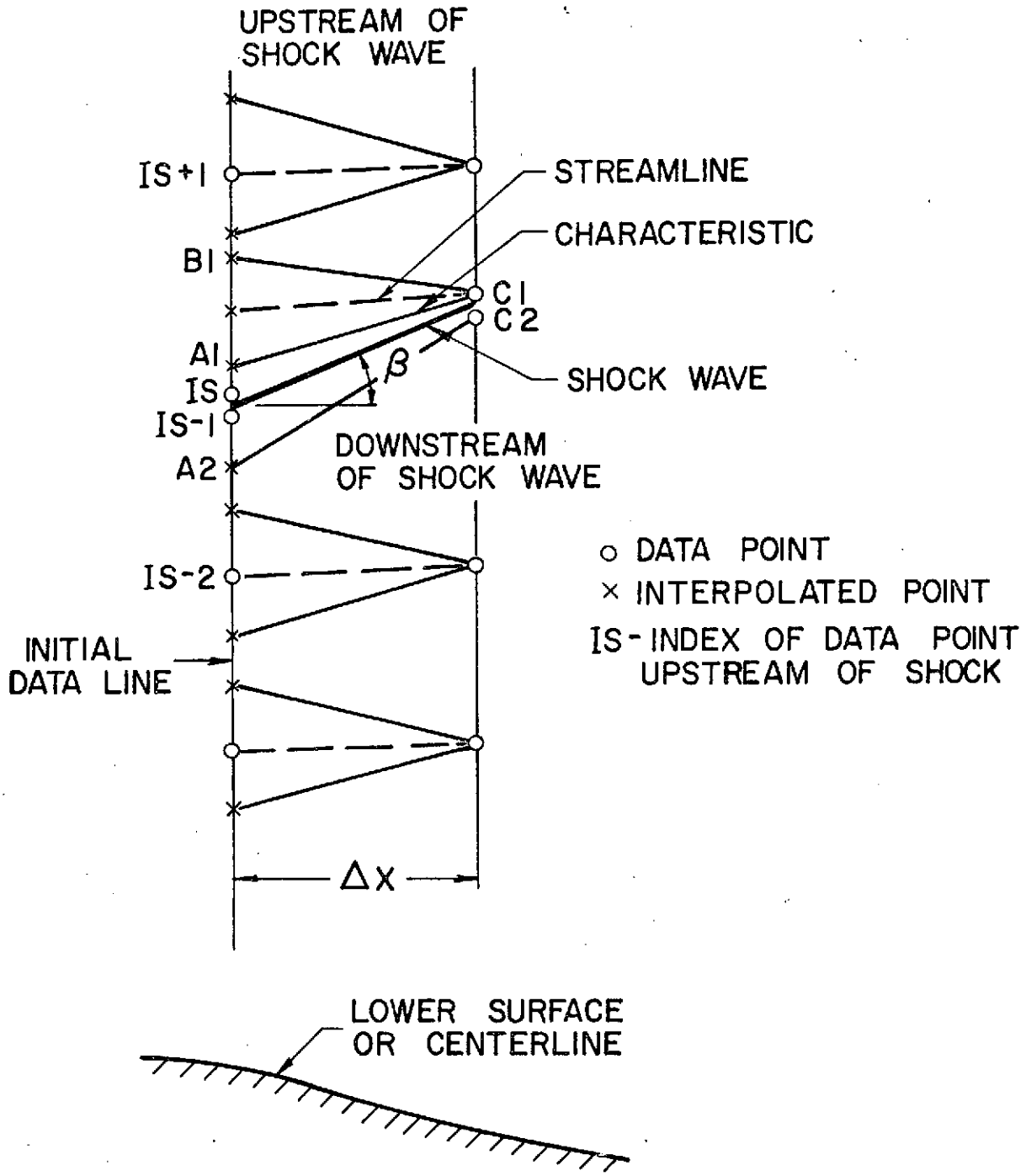
UPSTREAM OF
SHOCK WAVE
IS+1
B1
C1
C2
A1
IS
IS-1
A2
STREAMLINE
CHARACTERISTIC
SHOCK WAVE
β
DOWNSTREAM
OF SHOCK WAVE
IS-2
INITIAL
DATA LINE
ΔX
o DATA POINT
× INTERPOLATED POINT
IS - INDEX OF DATA POINT
UPSTREAM OF SHOCK
LOWER SURFACE
OR CENTERLINE

FIGURE 15.

viscous characteristic calculation yields properties at C1. The jump relations (Equations 45 - 49) are solved using the determined upstream conditions based on the assumed angle β_C. This yields all properties at C2. Using the deflection angle θ_{C_2} calculated from the jump conditions, a viscous-characteristic calculation performed along (C2-A2) yields an alternate value of the pressure at P_{C_2}. The pressures are compared and if the difference exceeds a specified tolerance, a new value of β_C is assumed and the process repeated until convergence is obtained.

B. Under-Expansion Interaction - The program developed has the capability of computing the interaction produced by pressure mismatch between a jet and a surrounding airstream, for the case of an under-expanded jet. This situation is depicted in Figure (16). It is assumed that during the under-expansion interaction, the species remain chemically frozen. The expansion is assumed to be isentropic and the local interaction is two dimensional and inviscid in the limit of vanishing radial distance with respect to the injector lip.

The basic equations describing the Prandtl-Meyer expansion process are

$$P/\rho^{\gamma} = \text{constant} \tag{50}$$

$$h + \frac{1}{2} V^2 = \text{constant} \tag{51}$$

$$\frac{dp}{\rho} + \frac{1}{2} d(V^2) = 0 \tag{52}$$

$$\frac{1}{\gamma} d \ln(P) \pm d\theta = 0 \tag{53}$$

For a small incremental step ΔP, Equations (52, (53) and (50) can be written

$$V_2^2 - V_1^2 = - \left(\frac{2\gamma}{\gamma-1}\right) \left[\left(\frac{P}{\rho}\right)_2 \left(\frac{P}{\rho}\right)_1\right] \tag{54}$$

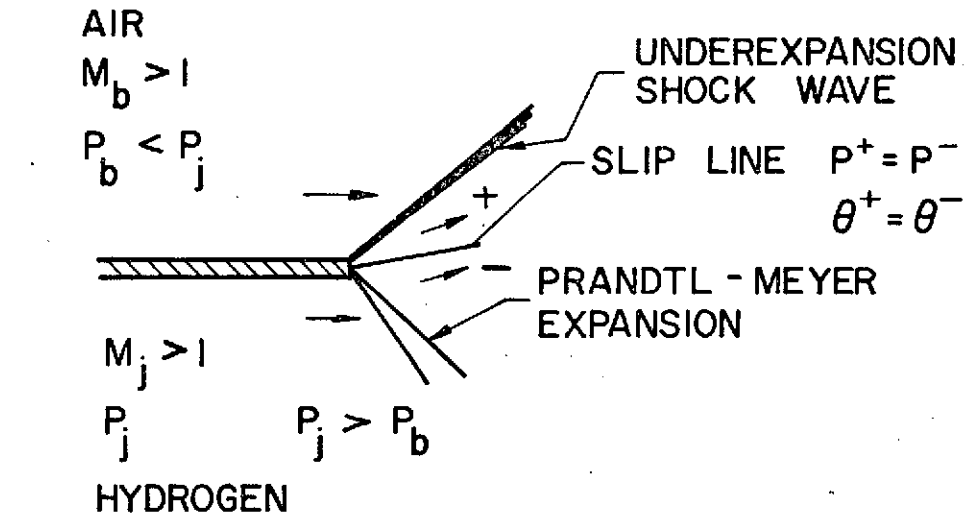
AIR
$M_b > 1$
$P_b < P_j$
UNDEREXPANSION
SHOCK WAVE
SLIP LINE $P^+ = P^-$
$\theta^+ = \theta^-$
PRANDTL - MEYER
EXPANSION
$M_j > 1$
P_j
$P_j > P_b$
HYDROGEN

FIGURE 16.

$$\frac{1}{\gamma} \ln (P_2/P_1) \pm (\theta_2-\theta_1) = 0 \tag{55}$$

$$P_2/\rho_2^{\gamma} = P_1/\rho_1^{\gamma} \tag{56}$$

where γ is held constant in the integration step, yielding values for V_2, ρ_2, and θ_2. Then Equation (51) yields h_2 and an inversion yields T_2. In this manner, the Prandtl-Meyer equations may be integrated.

Since the flow deflection and pressure downstream of the shock wave and Prandtl-Meyer are unknown an iteration process is required. A typical interaction calculation proceeds as follows. A shock wave angle is assumed for which flow properties (P,T,θ etc.) are computed downstream of the shock wave. Equations (50) through (53) are solved using small increments of ΔP with the pressure behind the shock as the final pressure and the jet pressure as the initial pressure. If the turning angle for the expansion does not agree with the flow angle behind the shock to within a specified tolerance, a new shock wave angle β is assumed and the process repeated until convergence is obtained. After this solution is obtained, the initial profile is adjusted by spreading the expansion over a small finite region and the program marches downstream carrying the shock wave as a discontinuity surface in the flow field.

C. Shock Coalescence - The presence of significant compression waves generated either by combustion phenomena or physical boundaries as shown in Figure (17) requires that the entropy rise associated with the focusing of these waves be included in the calculation. Since the numerical scheme follows streamlines, not characteristics, a detection technique based on pressure profiles must be employed, rather than a crossing of waves of the same family.

In strictly inviscid computations, detection of coalescence is based on determining the wave strength associated with the crossing of characteristics of the same family. However, the introduction of transport phenomena has the effect of dispersing the wave so as to weaken the usefulness of the above

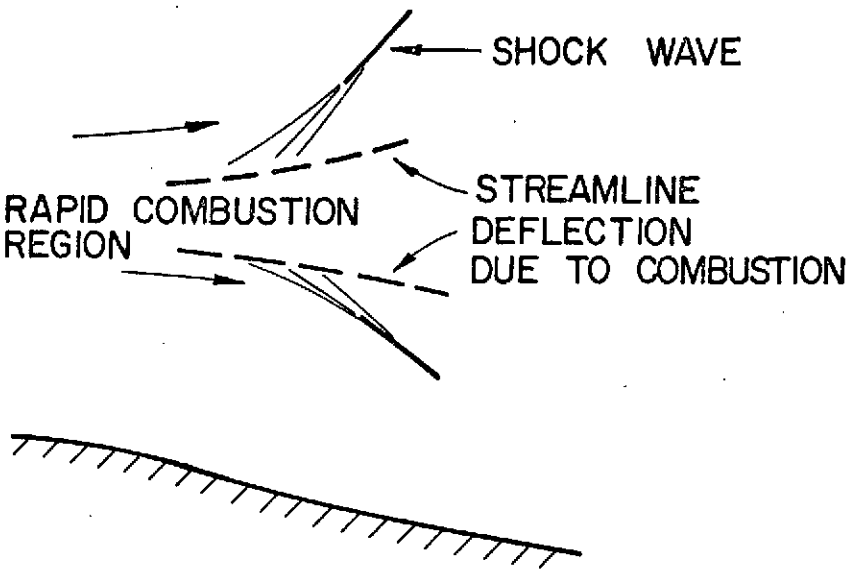

SCHEMATIC OF STRONG COMBUSTION WAVES

FIGURE 17.

detection criteria. A more practical approach is to locally determine the shape of the pressure curve once the above crossing has been detected. That is, a local polynomial of the form

$$y = a + bp + cp^2 + dp^3 \tag{57}$$

is fit using additional data from neighboring points in the region where crossing is detected. Then, the simultaneous vanishing of dy/dp and d^2y/dp^2 indicates the presence of a coalesced shock wave. Typical pressure distributions in the region of strong waves are shown in Figure (18).

The detection procedure is as follows. From data at the initial station the following equations for waves of the same family are solved for a crossing as shown in Figure (19).

$$\left.\frac{dy}{dx}\right|_{C,\,I} = \tan\,(\theta \pm \mu)_I; \qquad \left.\frac{dy}{dx}\right|_{C,\,I+1} = \tan\,(\theta \pm \mu)_{I+1}$$

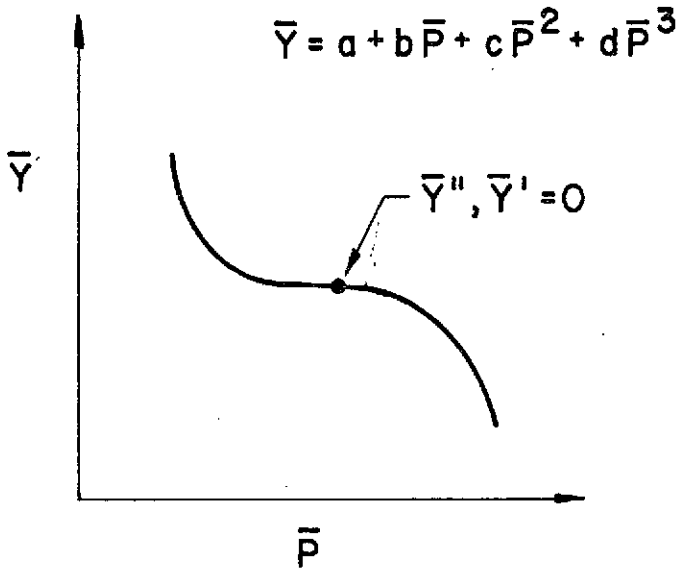

UP RUNNING SHOCK WAVE

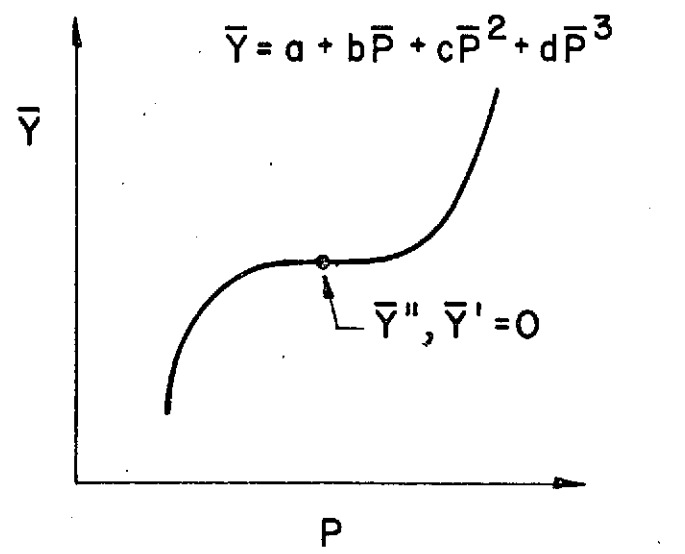

DOWN RUNNING SHOCK WAVE

FIGURE 18.

When a crossing is detected between points I and I+1, a polynomial of the form given in Equation (57) is fit using data at points I-1, I, I+1, I+2. If an inflection point exists for the above polynomial between I and I+1, it is determined if the magnitude of the slope y' at the inflection point is less than a specified tolerance. If so, an embedded shock wave is inserted between points I and I+1. The shock wave angle is assumed to be average of the characteristic angles,

$$\beta = ((\theta \pm \mu)_I + (\theta \pm \mu)_{I+1})/2 \tag{58}$$

the + sign for an uprunning shock and the - sign for a downrunning shock. The inserted shock wave replaces the grid points I and I+1. The program allows for only one embedded shock of a given family, and cannot handle shock crossings or shock-boundary interactions.

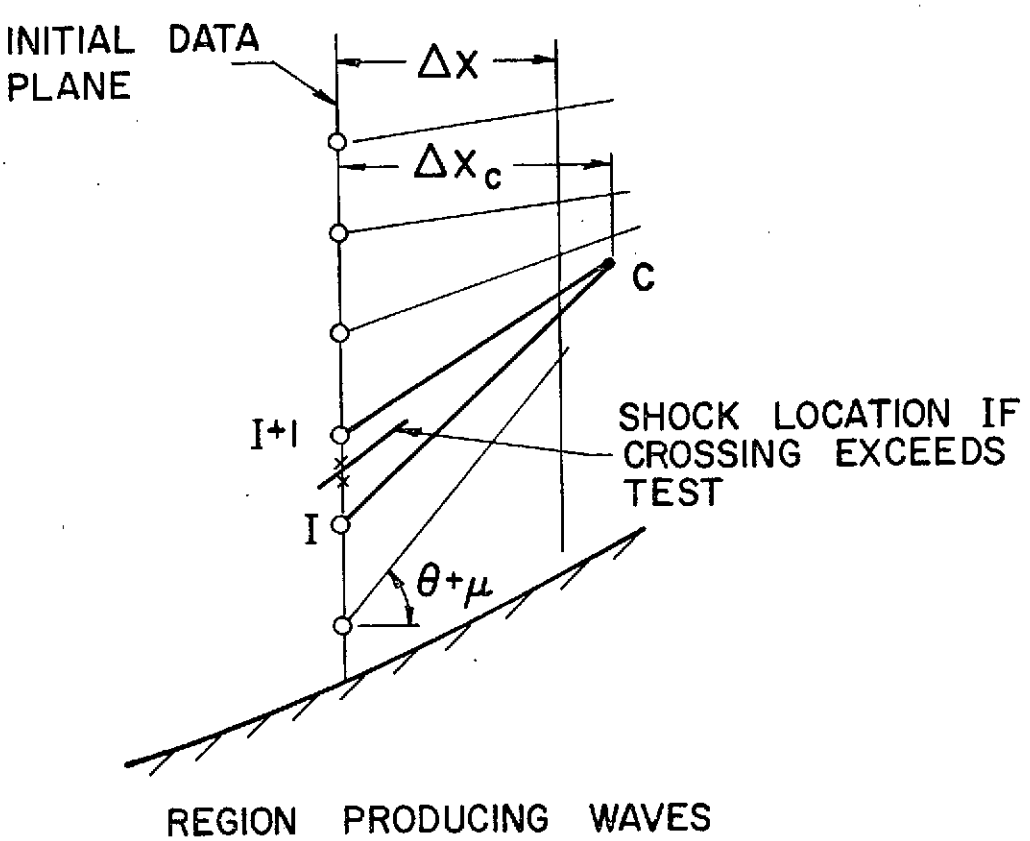

FIGURE 19.

VII. SAMPLE CALCULATIONS

Case I: An axially symmetric hydrogen jet is injected into a Mach 2 air stream as depicted in Figure (20).

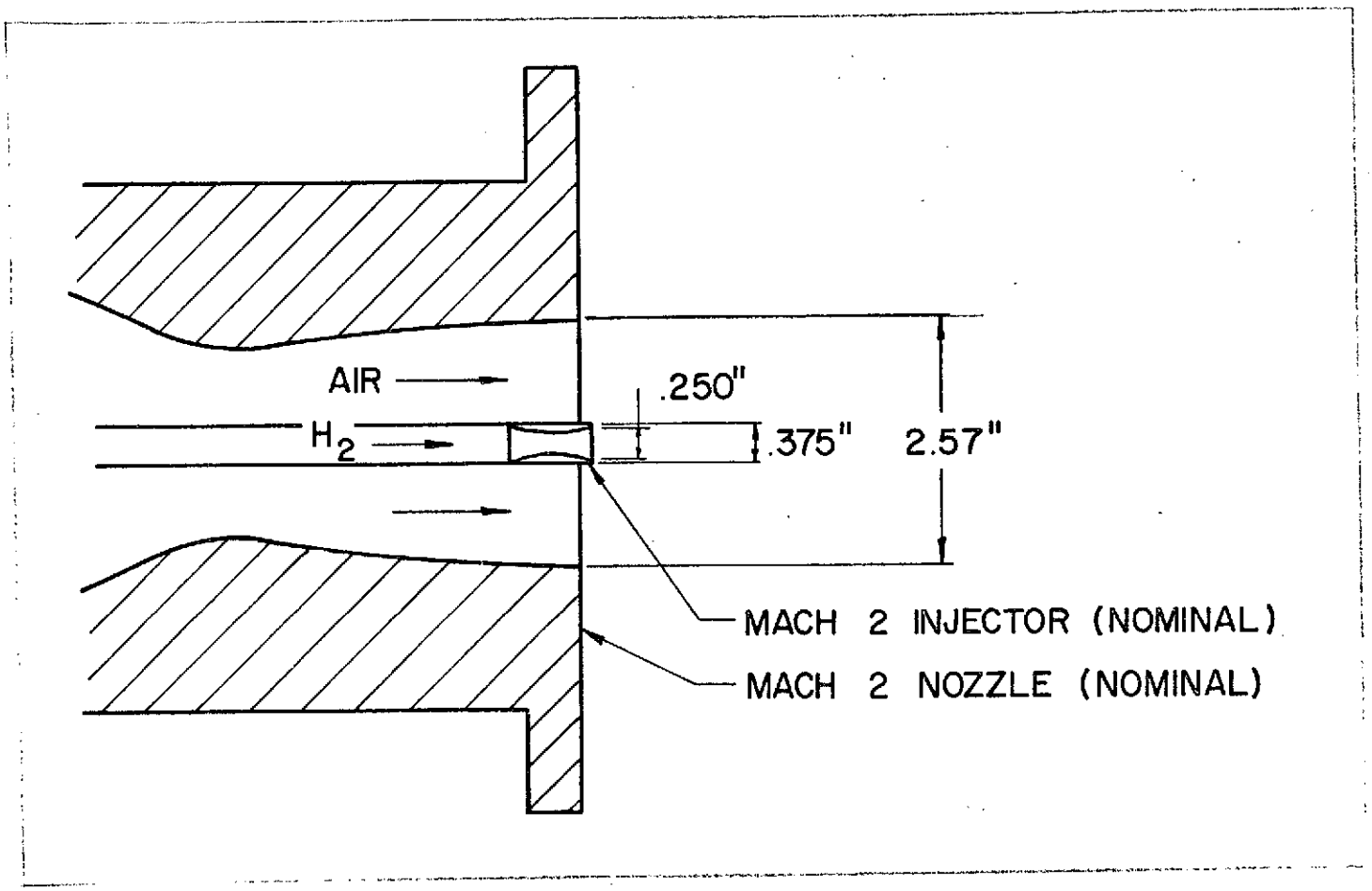

FIGURE 20.

Nominal conditions are

Hydrogen - injection velocity 6850 ft/sec
static temperature 190°K
static pressure 2 atm

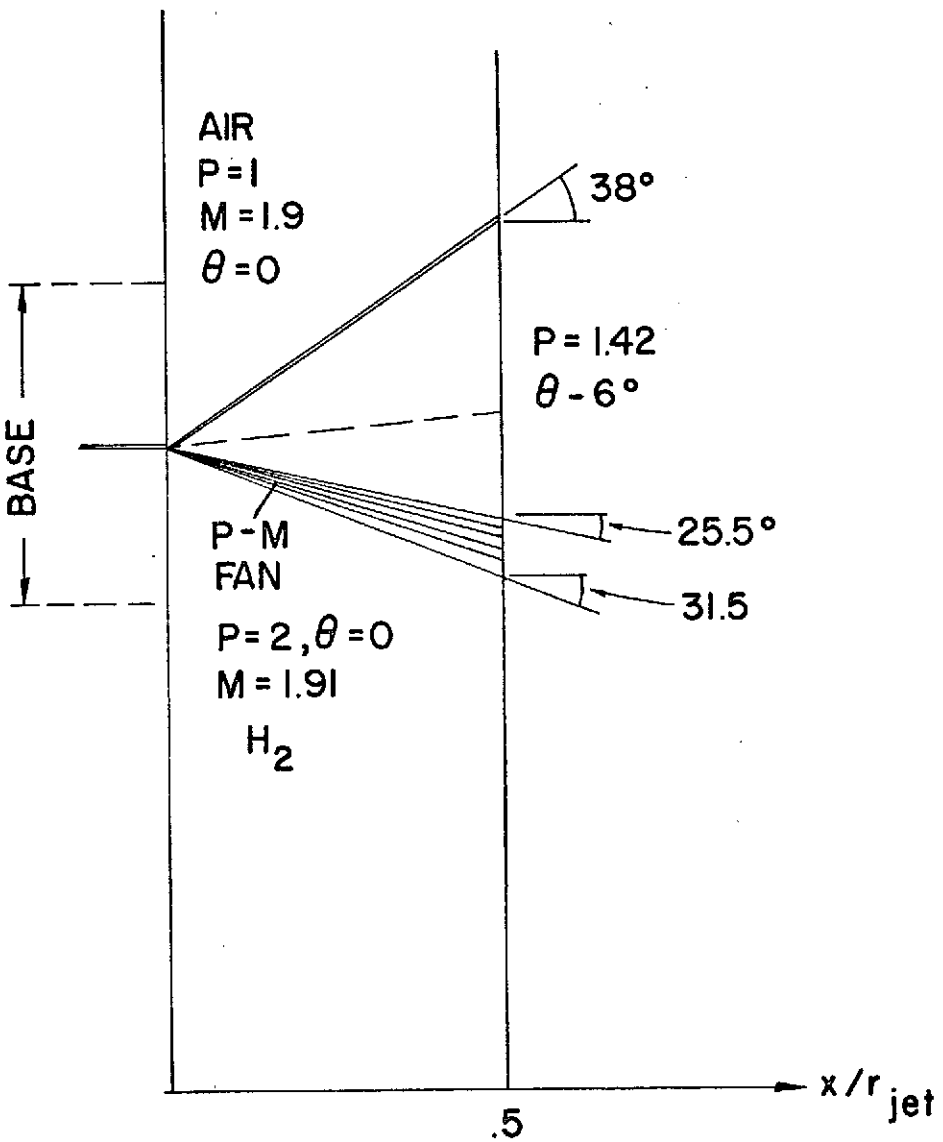

FIGURE 21.

Air - free stream velocity 4300 ft/sec
static temperature 1255^{o}K
static pressure 1 atm

The thickness of the injector lip and the effect of air side boundary layer leads to the formation of a base region downstream of the injector lip. Due to the large residence time in this region, combustion is assumed to initiate here. The pressure mismatch across this finite width region is accounted for by initiating the calculation a small distance downstream of the injector lip as depicted in Figure (21). The flow in the base region is assumed to be in chemical equilibrium and properties are obtained by assuming a smooth Φ variation between the hydrogen and air streams and obtaining the property variations by mass averaged formulas for the total enthalpy and velocity, with the pressure specified a priori. The program was run a total of 2000 axial stations (from x = 0 to x = 34). The overall flow field is depicted in Figure (22). The underexpansion shock is carried as a discrete discontinuity; its interactions with the upper constant pressure boundary (occurring at x = 10) was performed by a hand calculation. Representative flow streamlines, the isotherms T = .5, T = 1.2 and T = 1.5, and the Φ =1 line are also depicted in these figures. The wave field tends to significantly influence properties in the combustion zone as evidenced by the closing and reopening of the T = 1.5 isotherm. For example, this isotherm closes when the initial downward Prandtl-Meyer fan reflects off the axis and passes through the combustion zone (in the region $2 < x < 8$) and again closes after the expansion from the upper surface crosses (in the region $18 < x < 24$). The variation of pressure, Mach number and mass fraction of hydrogen along the axis is depicted in Figure (23). A Ferri-Kleinstein eddy viscosity model was used for the flow in the potential core (defined by $\alpha_{H_2} > .99$) the viscosity varying from 10^{-4} lb-sec/ft^2 at x = .5 to $2.14 * 10^{-4}$ at x = 10. Downstream of this station, the value was maintained at $2.14 * 10^{-4}$. Flow properties are tabulated at the following stations:

KOUNT = 0; x = .5
KOUNT = 100; x = 1.297
KOUNT = 500; x = 6.6346
KOUNT = 1000; x = 14.932
KOUNT = 1500; x = 24.97
KOUNT = 1800, x = 30.24

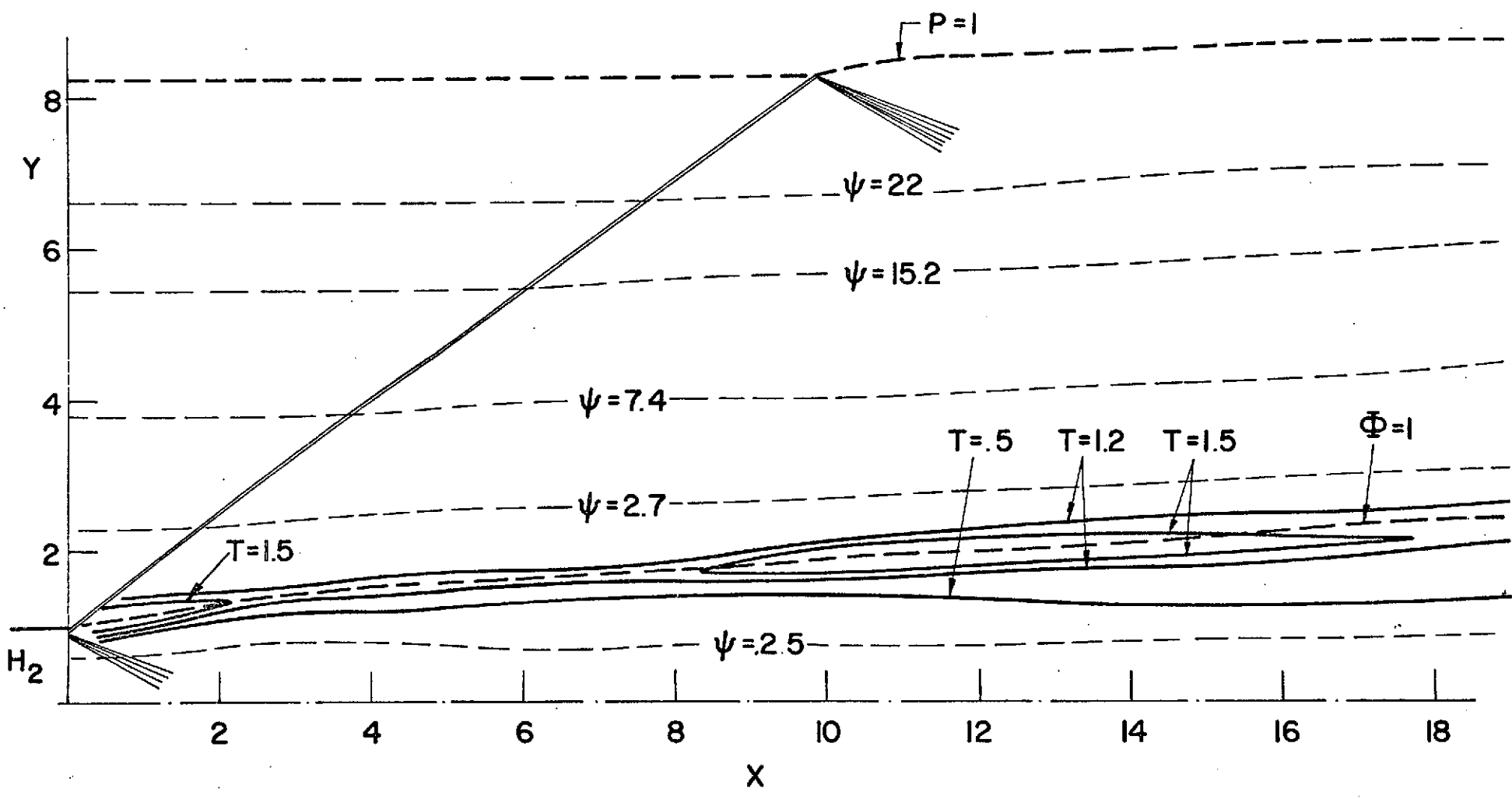
P=1
ψ=22
ψ=15.2
ψ=7.4
ψ=2.7
ψ=.2.5
T=.5
T=1.2
T=1.5
Φ=1
T=1.5
Y
X
H2
8
6
4
2
2
4
6
8
10
12
14
16
18

FIGURE 22a

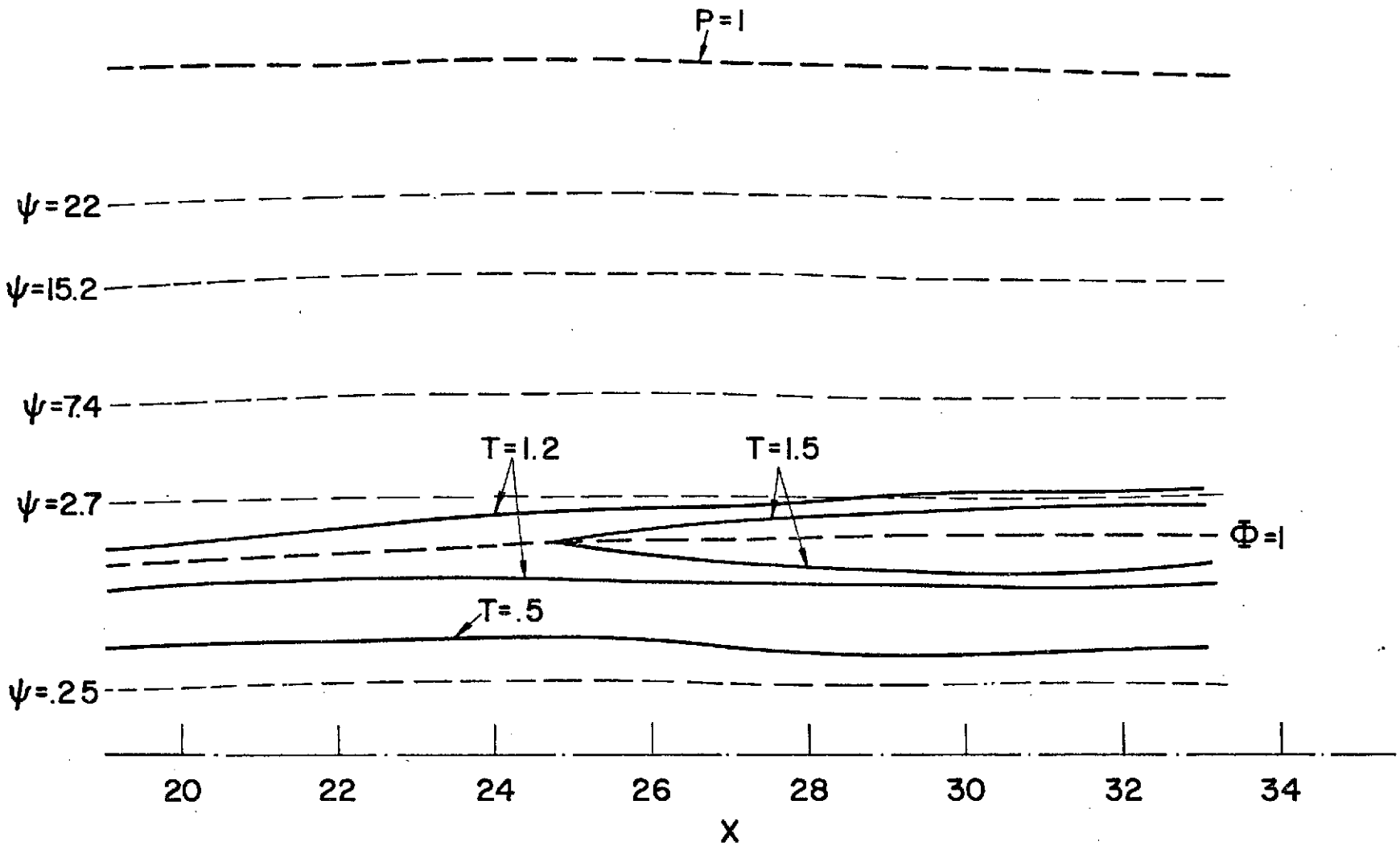

FIGURE 22b.

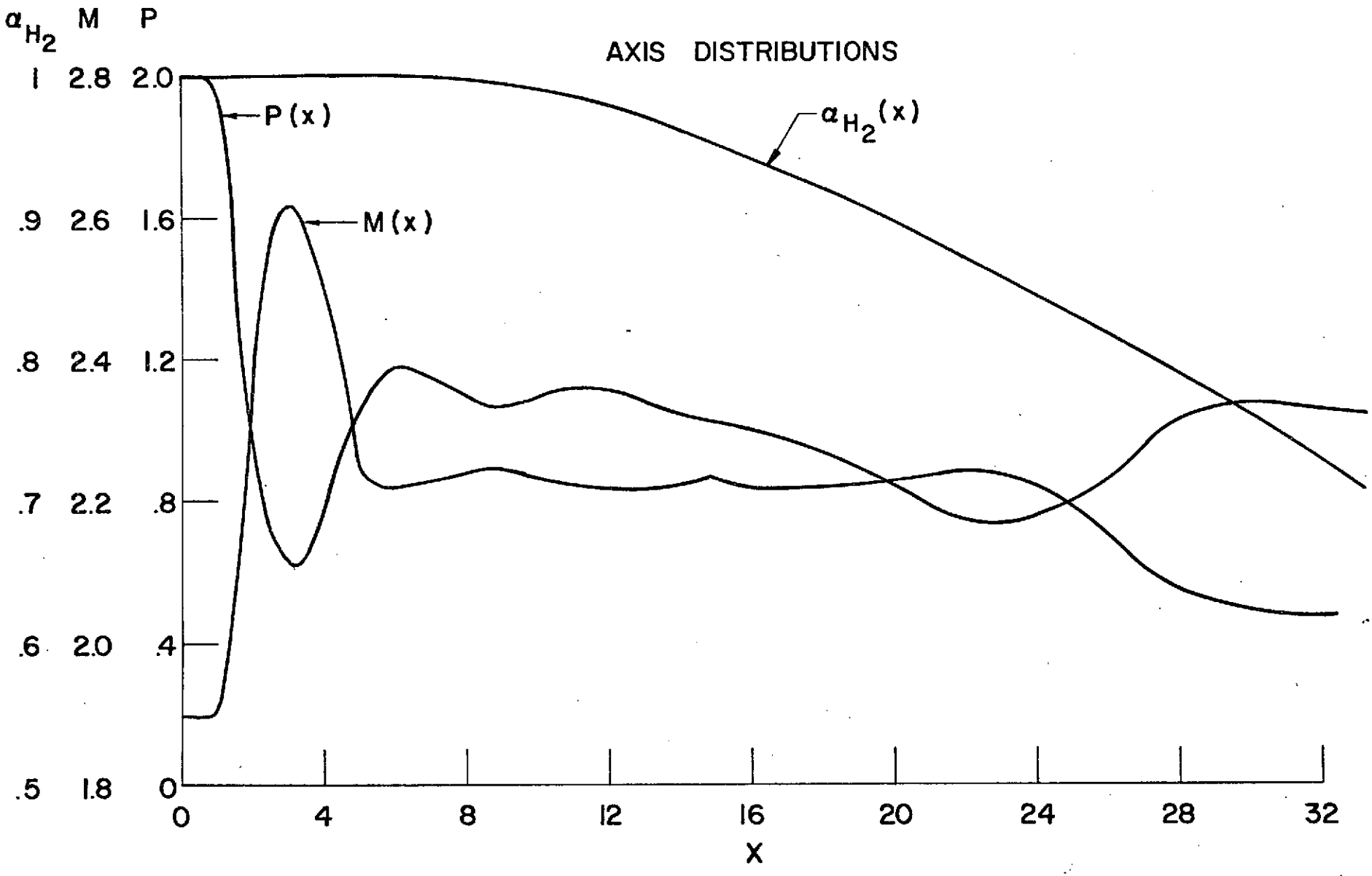
AXIS DISTRIBUTIONS
α_{H_2} M P
1 2.8 2.0
.9 2.6 1.6
.8 2.4 1.2
.7 2.2 .8
.6 2.0 .4
.5 1.8 0
P(x)
M(x)
$\alpha_{H_2}(x)$
0 4 8 12 16 20 24 28 32
X

FIGURE 23.

CASE I.

PROGRAM VIS-CHAR

WITH

EMBEDDED SUBSONIC FLOW

SHOCK WAVES

AND FINITE RATE H2-AIR CHEMISTRY

TYPE OF FLOW IS AXISYMMETRIC
CHEMISTRY IS FINITE RATE
JET OR NOZZLE RADIUS (RTH) = .13000E-01 FT.

REFERENCE CONDITIONS

MACH NO. (EMINF) = .19000E+01
VELOCITY (UIN) = .43089E+04 FT/SEC
TEMPERATURE (TIN) = .12550E+04 DEGREES K
PRESSURE (PRES) = .21160E+04 LB/FT**2
DENSITY (RHOINF) = .54305E-03 SLUGS/FT**3
FROZEN SPECIFIC HEAT RATIO (GAMINF) = .13199E+01
MOLECULAR WEIGHT (WINF) = .28850E+02
REYNOLDS NUMBER (RE) = .34450E+05
PRANDTL NUMBER (PR) = .10000E+01
LEWIS NUMBER (XLE) = .10000E+01

OUTPUT HEADINGS

X - X/RTH
Y - Y/RTH
Q - VELOCITY/UIN
T - TEMPERATURE/TIN
P - PRESSURE/PRES
TH - FLOW DEFLECTION (RADIANS)
EM - MACH NUMBER
GAM - SPECIFIC HEAT
XMASS - NON-DIMENSIONAL MASS FLOW
PHI - EQUIVALENCE RATIO
W - MOLECULAR WEIGHT

MASS FRACTIONS
ALP(1) - H
ALP(2) - O
ALP(3) - H2O
ALP(4) - H2
ALP(5) - O2
ALP(6) - OH
ALP(7) - N2

KOUNT= 0

X = .50000E+00

SHOCK TYPE 3 BETA = .662E+00

VISCOSITY = .99380E-04 (LB*SEC/FT**2)

PT.	Y	Q	T	P
1	.60000E+00	.15376E+01	.15150E+00	.20000E+01
2	.69400E+00	.15376E+01	.15150E+00	.20000E+01
3	.76200E+00	.16489E+01	.13700E+00	.14200E+01
4	.85000E+00	.12124E+01	.51400E+00	.14200E+01
5	.92000E+00	.11076E+01	.95000E+00	.14200E+01
6	.99000E+00	.10384E+01	.15000E+01	.14200E+01
7	.10530E+01	.94510E+00	.21000E+01	.14200E+01
8	.11100E+01	.92283E+00	.21600E+01	.14200E+01
9	.11800E+01	.94262E+00	.19700E+01	.14200E+01
10	.12500E+01	.93400E+00	.14600E+01	.14200E+01
11	.13200E+01	.91937E+00	.10850E+01	.14200E+01
12	.13900E+01	.91937E+00	.10850E+01	.14200E+01
13	.13900E+01	.10001E+01	.10000E+01	.10000E+01
14	.82500E+01	.10001E+01	.10000E+01	.10000E+01

PT.	ALP(1)	ALP(2)	ALP(3)	ALP(4)
1	.11000E-09	.11000E-09	.11000E-09	.10000E+01
2	.11000E-09	.11000E-09	.11000E-09	.10000E+01
3	.11000E-09	.11000E-09	.11000E-09	.10000E+01
4	.11000E-09	.11000E-09	.16300E+00	.34000E+00
5	.11000E-09	.11000E-09	.20800E+00	.18400E+00
6	.11000E-09	.11000E-09	.23300E+00	.78000E-01
7	.11000E-09	.11000E-09	.23700E+00	.13000E-01
8	.11000E-09	.24000E-02	.21200E+00	.11000E-09
9	.11000E-09	.20000E-02	.14500E+00	.11000E-09
10	.11000E-09	.11000E-09	.52000E-01	.11000E-09
11	.11000E-09	.11000E-09	.11000E-09	.11000E-09
12	.11000E-09	.11000E-09	.11000E-09	.11000E-09
13	.11000E-09	.11000E-09	.11000E-09	.11000E-09
14	.11000E-09	.11000E-09	.11000E-09	.11000E-09

TH	EM	RHO	GAM	XMASS
0.	.19100E+01	.92249E+00	.14243E+01	.25531E+00
0.	.19100E+01	.92249E+00	.14243E+01	.34158E+00
.10450E+00	.21500E+01	.72429E+00	.14295E+01	.40608E+00
.10450E+00	.13200E+01	.48997E+00	.13869E+01	.46916E+00
.10450E+00	.11300E+01	.41609E+00	.13414E+01	.50165E+00
.10450E+00	.11000E+01	.43052E+00	.12873E+01	.53183E+00
.10450E+00	.11000E+01	.50402E+00	.12485E+01	.56138E+00
.10450E+00	.11400E+01	.56660E+00	.12459E+01	.59201E+00
.10450E+00	.12400E+01	.64958E+00	.12596E+01	.63726E+00
.10450E+00	.14600E+01	.93850E+00	.12888E+01	.70023E+00
.10450E+00	.16800E+01	.13086E+01	.13151E+01	.79325E+00
.10450E+00	.16800E+01	.13086E+01	.13151E+01	.90674E+00
0.	.19000E+01	.99992E+00	.13200E+01	.90674E+00
0.	.19000E+01	.99992E+00	.13200E+01	.33971E+02

ALP(5)	ALP(6)	ALP(7)	PHI	W
.11000E-09	.11000E-09	-.55000E-09	-.26620E+12	.20160E+01
.11000E-09	.11000E-09	-.55000E-09	-.26620E+12	.20160E+01
.11000E-09	.11000E-09	-.55000E-09	-.26620E+12	.20160E+01
.11000E-09	.11000E-09	.49700E+00	.19142E+02	.51167E+01
.11000E-09	.11000E-09	.60800E+00	.89665E+01	.80309E+01
.11000E-09	.11000E-09	.68900E+00	.39835E+01	.13120E+02
.11000E-09	.55000E-02	.74450E+00	.14231E+01	.21504E+02
.15000E-01	.14000E-01	.75660E+00	.86316E+00	.24865E+02
.80000E-01	.85000E-02	.76450E+00	.58345E+00	.25999E+02
.18100E+00	.11000E-09	.76700E+00	.20071E+00	.27838E+02
.23200E+00	.11000E-09	.76800E+00	.81900E-08	.28848E+02
.23200E+00	.11000E-09	.76800E+00	.81900E-08	.28848E+02
.23200E+00	.11000E-09	.76800E+00	.81900E-08	.28848E+02
.23200E+00	.11000E-09	.76800E+00	.81900E-08	.28848E+02

KOUNT= 100

X = .12970E+01

SHOCK TYPE 3 BETA = .645E+00

VISCOSITY = .11356E-03 (LB*SEC/FT**2)

PT.	Y	Q	T	P
1	0.	.15802E+01	.14489E+00	.17290E+01
2	.10326E+00	.15839E+01	.14432E+00	.17069E+01
3	.20753E+00	.15943E+01	.14267E+00	.16434E+01
4	.31376E+00	.16099E+01	.14017E+00	.15499E+01
5	.42282E+00	.16284E+01	.13718E+00	.14428E+01
6	.53535E+00	.16463E+01	.13428E+00	.13421E+01
7	.65150E+00	.16587E+01	.13274E+00	.12689E+01
8	.76496E+00	.16526E+01	.14005E+00	.12477E+01
9	.85728E+00	.15847E+01	.18896E+00	.12600E+01
10	.95107E+00	.13477E+01	.37483E+00	.12359E+01
11	.10102E+01	.12266E+01	.62508E+00	.12348E+01
12	.10699E+01	.11345E+01	.98895E+00	.12403E+01
13	.11273E+01	.10692E+01	.13772E+01	.12483E+01
14	.11820E+01	.10257E+01	.16631E+01	.12554E+01
15	.12490E+01	.99254E+00	.17183E+01	.12622E+01
16	.13194E+01	.97145E+00	.14802E+01	.12695E+01
17	.13956E+01	.95295E+00	.11800E+01	.12785E+01
18	.15023E+01	.94849E+00	.10818E+01	.12643E+01
19	.16038E+01	.94709E+00	.10682E+01	.12679E+01
20	.17052E+01	.94499E+00	.10658E+01	.12779E+01
21	.18079E+01	.94176E+00	.10671E+01	.12951E+01
22	.19941E+01	.93222E+00	.10753E+01	.13473E+01
23	.19941E+01	.10001E+01	.10000E+01	.10000E+01
24	.82500E+01	.10001E+01	.10000E+01	.10000E+01

PT.	ALP(1)	ALP(2)	ALP(3)	ALP(4)
1	.11000E-09	.11000E-09	.11353E-09	.10000E+01
2	.11000E-09	.11000E-09	.15343E-09	.10000E+01
3	.11000E-09	.11000E-09	.13175E-08	.10000E+01
4	.11016E-09	.11000E-09	.35177E-07	.10000E+01
5	.11671E-09	.11000E-09	.93569E-06	.10000E+01
6	.36806E-09	.11011E-09	.21702E-04	.99991E+00
7	.90935E-08	.11327E-09	.41574E-03	.99833E+00
8	.25565E-06	.18863E-09	.56903E-02	.97712E+00
9	.43251E-05	.12752E-08	.38491E-01	.84542E+00
10	.48009E-04	.11778E-07	.13375E+00	.46248E+00
11	.19326E-03	.72556E-07	.17892E+00	.27374E+00
12	.55911E-03	.18134E-05	.20614E+00	.14340E+00
13	.12743E-02	.49932E-04	.21689E+00	.65675E-01
14	.20499E-02	.87296E-03	.21146E+00	.22949E-01
15	.10425E-02	.61256E-02	.15255E+00	.35832E-02
16	.15203E-03	.31695E-02	.72325E-01	.44560E-03
17	.99197E-05	.42284E-03	.17624E-01	.45960E-04
18	.31768E-06	.25394E-04	.32602E-02	.26649E-05
19	.28359E-07	.32632E-05	.12109E-02	.25785E-06
20	.94356E-08	.12869E-05	.57934E-03	.85813E-07
21	.46227E-08	.62972E-06	.28608E-03	.41584E-07
22	.11000E-09	.11000E-09	.11000E-09	.11000E-09
23	.11000E-09	.11000E-09	.11000E-09	.11000E-09

TH	EM	RHO	GAM	XMASS
0.	.20056E+01	.83388E+00	.14266E+01	0.
.16342E-01	.20141E+01	.82644E+00	.14268E+01	.70014E-02
.33855E-01	.20385E+01	.80488E+00	.14274E+01	.27995E-01
.52889E-01	.20762E+01	.77267E+00	.14283E+01	.62945E-01
.72650E-01	.21220E+01	.73499E+00	.14294E+01	.11187E+00
.90830E-01	.21676E+01	.69849E+00	.14306E+01	.17491E+00
.10434E+00	.21977E+01	.66900E+00	.14312E+01	.25241E+00
.11324E+00	.21550E+01	.63590E+00	.14282E+01	.33871E+00
.12140E+00	.19102E+01	.54301E+00	.14132E+01	.40979E+00
.11988E+00	.15118E+01	.45483E+00	.13935E+01	.47180E+00
.10812E+00	.13206E+01	.41393E+00	.13778E+01	.50410E+00
.94879E-01	.12310E+01	.40895E+00	.13345E+01	.53412E+00
.85926E-01	.12176E+01	.44002E+00	.12950E+01	.56346E+00
.81656E-01	.12509E+01	.49906E+00	.12736E+01	.59433E+00
.80118E-01	.13404E+01	.61396E+00	.12709E+01	.63984E+00
.81569E-01	.14883E+01	.80428E+00	.12862E+01	.70253E+00
.87625E-01	.16634E+01	.10685E+01	.13070E+01	.79521E+00
.93582E-01	.17340E+01	.11658E+01	.13146E+01	.95877E+00
.93206E-01	.17430E+01	.11858E+01	.13158E+01	.11337E+01
.93062E-01	.17413E+01	.11984E+01	.13160E+01	.13220E+01
.94949E-01	.17345E+01	.12133E+01	.13160E+01	.15263E+01
.10422E+00	.17108E+01	.12529E+01	.13156E+01	.19332E+01
.56521E-12	.19000E+01	.99992E+00	.13200E+01	.19332E+01
0.	.19000E+01	.99992E+00	.13200E+01	.33975E+02

ALP(5)	ALP(6)	ALP(7)	PHI	W
.11000E-09	.11000E-09	-.53926E-09	-.29833E+12	.20160E+01
.11000E-09	.11000E-09	-.41810E-09	.82356E+12	.20160E+01
.11002E-09	.11000E-09	.31156E-08	.74400E+10	.20160E+01
.11110E-09	.11000E-09	.10585E-06	.24956E+09	.20160E+01
.16051E-09	.11005E-09	.28361E-05	.93505E+07	.20160E+01
.22714E-08	.11128E-09	.65739E-04	.40333E+06	.20162E+01
.84238E-07	.14003E-09	.12578E-02	.21041E+05	.20191E+01
.26809E-05	.64085E-09	.17187E-01	.15074E+04	.20593E+01
.50438E-04	.50984E-08	.11603E+00	.19391E+03	.23494E+01
.60521E-03	.25731E-07	.40312E+00	.31338E+02	.39796E+01
.24574E-02	.51979E-06	.54470E+00	.14277E+02	.60450E+01
.65669E-02	.22442E-04	.64332E+00	.68762E+01	.94076E+01
.12758E-01	.47011E-03	.70288E+00	.34433E+01	.14006E+02
.22337E-01	.40222E-02	.73631E+00	.17631E+01	.19074E+02
.69350E-01	.10785E-01	.75656E+00	.78345E+00	.24114E+02
.15522E+00	.39004E-02	.76479E+00	.30871E+00	.27053E+02
.21394E+00	.50789E-03	.76745E+00	.70723E-01	.28451E+02
.22874E+00	.50370E-04	.76792E+00	.12720E-01	.28779E+02
.23080E+00	.12445E-04	.76797E+00	.46822E-02	.28823E+02
.23143E+00	.56240E-05	.76799E+00	.22380E-02	.28836E+02
.23172E+00	.27697E-05	.76799E+00	.11050E-02	.28842E+02
.23200E+00	.11000E-09	.76800E+00	.81900E-08	.28848E+02
.23200E+00	.11000E-09	.76800E+00	.81900E-08	.28848E+02
.23200E+00	.11000E-09	.76800E+00	.81900E-08	.28848E+02

KOUNT= 500

X = .66346E+01

SHOCK TYPE 3 BETA = .630E+00

VISCOSITY = .17496E-03 (LB*SEC/FT**2)

PT.	Y	Q	T	P
1	0.	.16763E+01	.12940E+00	.11649E+01
2	.23219E+00	.16777E+01	.12999E+00	.11603E+01
3	.46919E+00	.16597E+01	.13456E+00	.11476E+01
4	.72282E+00	.16160E+01	.16209E+00	.11269E+01
5	.96187E+00	.14475E+01	.25910E+00	.10976E+01
6	.11063E+01	.13139E+01	.39317E+00	.10850E+01
7	.11959E+01	.12363E+01	.52408E+00	.10788E+01
8	.13173E+01	.11466E+01	.77279E+00	.10729E+01
9	.14076E+01	.10955E+01	.10055E+01	.10698E+01
10	.15353E+01	.10454E+01	.13483E+01	.10676E+01
11	.17051E+01	.10082E+01	.13183E+01	.10701E+01
12	.18287E+01	.99714E+00	.11295E+01	.10521E+01
13	.21587E+01	.99911E+00	.10105E+01	.10043E+01
14	.25848E+01	.10002E+01	.10003E+01	.99302E+00
15	.30135E+01	.99864E+00	.10010E+01	.10022E+01
16	.34454E+01	.99451E+00	.10064E+01	.10225E+01
17	.39723E+01	.98804E+00	.10137E+01	.10557E+01
18	.44955E+01	.97997E+00	.10227E+01	.10967E+01
19	.50075E+01	.96949E+00	.10344E+01	.11506E+01
20	.59174E+01	.94327E+00	.10634E+01	.12880E+01
21	.59174E+01	.10001E+01	.10000E+01	.10000E+01
22	.82500E+01	.10001E+01	.10000E+01	.10000E+01

PT.	ALP(1)	ALP(2)	ALP(3)	ALP(4)
1	.69424E-06	.18468E-09	.22718E-03	.99907E+00
2	.30035E-05	.45433E-09	.81657E-03	.99664E+00
3	.24876E-04	.31283E-08	.52330E-02	.97831E+00
4	.19358E-03	.23481E-07	.29485E-01	.87648E+00
5	.91019E-03	.83942E-07	.96683E-01	.58884E+00
6	.18505E-02	.78039E-07	.14289E+00	.38524E+00
7	.26118E-02	.34760E-06	.16912E+00	.27388E+00
8	.38366E-02	.61792E-05	.19658E+00	.15182E+00
9	.48409E-02	.86322E-04	.21338E+00	.85077E-01
10	.56570E-02	.23471E-02	.21968E+00	.24280E-01
11	.19185E-02	.15036E-01	.10788E+00	.21859E-02
12	.33364E-03	.81582E-02	.32929E-01	.21706E-03
13	.13792E-04	.42260E-03	.19158E-02	.94351E-05
14	.30578E-06	.11055E-04	.60363E-04	.22668E-06
15	.55190E-08	.22035E-06	.14542E-05	.44601E-08
16	.18005E-09	.32147E-08	.24479E-07	.17070E-09
17	.11062E-09	.13989E-09	.42459E-09	.11060E-09
18	.11004E-09	.11204E-09	.15277E-09	.11005E-09
19	.11002E-09	.11094E-09	.13061E-09	.11002E-09
20	.11000E-09	.11000E-09	.11000E-09	.11000E-09
21	.11000E-09	.11000E-09	.11000E-09	.11000E-09
22	.11000E-09	.11000E-09	.11000E-09	.11000E-09

TH	EM	RHO	GAM	XMASS
0.	.22476E+01	.62961E+00	.14325E+01	0.
.20237E-02	.22471E+01	.62567E+00	.14323E+01	.28373E-01
.38683E-02	.22183E+01	.60809E+00	.14303E+01	.11419E+00
.66100E-02	.20636E+01	.54776E+00	.14204E+01	.25783E+00
.82240E-02	.17547E+01	.47438E+00	.14014E+01	.41608E+00
.68292E-02	.15465E+01	.43958E+00	.13935E+01	.51047E+00
.52904E-02	.14397E+01	.42587E+00	.13870E+01	.56743E+00
.34106E-02	.13511E+01	.42555E+00	.13612E+01	.64481E+00
.31890E-02	.13302E+01	.44079E+00	.13316E+01	.70451E+00
.58137E-02	.13489E+01	.48384E+00	.12970E+01	.79738E+00
.15803E-01	.15517E+01	.69021E+00	.12975E+01	.96271E+00
.21484E-01	.17510E+01	.89229E+00	.13106E+01	.11357E+01
.19506E-01	.18867E+01	.99153E+00	.13192E+01	.17542E+01
.13846E-01	.18998E+01	.99253E+00	.13199E+01	.27562E+01
.14484E-01	.18964E+01	.10011E+01	.13199E+01	.39517E+01
.19204E-01	.18838E+01	.10160E+01	.13196E+01	.53534E+01
.27682E-01	.18651E+01	.10414E+01	.13191E+01	.73456E+01
.38375E-01	.18420E+01	.10723E+01	.13186E+01	.96477E+01
.52638E-01	.18124E+01	.11122E+01	.13179E+01	.12235E+02
.88073E-01	.17403E+01	.12110E+01	.13163E+01	.17738E+02
.43743E-12	.19000E+01	.99992E+00	.13200E+01	.17738E+02
0.	.19000E+01	.99992E+00	.13200E+01	.34262E+02

ALP(5)	ALP(6)	ALP(7)	PHI	W
.45928E-05	.13984E-09	.69694E-03	.37929E+05	.20177E+01
.19203E-04	.23304E-09	.25193E-02	.10473E+05	.20222E+01
.15240E-03	.10164E-08	.16276E-01	.15928E+04	.20569E+01
.11351E-02	.53673E-08	.92705E-01	.25142E+03	.22731E+01
.52153E-02	.92133E-08	.30836E+00	.51560E+02	.32308E+01
.94741E-02	.29234E-07	.46054E+00	.23157E+02	.45957E+01
.11939E-01	.51247E-06	.54344E+00	.14371E+02	.59684E+01
.14013E-01	.20472E-04	.63372E+00	.74084E+01	.88428E+01
.13799E-01	.27951E-03	.68254E+00	.44041E+01	.11952E+02
.16338E-01	.42565E-02	.72744E+00	.19871E+01	.17629E+02
.10943E+00	.74650E-02	.75608E+00	.57954E+00	.24532E+02
.19125E+00	.20289E-02	.76508E+00	.15002E+00	.27637E+02
.22979E+00	.10429E-03	.76775E+00	.83619E-02	.28782E+02
.23194E+00	.28996E-05	.76799E+00	.25579E-03	.28846E+02
.23200E+00	.62268E-07	.76800E+00	.60491E-05	.28848E+02
.23200E+00	.10504E-08	.76800E+00	.10810E-06	.28848E+02
.23200E+00	.12020E-09	.76800E+00	.94598E-08	.28848E+02
.23200E+00	.11098E-09	.76800E+00	.83590E-08	.28848E+02
.23200E+00	.11046E-09	.76800E+00	.82713E-08	.28848E+02
.23200E+00	.11000E-09	.76800E+00	.81900E-08	.28848E+02
.23200E+00	.11000E-09	.76800E+00	.81900E-08	.28848E+02
.23200E+00	.11000E-09	.76800E+00	.81900E-08	.28848E+02

VISCOSITY = .21410E-03 (LB*SEC/FT**2)

PT.	Y	Q	T	P
1	0.	.15821E+01	.13664E+00	.10197E+01
2	.25032E+00	.16696E+01	.14223E+00	.10209E+01
3	.51344E+00	.16243E+01	.15340E+00	.10230E+01
4	.80340E+00	.15231E+01	.21477E+00	.10242E+01
5	.10703E+01	.13919E+01	.32198E+00	.10232E+01
6	.12208E+01	.13176E+01	.41909E+00	.10229E+01
7	.13103E+01	.12759E+01	.49461E+00	.10229E+01
8	.14294E+01	.12244E+01	.61499E+00	.10228E+01
9	.15197E+01	.11893E+01	.73355E+00	.10229E+01
10	.16554E+01	.11434E+01	.93947E+00	.10232E+01
11	.18779E+01	.10961E+01	.13519E+01	.10247E+01
12	.20783E+01	.10496E+01	.16701E+01	.10299E+01
13	.25131E+01	.10009E+01	.11989E+01	.10360E+01
14	.29206E+01	.99569E+00	.10277E+01	.10212E+01
15	.33073E+01	.99864E+00	.10058E+01	.10154E+01
16	.37071E+01	.99849E+00	.10020E+01	.10074E+01
17	.42134E+01	.10021E+01	.99776E+00	.99174E+00
18	.47367E+01	.10069E+01	.99210E+00	.96982E+00
19	.52710E+01	.10123E+01	.98577E+00	.94508E+00
20	.58196E+01	.10171E+01	.98019E+00	.92334E+00
21	.63778E+01	.10193E+01	.97752E+00	.91284E+00
22	.69396E+01	.10176E+01	.97956E+00	.92027E+00
23	.75016E+01	.10121E+01	.98594E+00	.94473E+00
24	.80553E+01	.10054E+01	.99384E+00	.97559E+00
25	.83750E+01	.10027E+01	.99701E+00	.98960E+00
26	.86495E+01	.10028E+01	.99698E+00	.10000E+01

PT.	ALP(1)	ALP(2)	ALP(3)	ALP(4)
1	.90024E-04	.61369E-08	.11497E-01	.95149E+00
2	.13371E-03	.78568E-08	.16475E-01	.93039E+00
3	.28720E-03	.11943E-07	.34252E-01	.85506E+00
4	.57928E-03	.11524E-07	.72738E-01	.69260E+00
5	.10562E-02	.40190E-08	.12120E+00	.49133E+00
6	.14560E-02	.65868E-08	.14875E+00	.38023E+00
7	.17395E-02	.25365E-07	.16433E+00	.31877E+00
8	.21684E-02	.16071E-06	.18372E+00	.24390E+00
9	.25277E-02	.74318E-06	.19706E+00	.19363E+00
10	.31100E-02	.74737E-05	.21456E+00	.12914E+00
11	.39813E-02	.26461E-03	.23361E+00	.52345E-01
12	.32385E-02	.52781E-02	.21704E+00	.12020E-01
13	.37956E-03	.90467E-02	.45877E-01	.30160E-03
14	.20243E-04	.16994E-02	.53838E-02	.14394E-04
15	.20882E-05	.14538E-03	.47210E-03	.16634E-05
16	.15075E-06	.86511E-05	.29321E-04	.11828E-06
17	.62143E-08	.31719E-06	.11143E-05	.48268E-08
18	.30655E-09	.98906E-08	.35677E-07	.26212E-09
19	.11539E-09	.37245E-09	.11185E-08	.11416E-09
20	.11013E-09	.11660E-09	.14524E-09	.11010E-09
21	.11000E-09	.11034E-09	.11611E-09	.11000E-09
22	.11000E-09	.11011E-09	.11280E-09	.11000E-09
23	.11000E-09	.11009E-09	.11135E-09	.11000E-09
24	.11000E-09	.11001E-09	.11067E-09	.11000E-09
25	.11000E-09	.11000E-09	.11019E-09	.11000E-09
26	.11000E-09	.11000E-09	.11007E-09	.11000E-09

TH	EM	RHO	GAM	XMASS
0.	.22442E+01	.54478E+00	.14296E+01	0.
.32695E-02	.22074E+01	.53477E+00	.14274E+01	.28341E-01
.72718E-02	.20870E+01	.50351E+00	.14201E+01	.11429E+00
.11961E-01	.18666E+01	.45441E+00	.14071E+01	.25842E+00
.15438E-01	.16362E+01	.41455E+00	.13965E+01	.41707E+00
.16643E-01	.15100E+01	.39273E+00	.13923E+01	.51143E+00
.17076E-01	.14440E+01	.38199E+00	.13888E+01	.56828E+00
.17409E-01	.13725E+01	.37210E+00	.13789E+01	.64522E+00
.17578E-01	.13316E+01	.36795E+00	.13663E+01	.70466E+00
.17900E-01	.12928E+01	.36820E+00	.13408E+01	.79717E+00
.19153E-01	.12740E+01	.38427E+00	.12981E+01	.96186E+00
.22911E-01	.13203E+01	.43576E+00	.12737E+01	.11352E+01
.37241E-01	.16973E+01	.81639E+00	.13054E+01	.17711E+01
.44481E-01	.18595E+01	.98569E+00	.13182E+01	.27658E+01
.45521E-01	.18856E+01	.10072E+01	.13198E+01	.39597E+01
.46660E-01	.18930E+01	.10035E+01	.13201E+01	.53643E+01
.49652E-01	.19037E+01	.99217E+00	.13203E+01	.73636E+01
.54461E-01	.19181E+01	.97577E+00	.13207E+01	.96750E+01
.59664E-01	.19342E+01	.95698E+00	.13211E+01	.12279E+02
.62965E-01	.19486E+01	.94029E+00	.13215E+01	.15201E+02
.61570E-01	.19554E+01	.93214E+00	.13216E+01	.18441E+02
.53967E-01	.19501E+01	.93777E+00	.13215E+01	.21997E+02
.42116E-01	.19337E+01	.95646E+00	.13211E+01	.25892E+02
.31336E-01	.19136E+01	.97986E+00	.13206E+01	.30096E+02
.27553E-01	.19056E+01	.99077E+00	.13204E+01	.32693E+02
.25906E-01	.19058E+01	.10012E+01	.13204E+01	.35025E+02

ALP(5)	ALP(6)	ALP(7)	PHI	W
.53610E-03	.12753E-08	.36389E-01	.69323E+03	.21097E+01
.80091E-03	.15236E-08	.52202E-01	.47274E+03	.21531E+01
.17608E-02	.19651E-08	.10864E+00	.20922E+03	.23242E+01
.37820E-02	.11279E-08	.23030E+00	.80520E+02	.28050E+01
.57327E-02	.53614E-09	.38068E+00	.35119E+02	.37699E+01
.61616E-02	.41513E-08	.46340E+00	.22703E+02	.46502E+01
.61172E-02	.43033E-07	.50905E+00	.17579E+02	.53382E+01
.57051E-02	.67725E-06	.56451E+00	.12467E+02	.65079E+01
.51548E-02	.51759E-05	.60162E+00	.95717E+01	.76259E+01
.40548E-02	.64558E-04	.64906E+00	.63512E+01	.97701E+01
.29518E-02	.14620E-02	.70538E+00	.30858E+01	.14651E+02
.13609E-01	.11144E-01	.73767E+00	.14365E+01	.20423E+02
.17793E+00	.28708E-02	.76356E+00	.20647E+00	.27303E+02
.22501E+00	.35240E-03	.76752E+00	.22578E-01	.28668E+02
.23139E+00	.34673E-04	.76795E+00	.20108E-02	.28831E+02
.23197E+00	.21423E-05	.76799E+00	.12609E-03	.28847E+02
.23200E+00	.79257E-07	.76800E+00	.48155E-05	.28848E+02
.23200E+00	.25761E-08	.76800E+00	.16164E-06	.28848E+02
.23200E+00	.17750E-09	.76800E+00	.12525E-07	.28848E+02
.23200E+00	.11178E-09	.76800E+00	.83365E-08	.28848E+02
.23200E+00	.11014E-09	.76800E+00	.82139E-08	.28848E+02
.23200E+00	.11009E-09	.76800E+00	.82009E-08	.28848E+02
.23200E+00	.11001E-09	.76800E+00	.81952E-08	.28848E+02
.23200E+00	.11000E-09	.76800E+00	.81926E-08	.28848E+02
.23200E+00	.11000E-09	.76800E+00	.81907E-08	.28848E+02
.23200E+00	.11000E-09	.76800E+00	.81903E-08	.28848E+02

VISCOSITY = .21410E-03 (LB*SEC/FT**2)

PT.	Y	Q	T	P
1	0.	.16756E+01	.16132E+00	.78316E+00
2	.29265E+00	.16599E+01	.16998E+00	.78545E+00
3	.60041E+00	.16107E+01	.19984E+00	.79182E+00
4	.93378E+00	.15255E+01	.26357E+00	.80038E+00
5	.12280E+01	.14354E+01	.36019E+00	.80845E+00
6	.13868E+01	.13860E+01	.43583E+00	.81244E+00
7	.14785E+01	.13579E+01	.48850E+00	.81462E+00
8	.15983E+01	.13221E+01	.56788E+00	.81732E+00
9	.16877E+01	.12962E+01	.63537E+00	.81924E+00
10	.18209E+01	.12594E+01	.74901E+00	.82201E+00
11	.20393E+01	.12041E+01	.95585E+00	.82668E+00
12	.22434E+01	.11593E+01	.11809E+01	.83151E+00
13	.27923E+01	.10742E+01	.15176E+01	.85998E+00
14	.33121E+01	.10409E+01	.10986E+01	.85802E+00
15	.37192E+01	.10315E+01	.99326E+00	.86623E+00
16	.41149E+01	.10279E+01	.97574E+00	.87905E+00
17	.45987E+01	.10242E+01	.97683E+00	.89590E+00
18	.51146E+01	.10204E+01	.98038E+00	.91132E+00
19	.56257E+01	.10180E+01	.98379E+00	.92506E+00
20	.61439E+01	.10152E+01	.98700E+00	.93782E+00
21	.66656E+01	.10126E+01	.99011E+00	.95011E+00
22	.71888E+01	.10099E+01	.99320E+00	.96232E+00
23	.77146E+01	.10073E+01	.99629E+00	.97461E+00
24	.82442E+01	.10049E+01	.99917E+00	.98682E+00
25	.87541E+01	.10033E+01	.10003E+01	.99397E+00
26	.88224E+01	.10035E+01	.10009E+01	.10000E+01

PT.	ALP(1)	ALP(2)	ALP(3)	ALP(4)
1	.31555E-03	.87945E-08	.41102E-01	.82706E+00
2	.35679E-03	.84702E-08	.47578E-01	.80018E+00
3	.46919E-03	.87404E-08	.67818E-01	.71662E+00
4	.70192E-03	.35373E-08	.10246E+00	.57542E+00
5	.10673E-02	.14370E-08	.13848E+00	.43124E+00
6	.13385E-02	.42138E-08	.15764E+00	.35532E+00
7	.15209E-02	.12366E-07	.16425E+00	.31335E+00
8	.17888E-02	.49530E-07	.18140E+00	.26130E+00
9	.20127E-02	.15132E-06	.19052E+00	.22500E+00
10	.23869E-02	.78392E-06	.20266E+00	.17531E+00
11	.31137E-02	.10409E-04	.21942E+00	.10641E+00
12	.38573E-02	.14383E-03	.22656E+00	.56830E-01
13	.17592E-02	.13319E-01	.14745E+00	.29217E-02
14	.22276E-03	.67443E-02	.31869E-01	.13823E-03
15	.21668E-04	.17434E-02	.60309E-02	.12130E-04
16	.31072E-05	.24331E-03	.82712E-03	.20174E-05
17	.23499E-06	.20765E-04	.69511E-04	.19513E-06
18	.21049E-07	.14233E-05	.47846E-05	.14817E-07
19	.13973E-08	.83685E-07	.25170E-06	.10354E-08
20	.17792E-09	.43651E-08	.14505E-07	.15992E-09
21	.11317E-09	.30230E-09	.75972E-09	.11237E-09
22	.11013E-09	.11791E-09	.13990E-09	.11010E-09
23	.11000E-09	.11037E-09	.11255E-09	.11000E-09
24	.11000E-09	.11003E-09	.11076E-09	.11000E-09
25	.11000E-09	.11001E-09	.11040E-09	.11000E-09

TH	EM	RHO	GAM	XMASS
0.	.21992E+01	.40233E+00	.14206E+01	0.
-.25026E-02	.21560E+01	.39447E+00	.14180E+01	.28454E-01
-.50350E-02	.20320E+01	.37321E+00	.14106E+01	.11475E+00
-.79705E-02	.18508E+01	.34648E+00	.14009E+01	.25919E+00
-.10851E-01	.16856E+01	.32638E+00	.13944E+01	.41772E+00
-.12412E-01	.16013E+01	.31673E+00	.13913E+01	.51190E+00
-.13317E-01	.15574E+01	.31239E+00	.13886E+01	.56864E+00
-.14521E-01	.15082E+01	.30880E+00	.13829E+01	.64533E+00
-.15409E-01	.14781E+01	.30780E+00	.13763E+01	.70460E+00
-.16699E-01	.14446E+01	.30954E+00	.13631E+01	.79675E+00
-.18497E-01	.14194E+01	.32197E+00	.13350E+01	.96060E+00
-.19239E-01	.14298E+01	.34776E+00	.13097E+01	.11334E+01
-.10152E-01	.15263E+01	.46739E+00	.12824E+01	.17588E+01
.39287E-03	.18565E+01	.75160E+00	.13118E+01	.27777E+01
.11496E-02	.19582E+01	.86466E+00	.13202E+01	.39762E+01
-.13143E-03	.19727E+01	.89843E+00	.13217E+01	.53831E+01
-.11481E-02	.19654E+01	.91541E+00	.13217E+01	.73872E+01
-.97324E-03	.19559E+01	.92788E+00	.13214E+01	.97055E+01
-.50668E-04	.19470E+01	.93860E+00	.13212E+01	.12317E+02
.11128E-02	.19387E+01	.94844E+00	.13210E+01	.15242E+02
.21632E-02	.19307E+01	.95787E+00	.13208E+01	.18471E+02
.29172E-02	.19228E+01	.96715E+00	.13206E+01	.21999E+02
.33228E-02	.19149E+01	.97647E+00	.13204E+01	.25850E+02
.33889E-02	.19077E+01	.98586E+00	.13203E+01	.30010E+02
.33090E-02	.19048E+01	.99184E+00	.13202E+01	.32596E+02
.31709E-02	.19035E+01	.99733E+00	.13202E+01	.34922E+02

ALP(5)	ALP(6)	ALP(7)	PHI	W
.19646E-02	.13811E-08	.12955E+00	.16980E+03	.23950E+01
.22182E-02	.12662E-08	.14967E+00	.14235E+03	.24672E+01
.29248E-02	.78670E-09	.21216E+00	.90263E+02	.27221E+01
.37768E-02	.26490E-09	.31764E+00	.48859E+02	.32974E+01
.41342E-02	.37800E-09	.42508E+00	.27809E+02	.42024E+01
.41748E-02	.42927E-08	.48152E+00	.20514E+02	.49104E+01
.41862E-02	.24301E-07	.51269E+00	.17174E+02	.54139E+01
.42182E-02	.18620E-06	.55129E+00	.13561E+02	.62008E+01
.42867E-02	.82157E-06	.57818E+00	.11329E+02	.68989E+01
.44938E-02	.58546E-05	.61492E+00	.85947E+01	.81512E+01
.52518E-02	.83131E-04	.66572E+00	.53098E+01	.10872E+02
.76892E-02	.64391E-03	.70227E+00	.32390E+01	.14274E+02
.71432E-01	.11667E-01	.75145E+00	.76681E+00	.23836E+02
.19447E+00	.15705E-02	.76498E+00	.13842E+00	.27811E+02
.22439E+00	.30935E-03	.76745E+00	.24948E-01	.28654E+02
.23097E+00	.48253E-04	.76790E+00	.34481E-02	.28821E+02
.23192E+00	.43070E-05	.76799E+00	.29196E-03	.28845E+02
.23199E+00	.30666E-06	.76800E+00	.20214E-04	.28847E+02
.23200E+00	.18640E-07	.76800E+00	.12023E-05	.28848E+02
.23200E+00	.10785E-08	.76800E+00	.69438E-07	.28848E+02
.23200E+00	.15485E-09	.76800E+00	.11003E-07	.28848E+02
.23200E+00	.11193E-09	.76800E+00	.83166E-08	.28848E+02
.23200E+00	.11009E-09	.76800E+00	.82002E-08	.28848E+02
.23200E+00	.11001E-09	.76800E+00	.81929E-08	.28848E+02
.23200E+00	.11000E-09	.76800E+00	.81915E-08	.28848E+02
.23200E+00	.11000E-09	.76800E+00	.81912E-08	.28848E+02

VISCOSITY = .21410E-03 (LB*SEC/FT**2)

PT.	Y	Q	T	P
1	0.	.15496E+01	.20199E+00	.10703E+01
2	.28012E+00	.15327E+01	.21237E+00	.10695E+01
3	.57579E+00	.14814E+01	.24710E+00	.10657E+01
4	.89684E+00	.13965E+01	.31677E+00	.10607E+01
5	.11803E+01	.13093E+01	.41657E+00	.10563E+01
6	.13331E+01	.12620E+01	.49061E+00	.10543E+01
7	.14213E+01	.12354E+01	.54072E+00	.10533E+01
8	.15364E+01	.12018E+01	.61473E+00	.10520E+01
9	.16223E+01	.11780E+01	.67567E+00	.10511E+01
10	.17508E+01	.11446E+01	.78016E+00	.10498E+01
11	.19635E+01	.10962E+01	.97996E+00	.10483E+01
12	.21668E+01	.10569E+01	.11973E+01	.10473E+01
13	.27593E+01	.99943E+00	.18372E+01	.10537E+01
14	.33182E+01	.99611E+00	.12585E+01	.10312E+01
15	.37184E+01	.99947E+00	.10607E+01	.10097E+01
16	.40955E+01	.10027E+01	.10113E+01	.99325E+00
17	.45695E+01	.10061E+01	.99576E+00	.97799E+00
18	.50633E+01	.10086E+01	.99495E+00	.96756E+00
19	.55685E+01	.10098E+01	.99339E+00	.96229E+00
20	.60849E+01	.10100E+01	.99319E+00	.96169E+00
21	.66072E+01	.10092E+01	.99405E+00	.96550E+00
22	.71326E+01	.10078E+01	.99566E+00	.97203E+00
23	.76613E+01	.10060E+01	.99773E+00	.98045E+00
24	.81917E+01	.10043E+01	.99976E+00	.98981E+00
25	.85630E+01	.10035E+01	.10004E+01	.99529E+00
26	.87725E+01	.10038E+01	.10004E+01	.10000E+01

PT.	ALP(1)	ALP(2)	ALP(3)	ALP(4)
1	.39906E-03	.73339E-08	.57403E-01	.75991E+00
2	.41839E-03	.64793E-08	.63619E-01	.73448E+00
3	.47899E-03	.37789E-08	.82637E-01	.65705E+00
4	.68730E-03	.87190E-09	.11371E+00	.53157E+00
5	.99116E-03	.14487E-08	.14477E+00	.40732E+00
6	.12093E-02	.73842E-08	.16112E+00	.34220E+00
7	.13537E-02	.19610E-07	.17020E+00	.30613E+00
8	.15636E-02	.65611E-07	.18158E+00	.26119E+00
9	.17369E-02	.16124E-06	.18964E+00	.22957E+00
10	.20231E-02	.60176E-06	.20096E+00	.18571E+00
11	.25639E-02	.52733E-05	.21755E+00	.12287E+00
12	.30912E-02	.52538E-04	.22962E+00	.74877E-01
13	.18595E-02	.74902E-02	.19760E+00	.61424E-02
14	.30415E-03	.85388E-02	.51914E-01	.26883E-03
15	.44295E-04	.31967E-02	.12251E-01	.23405E-04
16	.81407E-05	.52365E-03	.21986E-02	.45325E-05
17	.92466E-06	.71784E-04	.24464E-03	.56500E-06
18	.87332E-07	.65400E-05	.22033E-04	.56734E-07
19	.70815E-08	.50078E-06	.16824E-05	.48362E-08
20	.59003E-09	.33133E-07	.11115E-06	.44511E-09
21	.13915E-09	.20406E-08	.66205E-08	.13080E-09
22	.11158E-09	.21165E-09	.45646E-09	.11115E-09
23	.11006E-09	.11490E-09	.12802E-09	.11006E-09
24	.11000E-09	.11028E-09	.11164E-09	.11000E-09
25	.11000E-09	.11004E-09	.11058E-09	.11000E-09
26	.11000E-09	.11001E-09	.11042E-09	.11000E-09

TH	EM	RHO	GAM	XMASS
0.	.18946E+01	.47376E+00	.14104E+01	0.
.24458E-02	.18569E+01	.46412E+00	.14083E+01	.28356E-01
.46158E-02	.17512E+01	.43862E+00	.14030E+01	.11447E+00
.60560E-02	.16013E+01	.40898E+00	.13968E+01	.25878E+00
.64129E-02	.14648E+01	.38652E+00	.13924E+01	.41733E+00
.62332E-02	.13963E+01	.37640E+00	.13891E+01	.51153E+00
.60242E-02	.13608E+01	.37184E+00	.13858E+01	.56827E+00
.56785E-02	.13205E+01	.36778E+00	.13795E+01	.64497E+00
.53942E-02	.12951E+01	.36618E+00	.13729E+01	.70424E+00
.49986E-02	.12649E+01	.36639E+00	.13610E+01	.79638E+00
.46625E-02	.12364E+01	.37385E+00	.13353E+01	.96016E+00
.50407E-02	.12314E+01	.38969E+00	.13107E+01	.11329E+01
.12290E-01	.12575E+01	.44407E+00	.12655E+01	.17574E+01
.17455E-01	.16502E+01	.77297E+00	.13010E+01	.27876E+01
.14193E-01	.18327E+01	.93773E+00	.13156E+01	.39894E+01
.73657E-02	.18905E+01	.97796E+00	.13194E+01	.54019E+01
-.15641E-02	.19103E+01	.97715E+00	.13203E+01	.74186E+01
-.92232E-02	.19186E+01	.97068E+00	.13205E+01	.97517E+01
-.14971E-01	.19224E+01	.96694E+00	.13206E+01	.12377E+02
-.18893E-01	.19229E+01	.96673E+00	.13206E+01	.15315E+02
-.21249E-01	.19206E+01	.96952E+00	.13206E+01	.18553E+02
-.22381E-01	.19165E+01	.97449E+00	.13205E+01	.22087E+02
-.22611E-01	.19113E+01	.98090E+00	.13204E+01	.25940E+02
-.22191E-01	.19062E+01	.98826E+00	.13202E+01	.30100E+02
-.21707E-01	.19046E+01	.99309E+00	.13202E+01	.32685E+02
-.21136E-01	.19045E+01	.99774E+00	.13202E+01	.35010E+02

ALP(5)	ALP(6)	ALP(7)	PHI	W
.25091E-02	.98030E-09	.17978E+00	.11271E+03	.25839E+01
.26832E-02	.75228E-09	.19880E+00	.98634E+02	.26634E+01
.31518E-02	.25614E-09	.25669E+00	.68617E+02	.29391E+01
.37002E-02	.10127E-09	.35033E+00	.41073E+02	.35299E+01
.40392E-02	.12500E-08	.44288E+00	.25296E+02	.44053E+01
.41692E-02	.15205E-07	.49131E+00	.19410E+02	.50620E+01
.42162E-02	.63282E-07	.51810E+00	.16626E+02	.55168E+01
.42309E-02	.34645E-06	.55144E+00	.13540E+02	.62110E+01
.41859E-02	.11601E-05	.57486E+00	.11585E+02	.68131E+01
.40011E-02	.60174E-05	.60730E+00	.91278E+01	.78689E+01
.33342E-02	.62230E-04	.65361E+00	.60415E+01	.10100E+02
.30351E-02	.42160E-03	.68890E+00	.39670E+01	.12875E+02
.26051E-01	.16044E-01	.74440E+00	.10998E+01	.22375E+02
.17260E+00	.33458E-02	.76303E+00	.22715E+00	.27264E+02
.21700E+00	.60379E-03	.76688E+00	.50634E-01	.28468E+02
.22927E+00	.11280E-03	.76778E+00	.91030E-02	.28777E+02
.23170E+00	.13503E-04	.76797E+00	.10175E-02	.28840E+02
.23197E+00	.12931E-05	.76800E+00	.92117E-04	.28847E+02
.23200E+00	.10335E-06	.76800E+00	.70747E-05	.28848E+02
.23200E+00	.71504E-08	.76800E+00	.47656E-06	.28848E+02
.23200E+00	.53290E-09	.76800E+00	.35745E-07	.28848E+02
.23200E+00	.13282E-09	.76800E+00	.96597E-08	.28848E+02
.23200E+00	.11112E-09	.76800E+00	.82660E-08	.28848E+02
.23200E+00	.11006E-09	.76800E+00	.81967E-08	.28848E+02
.23200E+00	.11001E-09	.76800E+00	.81923E-08	.28848E+02
.23200E+00	.11000E-09	.76800E+00	.81916E-08	.28848E+02

Case II: An axially symmetric Mach 1.2 hydrogen jet is injected into a Mach 3 airstream as depicted in Figure (24). The initial conditions for this case are tabulated under KOUNT = 0. The pressures of the jet and airstream are balanced and the effect of the initial airside boundary layer and base region are analyzed by assuming chemical equilibrium to prevail in this region as described for Case I. The combustion generates a mild compression field, the pressure increasing to about 1.25 of the initial value in a distance of about 2 slot heights. The axial pressure distribution for several streamlines is depicted in Figure (25). Note that initially the pressure is highest in the combustion zone, but when the compression waves generated by combustion reflect off the centerbody, the pressure becomes highest at the lower boundary. The overall flow field properties are tabulated. . The flow becomes subsonic at the axial station X = 2. Details of the sonic line and streamlines in this region are depicted in Figure (26). Note that the combustion zone is in the vicinity y = 6, hence the streamlines are closer together in this region so that the mixing can be accurately calculated.

In the region $2 < X < 2 \cdot 2$, the upper subsonic streamline ($\psi = .591$) is specified by the coefficients A thru D specified by the values of y, θ, θ_s and θ_{ss} at the station KOUNT = 365, while downstream of X = 2.2 a higher order term is added to turn this streamline down and hence re-accelerate the flow. The Ferri-Kleinstein viscosity model is also employed for this case, the viscosity varying from $.6643 * 10^{-4}$ lb.sec/ft^2 at X = 0 to $.8252 * 10^{-3}$ at X = 2.4. The flow field properties are tabulated at the following stations:

KOUNT	= 0;	x = 0
	= 100;	= .731
	= 200;	= 1.32
	= 300;	= 1.77
	= 365;	= 1.96
	= 370;	= 2.03
	= 375;	= 2.09
	= 385;	= 2.20
	= 390;	= 2.25
	= 390;	= 2.30
	= 400;	= 2.35
	= 405;	= 2.4

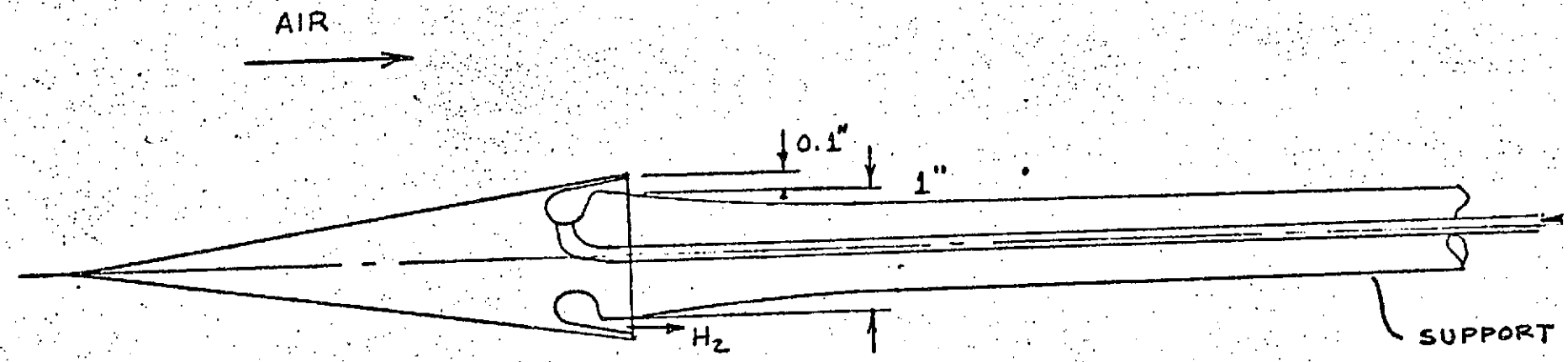

FIGURE 24.

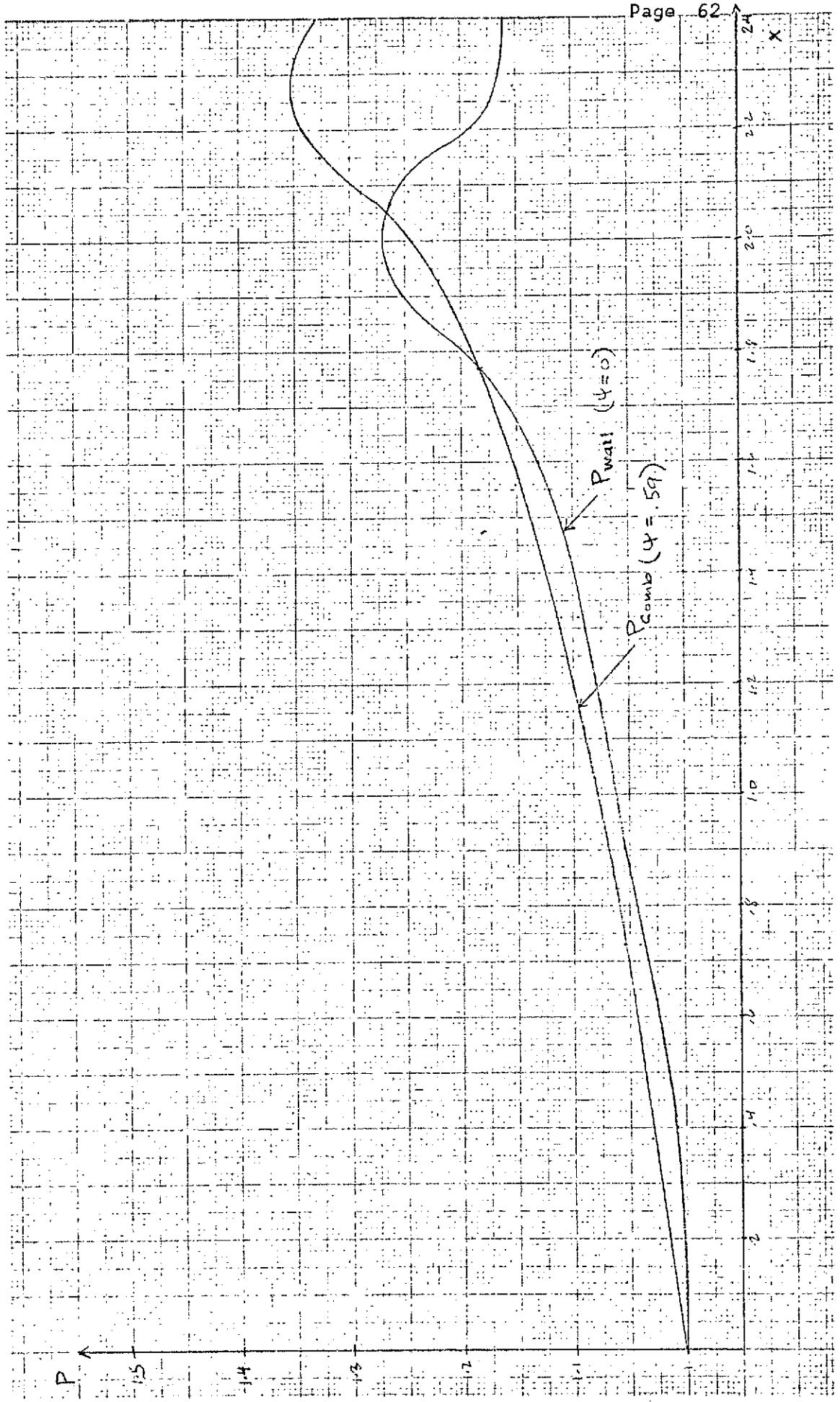

FIGURE 25.

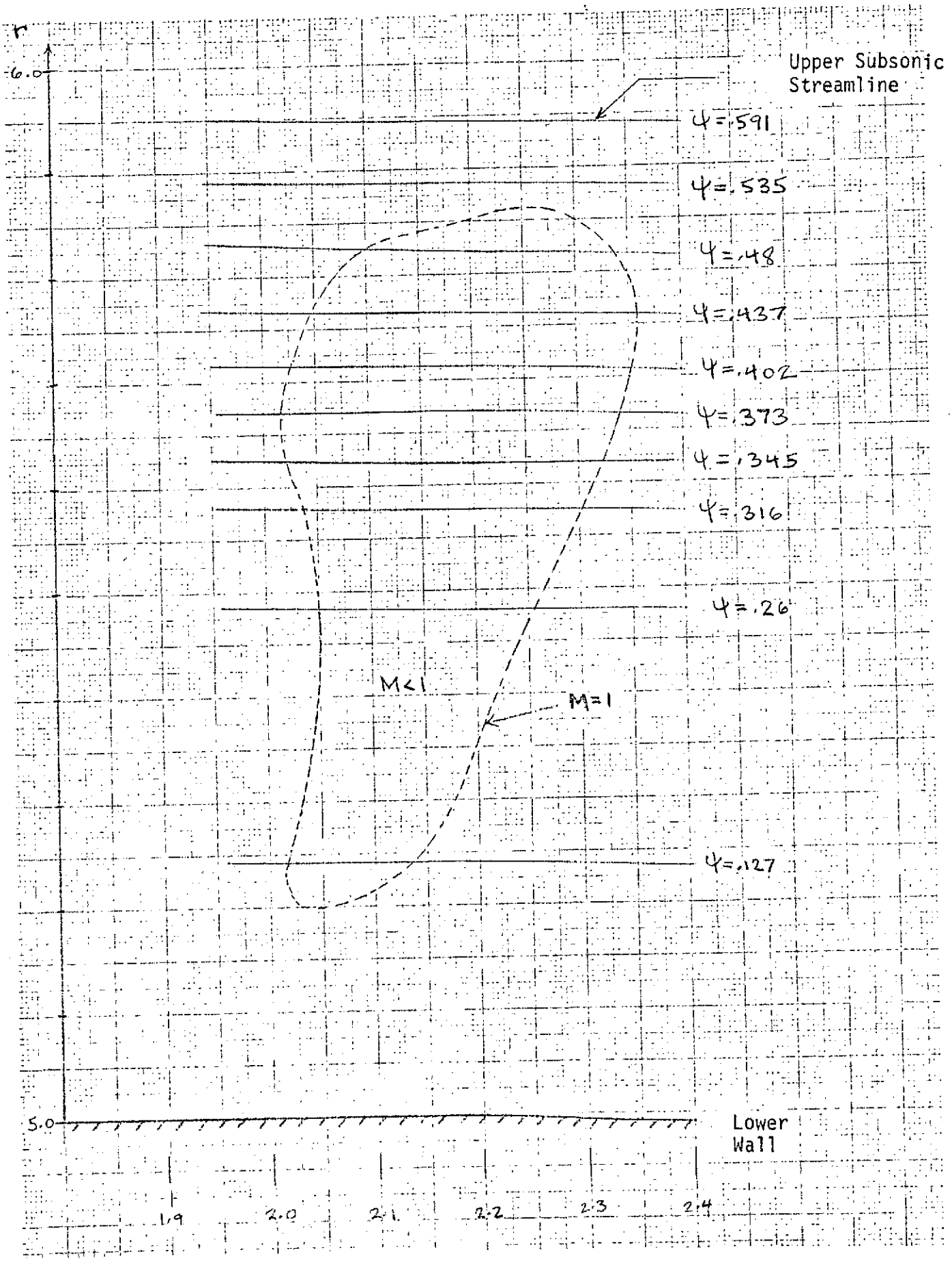
r
6.0
5.0
Upper Subsonic Streamline
ψ=.591
ψ=.535
ψ=.48
ψ=.437
ψ=.402
ψ=.373
ψ=.345
ψ=.316
ψ=.26
ψ=.127
M<1
M=1
Lower Wall
1.9
2.0
2.1
2.2
2.3
2.4

FIGURE 26.

The flow field is calculated by "viscous-characteristics" from station KOUNT = 0 to KOUNT = 365, while the subsonic routine is used to calculate the flow between KOUNT = 365 and 405, below streamline 11. The flow downstream of KOUNT = 405, is calculable by "viscous-characteristics" provided that the lower wall continues slope downward, hence, accelerating the flow . Note that the sonic line does not reach the wall since at station KOUNT=365, the wall is turned down hence accelerating the streamtubes in the vicinity of the wall. The wall pressure (as depicted in Figure 25) in the subsonic region continuously decreases as the wall turns down, consistent with the flow being supersonic adjacent to the wall. Hence, the neccesity of providing a variable pressure in the subsonic region, employing the normal momentum equation is quite evident. A constant pressure scheme certainly would not provide the details of the flow field as obtained in this analysis.

CASE II.

PROGRAM VIS-CHAR
WITH
EMBEDDED SUBSONIC FLOW
SHOCK WAVES
AND FINITE RATE H2-AIR CHEMISTRY

TYPE OF FLOW IS AXISYMMETRIC
CHEMISTRY IS FINITE RATE
JET OR NOZZLE RADIUS (RTH) = .83500E-01 FT.

REFERENCE CONDITIONS

MACH NO. (FMINF) = .30000E+01
VELOCITY (UIN) = .49127E+04 FT/SEC
TEMPERATURE (TIN) = .63000E+03 DEGREES K
PRESSURE (PRES) = .21160E+04 LB/FT**2
DENSITY (RHOINF) = .10618E-02 SLUGS/FT**3
FROZEN SPECIFIC HEAT RATIO (GAMINF) = .13710E+01
MOLECULAR WEIGHT (WINF) = .28850E+02
REYNOLDS NUMBER (RE) = .66800E+06
PRANDTL NUMBER (PR) = .10000E+01
LEWIS NUMBER (XLE) = .10000E+01

OUTPUT HEADINGS

X - X/RTH
Y - Y/RTH
Q - VELOCITY/UIN
T - TEMPERATURE/TIN
P - PRESSURE/PRES
TH - FLOW DEFLECTION (RADIANS)
EM - MACH NUMBER
GAM - SPECIFIC HEAT
XMASS - NON-DIMENSIONAL MASS FLOW
PHI - EQUIVALENCE RATIO
W - MOLECULAR WEIGHT

MASS FRACTIONS
ALP(1) - H
ALP(2) - O
ALP(3) - H2O
ALP(4) - H2
ALP(5) - O2
ALP(6) - OH
ALP(7) - N2

TH	EM	RHO	GAM	XMASS
0.	.12000E+01	.59879E-01	.13927E+01	0.
0.	.12000E+01	.59879E-01	.13927E+01	.12640E+00
0.	.12000E+01	.59879E-01	.13927E+01	.25896E+00
0.	.12000E+01	.59879E-01	.13927E+01	.31372E+00
0.	.12000E+01	.59879E-01	.13927E+01	.34146E+00
0.	.12000E+01	.59879E-01	.13927E+01	.36945E+00
0.	.12000E+01	.59879E-01	.13927E+01	.39769E+00
0.	.13200E+01	.10079E+00	.13608E+01	.43203E+00
0.	.13200E+01	.16659E+00	.12664E+01	.47743E+00
0.	.14000E+01	.18448E+00	.12514E+01	.53091E+00
0.	.13800E+01	.17880E+00	.12496E+01	.58678E+00
0.	.14200E+01	.18944E+00	.12497E+01	.64390E+00
0.	.15600E+01	.22921E+00	.12521E+01	.70937E+00
0.	.16800E+01	.27033E+00	.12644E+01	.78797E+00
0.	.22400E+01	.49255E+00	.13120E+01	.90928E+00
0.	.30000E+01	.99992E+00	.13710E+01	.11428E+01

ALP(5)	ALP(6)	ALP(7)	PHI	W
.11000E-09	.11000E-09	-.55000E-09	-.26620E+12	.20160E+01
.11000E-09	.11000E-09	-.55000E-09	-.26620E+12	.20160E+01
.11000E-09	.11000E-09	-.55000E-09	-.26620E+12	.20160E+01
.11000E-09	.11000E-09	-.55000E-09	-.26620E+12	.20160E+01
.11000E-09	.11000E-09	-.55000E-09	-.26620E+12	.20160E+01
.11000E-09	.11000E-09	-.55000E-09	-.26620E+12	.20160E+01
.11000E-09	.11000E-09	-.55000E-09	-.26620E+12	.20160E+01
.11000E-09	.11000E-09	.48830E+00	.19763E+02	.50306E+01
.11000E-09	.40000E-03	.71710E+00	.24759E+01	.16918E+02
.15000E-03	.30000E-02	.73737E+00	.15032E+01	.21076E+02
.60000E-02	.14000E-01	.74660E+00	.11941E+01	.22490E+02
.16200E-01	.16100E-01	.75190E+00	.99661E+00	.23664E+02
.40000E-01	.70000E-02	.75610E+00	.78386E+00	.25261E+02
.87000E-01	.30000E-02	.75800E+00	.59968E+00	.26048E+02
.18400E+00	.11000E-09	.76420E+00	.19993E+00	.27852E+02
.23200E+00	.11000E-09	.76800E+00	.81900E-08	.28848E+02

KOUNT= 0

X = -0.

VISCOSITY = .66431E-04 (LB*SEC/FT**2)

PT.	Y	Q	T	P
1	.50000E+01	.16475E+01	.11670E+01	.10000E+01
2	.52500E+01	.16475E+01	.11670E+01	.10000E+01
3	.55000E+01	.16475E+01	.11670E+01	.10000E+01
4	.56000E+01	.16475E+01	.11670E+01	.10000E+01
5	.56500E+01	.16475E+01	.11670E+01	.10000E+01
6	.57000E+01	.16475E+01	.11670E+01	.10000E+01
7	.57500E+01	.16475E+01	.11670E+01	.10000E+01
8	.58000E+01	.13308E+01	.17300E+01	.10000E+01
9	.58500E+01	.10361E+01	.35200E+01	.10000E+01
10	.59000E+01	.10381E+01	.39600E+01	.10000E+01
11	.59500E+01	.10386E+01	.43600E+01	.10000E+01
12	.60000E+01	.10363E+01	.43300E+01	.10000E+01
13	.60500E+01	.10380E+01	.38200E+01	.10000E+01
14	.61000E+01	.10344E+01	.33400E+01	.10000E+01
15	.61500E+01	.10408E+01	.19600E+01	.10000E+01
16	.62000E+01	.10001E+01	.10000E+01	.10000E+01

PT.	ALP(1)	ALP(2)	ALP(3)	ALP(4)
1	.11000E-09	.11000E-09	.11000E-09	.10000E+01
2	.11000E-09	.11000E-09	.11000E-09	.10000E+01
3	.11000E-09	.11000E-09	.11000E-09	.10000E+01
4	.11000E-09	.11000E-09	.11000E-09	.10000E+01
5	.11000E-09	.11000E-09	.11000E-09	.10000E+01
6	.11000E-09	.11000E-09	.11000E-09	.10000E+01
7	.11000E-09	.11000E-09	.11000E-09	.10000E+01
8	.11000E-09	.11000E-09	.16450E+00	.34720E+00
9	.20000E-03	.11000E-09	.24230E+00	.40000E-01
10	.40000E-03	.80000E-04	.24500E+00	.14000E-01
11	.80000E-03	.20000E-02	.22360E+00	.70000E-02
12	.50000E-03	.29000E-02	.20900E+00	.34000E-02
13	.11000E-09	.90000E-03	.19600E+00	.11000E-09
14	.11000E-09	.11000E-09	.15200E+00	.11000E-09
15	.11000E-09	.11000E-09	.51800E-01	.11000E-09
16	.11000E-09	.11000E-09	.11000E-09	.11000E-09

KOUNT= 100

X = .73128E+00

VISCOSITY = .28642E-03 (LB*SEC/FT**2)

PT.	Y	Q	T	P
1	.50000E+01	.16135E+01	.11805E+01	.10415E+01
2	.52483E+01	.16143E+01	.11802E+01	.10406E+01
3	.54965E+01	.16161E+01	.11796E+01	.10383E+01
4	.55959E+01	.16144E+01	.11825E+01	.10367E+01
5	.56453E+01	.16013E+01	.11966E+01	.10356E+01
6	.56941E+01	.15614E+01	.12376E+01	.10341E+01
7	.57415E+01	.14726E+01	.13389E+01	.10343E+01
8	.57925E+01	.13199E+01	.15933E+01	.10485E+01
9	.58475E+01	.11345E+01	.23143E+01	.10520E+01
10	.59056E+01	.10408E+01	.34824E+01	.10601E+01
11	.59579E+01	.10198E+01	.41269E+01	.10533E+01
12	.60059E+01	.10184E+01	.41675E+01	.10497E+01
13	.60539E+01	.10202E+01	.42089E+01	.10517E+01
14	.61011E+01	.10213E+01	.31912E+01	.10508E+01
15	.61500E+01	.10221E+01	.21046E+01	.10663E+01
16	.62006E+01	.99542E+00	.10617E+01	.10657E+01
17	.67005E+01	.99955E+00	.10028E+01	.10067E+01
18	.72001E+01	.10000E+01	.10012E+01	.10011E+01
19	.77000E+01	.10001E+01	.10010E+01	.10001E+01
20	.82000E+01	.10001E+01	.10009E+01	.10000E+01

PT.	ALP(1)	ALP(2)	ALP(3)	ALP(4)
1	.11135E-09	.11000E-09	.10094E-07	.10000E+01
2	.22142E-09	.11006E-09	.69996E-06	.10000E+01
3	.15219E-07	.11551E-09	.77656E-04	.99969E+00
4	.47629E-06	.26989E-09	.19082E-02	.99243E+00
5	.30591E-05	.81250E-09	.93594E-02	.96268E+00
6	.13055E-04	.15540E-08	.29920E-01	.88135E+00
7	.44911E-04	.17690E-09	.72542E-01	.71233E+00
8	.13830E-03	.86219E-08	.14098E+00	.44081E+00
9	.38439E-03	.64430E-06	.20721E+00	.17685E+00
10	.87163E-03	.41976E-04	.23695E+00	.48842E-01
11	.10850E-02	.10022E-02	.23349E+00	.13126E-01
12	.59267E-03	.28392E-02	.21283E+00	.40173E-02
13	.15590E-03	.23098E-02	.13441E+00	.97011E-03
14	.22702E-04	.91237E-03	.13620E+00	.15442E-03
15	.22141E-05	.15993E-03	.59353E-01	.13915E-04
16	.12892E-07	.12170E-05	.11544E-02	.10304E-06
17	.11321E-09	.47379E-09	.51039E-04	.14022E-09
18	.11000E-09	.11009E-09	.50447E-04	.11001E-09
19	.11000E-09	.11000E-09	.50447E-04	.11000E-09
20	.11000E-09	.11000E-09	.50447E-04	.11000E-09

TH	EM	RHO	GAM	XMASS
0.	.11686E+01	.61650E-01	.13924E+01	0.
-.35941E-02	.11693E+01	.61612E-01	.13924E+01	.12654E+00
-.64488E-02	.11711E+01	.61526E-01	.13924E+01	.25922E+00
-.79781E-02	.11724E+01	.61689E-01	.13923E+01	.31400E+00
-.95426E-02	.11724E+01	.62612E-01	.13918E+01	.34176E+00
-.12427E-01	.11710E+01	.65523E-01	.13901E+01	.36979E+00
-.16151E-01	.11703E+01	.73345E-01	.13853E+01	.39828E+00
-.15004E-01	.11882E+01	.94435E-01	.13712E+01	.43248E+00
-.95061E-02	.12154E+01	.12959E+00	.13243E+01	.47599E+00
.10797E-02	.12811E+01	.16557E+00	.12720E+01	.53049E+00
.85817E-02	.13441E+01	.18585E+00	.12534E+01	.58658E+00
.81635E-02	.14127E+01	.20480E+00	.12510E+01	.64377E+00
.51814E-02	.15254E+01	.23922E+00	.12555E+01	.70922E+00
.90512E-03	.16989E+01	.29921E+00	.12696E+01	.78814E+00
.19596E-03	.21215E+01	.48635E+00	.13061E+01	.90837E+00
.23302E-02	.29016E+01	.10029E+01	.13664E+01	.11417E+01
.17395E-02	.29945E+01	.10038E+01	.13708E+01	.43691E+01
.24823E-03	.29981E+01	.99972E+00	.13709E+01	.78465E+01
.38064E-04	.29987E+01	.99904E+00	.13709E+01	.11569E+02
.70068E-05	.29987E+01	.99895E+00	.13709E+01	.15540E+02

ALP(5)	ALP(6)	ALP(7)	PHI	W
.11010E-09	.11013E-09	.29071E-07	.89398E+09	.20160E+01
.12000E-09	.11934E-09	.20756E-05	.12712E+08	.20160E+01
.17449E-08	.11229E-08	.23035E-03	.11453E+06	.20166E+01
.64019E-07	.23628E-07	.56594E-02	.46287E+04	.20301E+01
.51288E-06	.98543E-07	.27755E-01	.91649E+03	.20871E+01
.26877E-05	.19852E-06	.88714E-01	.26316E+03	.22623E+01
.11534E-04	.28217E-07	.21507E+00	.88396E+02	.27391E+01
.44862E-04	.98360E-06	.41803E+00	.28829E+02	.41401E+01
.15881E-03	.41337E-04	.61535E+00	.85960E+01	.82248E+01
.45379E-03	.11123E-02	.71173E+00	.28324E+01	.15691E+02
.28409E-02	.79213E-02	.74053E+00	.14590E+01	.21009E+02
.16400E-01	.12961E-01	.75036E+00	.10313E+01	.23457E+02
.47572E-01	.92009E-02	.75538E+00	.78242E+00	.24995E+02
.10030E+00	.33998E-02	.75901E+00	.54414E+00	.26216E+02
.17625E+00	.35321E-03	.76386E+00	.23057E+00	.27693E+02
.23092E+00	.37132E-05	.76792E+00	.44418E-02	.28825E+02
.23195E+00	.15324E-08	.76800E+00	.19587E-03	.28847E+02
.23195E+00	.11040E-09	.76800E+00	.19359E-03	.28847E+02
.23195E+00	.11000E-09	.76800E+00	.19359E-03	.28847E+02
.23195E+00	.11000E-09	.76800E+00	.19359E-03	.28847E+02

KOUNT= 200

X = .13203E+01

VISCOSITY = .46714E-03 (LB*SEC/FT**2)

PT.	Y	Q	T	P
1	.50000E+01	.15712E+01	.11969E+01	.10936E+01
2	.52462E+01	.15704E+01	.11972E+01	.10945E+01
3	.54923E+01	.15665E+01	.12008E+01	.10943E+01
4	.55900E+01	.15400E+01	.12256E+01	.10922E+01
5	.56351E+01	.15026E+01	.12516E+01	.10923E+01
6	.56852E+01	.14459E+01	.13233E+01	.10929E+01
7	.57309E+01	.13714E+01	.14232E+01	.10948E+01
8	.57819E+01	.12721E+01	.16110E+01	.10997E+01
9	.58394E+01	.11560E+01	.19930E+01	.11075E+01
10	.59022E+01	.10641E+01	.27378E+01	.11111E+01
11	.59586E+01	.10188E+01	.35247E+01	.11130E+01
12	.60078E+01	.10034E+01	.38916E+01	.11138E+01
13	.60549E+01	.10017E+01	.39921E+01	.11125E+01
14	.61000E+01	.10044E+01	.31142E+01	.11114E+01
15	.61464E+01	.10053E+01	.22144E+01	.11183E+01
16	.62007E+01	.99120E+00	.11559E+01	.11255E+01
17	.67024E+01	.99941E+00	.10068E+01	.10208E+01
18	.72005E+01	.99965E+00	.10024E+01	.10055E+01
19	.77001E+01	.10000E+01	.10012E+01	.10011E+01
20	.82000E+01	.10001E+01	.10010E+01	.10002E+01
21	.87000E+01	.10001E+01	.10009E+01	.10000E+01

PT.	ALP(1)	ALP(2)	ALP(3)	ALP(4)
1	.14300E-08	.11019E-09	.32430E-05	.99999E+00
2	.34286E-07	.11333E-09	.69379E-04	.99972E+00
3	.14140E-05	.18765E-09	.22482E-02	.99108E+00
4	.13784E-04	.40696E-09	.16097E-01	.93614E+00
5	.37184E-04	.42838E-09	.33907E-01	.86544E+00
6	.82532E-04	.33766E-09	.60163E-01	.76104E+00
7	.16337E-03	.17610E-09	.93758E-01	.62747E+00
8	.31786E-03	.32259E-08	.13697E+00	.45510E+00
9	.60766E-03	.11674E-06	.18387E+00	.26686E+00
10	.10960E-02	.55425E-05	.22029E+00	.11734E+00
11	.15900E-02	.15489E-03	.23515E+00	.43126E-01
12	.19335E-02	.19192E-02	.22671E+00	.12386E-01
13	.63489E-03	.50410E-02	.18447E+00	.26192E-02
14	.15849E-03	.35348E-02	.12927E+00	.50217E-03
15	.28232E-04	.11565E-02	.64833E-01	.67220E-04
16	.43027E-06	.20969E-04	.32165E-02	.13579E-05
17	.38463E-09	.16146E-07	.55056E-04	.12407E-08
18	.11015E-09	.11994E-09	.50452E-04	.11074E-09
19	.11000E-09	.11001E-09	.50447E-04	.11000E-09
20	.11000E-09	.11000E-09	.50447E-04	.11000E-09
21	.11000E-09	.11000E-09	.50447E-04	.11000E-09

TH	EM	RHO	GAM	XMASS
0.	.11303E+01	.63851E-01	.13920E+01	0.
-.43718E-02	.11297E+01	.63901E-01	.13920E+01	.12656E+00
-.93286E-02	.11300E+01	.64207E-01	.13918E+01	.25931E+00
-.12676E-01	.11289E+01	.66151E-01	.13908E+01	.31412E+00
-.15111E-01	.11256E+01	.69011E-01	.13893E+01	.34190E+00
-.17768E-01	.11217E+01	.73917E-01	.13864E+01	.36996E+00
-.19971E-01	.11194E+01	.81652E-01	.13813E+01	.39849E+00
-.20552E-01	.11236E+01	.95327E-01	.13709E+01	.43271E+00
-.17649E-01	.11465E+01	.11835E+00	.13450E+01	.47589E+00
-.12076E-01	.11942E+01	.14788E+00	.13040E+01	.53011E+00
-.64904E-02	.12661E+01	.17716E+00	.12718E+01	.58661E+00
-.27436E-02	.13592E+01	.20840E+00	.12583E+01	.64399E+00
-.19266E-02	.14924E+01	.25224E+00	.12602E+01	.70949E+00
-.38918E-02	.16826E+01	.32195E+00	.12735E+01	.78845E+00
-.48002E-02	.20307E+01	.48168E+00	.13024E+01	.90822E+00
-.19634E-02	.27741E+01	.97143E+00	.13595E+01	.11419E+01
.48989E-02	.29855E+01	.10139E+01	.13705E+01	.43385E+01
.12919E-02	.29953E+01	.10030E+01	.13708E+01	.78262E+01
.27212E-03	.29980E+01	.99978E+00	.13709E+01	.11553E+02
.49548E-04	.29986E+01	.99908E+00	.13709E+01	.15525E+02
.13153E-04	.29987E+01	.99895E+00	.13709E+01	.19747E+02

ALP(5)	ALP(6)	ALP(7)	PHI	W
.40340E-09	.13765E-09	.96165E-05	.27440E+07	.20160E+01
.86450E-08	.59636E-09	.20575E-03	.12822E+06	.20165E+01
.40027E-06	.11457E-07	.66674E-02	.39235E+04	.20326E+01
.44102E-05	.45238E-07	.47746E-01	.51840E+03	.21415E+01
.12790E-04	.53879E-07	.10061E+00	.22802E+03	.22999E+01
.29709E-04	.51127E-07	.17866E+00	.11343E+03	.25820E+01
.60252E-04	.43216E-07	.27855E+00	.60470E+02	.30623E+01
.11746E-03	.55397E-06	.40749E+00	.30501E+02	.40288E+01
.21618E-03	.10845E-04	.54844E+00	.13874E+02	.61439E+01
.36786E-03	.22202E-03	.66067E+00	.57269E+01	.10512E+02
.95832E-03	.22233E-02	.71680E+00	.26273E+01	.16187E+02
.66041E-02	.95903E-02	.74125E+00	.14237E+01	.21006E+02
.41818E-01	.12718E-01	.75269E+00	.86669E+00	.24151E+02
.10159E+00	.61533E-02	.75879E+00	.53951E+00	.26026E+02
.16934E+00	.10061E-02	.76356E+00	.25600E+00	.27518E+02
.22896E+00	.25377E-04	.76778E+00	.12460E-01	.28782E+02
.23195E+00	.25985E-07	.76800E+00	.21138E-03	.28847E+02
.23195E+00	.12990E-09	.76800E+00	.19361E-03	.28847E+02
.23195E+00	.11001E-09	.76800E+00	.19359E-03	.28847E+02
.23195E+00	.11000E-09	.76800E+00	.19359E-03	.28847E+02
.23195E+00	.11000E-09	.76800E+00	.19359E-03	.28847E+02

KOUNT= 300

X = .17676E+01

VISCOSITY = .60750E-03 (LB*SEC/FT**2)

PT.	Y	Q	T	P
1	.50000E+01	.15044E+01	.12218E+01	.11765E+01
2	.52440E+01	.15042E+01	.12223E+01	.11763E+01
3	.54874E+01	.14942E+01	.12331E+01	.11704E+01
4	.55834E+01	.14474E+01	.12771E+01	.11680E+01
5	.56305E+01	.14067E+01	.13214E+01	.11681E+01
6	.56765E+01	.13552E+01	.13662E+01	.11686E+01
7	.57212E+01	.12956E+01	.14790E+01	.11698E+01
8	.57718E+01	.12215E+01	.16356E+01	.11726E+01
9	.58302E+01	.11365E+01	.19199E+01	.11777E+01
10	.58947E+01	.10578E+01	.24291E+01	.11813E+01
11	.59530E+01	.10111E+01	.30571E+01	.11835E+01
12	.60039E+01	.98988E+00	.35510E+01	.11864E+01
13	.60521E+01	.98311E+00	.36420E+01	.11914E+01
14	.60975E+01	.98481E+00	.31537E+01	.11901E+01
15	.61460E+01	.98869E+00	.23085E+01	.11882E+01
16	.61995E+01	.98586E+00	.12577E+01	.11919E+01
17	.67053E+01	.99725E+00	.10109E+01	.10351E+01
18	.72013E+01	.99916E+00	.10041E+01	.10115E+01
19	.77003E+01	.99984E+00	.10018E+01	.10031E+01
20	.82001E+01	.10000E+01	.10011E+01	.10007E+01
21	.87000E+01	.10001E+01	.10010E+01	.10001E+01
22	.92000E+01	.10001E+01	.10009E+01	.10000E+01

PT.	ALP(1)	ALP(2)	ALP(3)	ALP(4)
1	.30647E-07	.11133E-09	.41620E-04	.99983E+00
2	.42722E-06	.12110E-09	.47404E-03	.99812E+00
3	.93399E-05	.21777E-09	.79274E-02	.96853E+00
4	.50176E-04	.25271E-09	.31014E-01	.87679E+00
5	.99345E-04	.19600E-09	.50356E-01	.79981E+00
6	.17279E-03	.94415E-10	.74449E-01	.70380E+00
7	.28181E-03	.49405E-09	.10196E+00	.59398E+00
8	.46133E-03	.40992E-08	.13569E+00	.45892E+00
9	.76307E-03	.64478E-07	.17359E+00	.30506E+00
10	.12489E-02	.17612E-05	.20832E+00	.16523E+00
11	.18441E-02	.40731E-04	.22382E+00	.77241E-01
12	.23168E-02	.63599E-03	.23391E+00	.29760E-01
13	.17007E-02	.52937E-02	.20583E+00	.71302E-02
14	.55963E-03	.72041E-02	.14049E+00	.13375E-02
15	.12304E-03	.32554E-02	.70563E-01	.18622E-03
16	.31565E-05	.96586E-04	.55505E-02	.55682E-05
17	.33329E-06	.12181E-06	.63773E-04	.75226E-06
18	.11286E-09	.23707E-09	.50470E-04	.11818E-09
19	.11000E-09	.11011E-09	.50447E-04	.11001E-09
20	.11000E-09	.11000E-09	.50447E-04	.11000E-09
21	.11000E-09	.11000E-09	.50447E-04	.11000E-09
22	.11000E-09	.11000E-09	.50447E-04	.11000E-09

TH	EM	RHO	GAM	XMASS
0.	.10715E+01	.67299E-01	.13914E+01	0.
-.54376E-02	.10719E+01	.67363E-01	.13913E+01	.12658E+00
-.12365E-01	.10751E+01	.68299E-01	.13909E+01	.25940E+00
-.16435E-01	.10715E+01	.72047E-01	.13890E+01	.31423E+00
-.18837E-01	.10679E+01	.75658E-01	.13869E+01	.34201E+00
-.21123E-01	.10646E+01	.80877E-01	.13837E+01	.37008E+00
-.22965E-01	.10632E+01	.88037E-01	.13788E+01	.39862E+00
-.24047E-01	.10672E+01	.99373E-01	.13699E+01	.43284E+00
-.23396E-01	.10857E+01	.11763E+00	.13507E+01	.47598E+00
-.20893E-01	.11289E+01	.14397E+00	.13203E+01	.53007E+00
-.17878E-01	.11956E+01	.17299E+00	.12899E+01	.58656E+00
-.14722E-01	.12842E+01	.20549E+00	.12698E+01	.64406E+00
-.10593E-01	.14122E+01	.25175E+00	.12635E+01	.70962E+00
-.71413E-02	.16132E+01	.32976E+00	.12741E+01	.78855E+00
-.54104E-02	.19483E+01	.48590E+00	.12999E+01	.90809E+00
-.25237E-02	.26497E+01	.94369E+00	.13524E+01	.11413E+01
.80628E-02	.29762E+01	.10238E+01	.13702E+01	.43249E+01
.26899E-02	.29915E+01	.10073E+01	.13707E+01	.78214E+01
.73137E-03	.29968E+01	.10012E+01	.13709E+01	.11553E+02
.16819E-03	.29983E+01	.99945E+00	.13709E+01	.15527E+02
.37248E-04	.29987E+01	.99903E+00	.13709E+01	.19749E+02
.90959E-05	.29987E+01	.99895E+00	.13709E+01	.24220E+02

ALP(5)	ALP(6)	ALP(7)	PHI	W
.93859E-08	.30703E-09	.12345E-03	.21372E+06	.20163E+01
.13836E-06	.17822E-08	.14064E-02	.18730E+05	.20195E+01
.32030E-05	.17287E-07	.23529E-01	.10874E+04	.20759E+01
.17827E-04	.28966E-07	.92131E-01	.25221E+03	.22729E+01
.34980E-04	.25242E-07	.14970E+00	.14205E+03	.24693E+01
.60891E-04	.19319E-07	.22152E+00	.84902E+02	.27676E+01
.97116E-04	.91238E-07	.30369E+00	.52671E+02	.32112E+01
.15228E-03	.61465E-06	.40478E+00	.30972E+02	.39987E+01
.23239E-03	.63603E-05	.51925E+00	.16606E+02	.55323E+01
.33720E-03	.86372E-04	.62478E+00	.80332E+01	.85412E+01
.59265E-03	.81172E-03	.69065E+00	.40119E+01	.12892E+02
.24715E-02	.45686E-02	.72633E+00	.21316E+01	.17744E+02
.20767E-01	.13306E-01	.74597E+00	.11575E+01	.22203E+02
.84580E-01	.94026E-02	.75643E+00	.63479E+00	.25211E+02
.16091E+00	.19525E-02	.76291E+00	.28813E+00	.27236E+02
.22667E+00	.64555E-04	.76761E+00	.21743E-01	.28729E+02
.23194E+00	.11497E-06	.76800E+00	.24532E-03	.28846E+02
.23195E+00	.26267E-09	.76800E+00	.19368E-03	.28847E+02
.23195E+00	.11016E-09	.76800E+00	.19359E-03	.28847E+02
.23195E+00	.11000E-09	.76800E+00	.19359E-03	.28847E+02
.23195E+00	.11000E-09	.76800E+00	.19359E-03	.28847E+02
.23195E+00	.11000E-09	.76800E+00	.19359E-03	.28847E+02

KOUNT= 365

X = .19614E+01

VISCOSITY = .67146E-03 (LB*SEC/FT**2)

PT.	Y	Q	T	P
1	.50000E+01	.14325E+01	.12467E+01	.12679E+01
2	.52429E+01	.14365E+01	.12461E+01	.12657E+01
3	.54864E+01	.14414E+01	.12464E+01	.12592E+01
4	.55802E+01	.13533E+01	.13083E+01	.12555E+01
5	.56264E+01	.13452E+01	.13543E+01	.12534E+01
6	.56723E+01	.12988E+01	.14189E+01	.12512E+01
7	.57166E+01	.12465E+01	.15082E+01	.12459E+01
8	.57672E+01	.11327E+01	.16539E+01	.12462E+01
9	.58256E+01	.11096E+01	.18090E+01	.12427E+01
10	.58905E+01	.10406E+01	.23513E+01	.12386E+01
11	.59493E+01	.99434E+00	.29085E+01	.12346E+01
12	.60007E+01	.97826E+00	.34058E+01	.12357E+01
13	.60408E+01	.97203E+00	.36266E+01	.12400E+01
14	.60960E+01	.97420E+00	.32199E+01	.12394E+01
15	.61451E+01	.97665E+00	.23710E+01	.12335E+01
16	.61992E+01	.98321E+00	.13111E+01	.12308E+01
17	.62706E+01	.99732E+00	.10125E+01	.10436E+01
18	.72019E+01	.99961E+00	.10041E+01	.10150E+01
19	.77005E+01	.10005E+01	.10012E+01	.10044E+01
20	.82001E+01	.10007E+01	.10003E+01	.10011E+01
21	.87004E+01	.10008E+01	.10001E+01	.10002E+01
22	.92000E+01	.10008E+01	.10000E+01	.10000E+01

TH	EM	RHO	GAM	XMASS
0.	.10092E+01	.70975E-01	.13907E+01	0.
-.54400E-02	.10136E+01	.71080E-01	.13907E+01	.12677E+00
-.12600E-01	.10257E+01	.72864E-01	.13901E+01	.26075E+00
-.16510E-01	.10239E+01	.77405E-01	.13878E+01	.31643E+00
-.18640E-01	.10216E+01	.81229E-01	.13856E+01	.34468E+00
-.20600E-01	.10199E+01	.86500E-01	.13823E+01	.37319E+00
-.22200E-01	.10202E+01	.93466E-01	.13776E+01	.40215E+00
-.23310E-01	.10258E+01	.10410E+00	.13691E+01	.43680E+00
-.23330E-01	.10452E+01	.12088E+00	.13519E+01	.48032E+00
-.21940E-01	.10888E+01	.14565E+00	.13250E+01	.53463E+00
-.19470E-01	.11548E+01	.17369E+00	.12966E+01	.59118E+00
-.17340E-01	.12406E+01	.20555E+00	.12753E+01	.64867E+00
-.13040E-01	.13606E+01	.24926E+00	.12650E+01	.71422E+00
-.76400E-02	.15592E+01	.32794E+00	.12731E+01	.79316E+00
-.42000E-02	.18977E+01	.48627E+00	.12982E+01	.91265E+00
-.11100E-02	.25871E+01	.93223E+00	.13488E+01	.11453E+01
.99200E-02	.29706E+01	.10288E+01	.13701E+01	.43283E+01
.35000E-02	.29893E+01	.10091E+01	.13707E+01	.78298E+01
.10300E-02	.29960E+01	.10014E+01	.13709E+01	.11564E+02
.26000E-03	.29981E+01	.99895E+00	.13710E+01	.15539E+02
.60000E-04	.29996E+01	.99831E+00	.13710E+01	.19761E+02
.20000E-04	.29988E+01	.99816E+00	.13710E+01	.24232E+02

KOUNT= 370

X = .20282E+01

VISCOSITY = .69346E-03 (LB*SEC/FT**2)

PT.	Y	Q	T	P	EM
1	.50000E+01	.14267E+01	.12480E+01	.12727E+01	.10060E+01
2	.52424E+01	.14165E+01	.12524E+01	.12879E+01	.99905E+00
3	.54841E+01	.14036E+01	.12569E+01	.12912E+01	.10041E+01
4	.55791E+01	.13536E+01	.13221E+01	.12893E+01	.10009E+01
5	.56256E+01	.13157E+01	.13690E+01	.12877E+01	.99833E+00
6	.56711E+01	.12707E+01	.14336E+01	.12857E+01	.99666E+00
7	.57154E+01	.12206E+01	.15224E+01	.12934E+01	.99708E+00
8	.57658E+01	.11603E+01	.16652E+01	.12803E+01	.10031E+01
9	.58242E+01	.10917E+01	.19121E+01	.12760E+01	.10227E+01
10	.58992E+01	.10273E+01	.23355E+01	.12705E+01	.10669E+01
11	.59480E+01	.99478E+00	.29704E+01	.12647E+01	.11335E+01
12	.59995E+01	.97081E+00	.33609E+01	.12603E+01	.12215E+01
13	.60486E+01	.96570E+00	.35171E+01	.12598E+01	.13414E+01
14	.60955E+01	.96374E+00	.32513E+01	.12597E+01	.15375E+01
15	.61468E+01	.97208E+00	.23994E+01	.12527E+01	.18768E+01
16	.61991E+01	.99179E+00	.13314E+01	.12469E+01	.25638E+01
17	.62677E+01	.99704E+00	.10135E+01	.10470E+01	.29684E+01
18	.72022E+01	.99950E+00	.10044E+01	.10164E+01	.29885E+01
19	.77005E+01	.10004E+01	.10013E+01	.10049E+01	.29957E+01
20	.82001E+01	.10007E+01	.10003E+01	.10012E+01	.29980E+01
21	.87006E+01	.10008E+01	.10001E+01	.10003E+01	.29986E+01
22	.92000E+01	.10008E+01	.10000E+01	.10000E+01	.29987E+01

KOUNT= 375

X = .20908E+01

VISCOSITY = .71431E-03 (LB*SEC/FT**2)

PT.	Y	Q	T	P	EM
1	.49997E+01	.14394E+01	.12456E+01	.12531E+01	.10121E+01
2	.52417E+01	.14124E+01	.12548E+01	.12958E+01	.99396E+00
3	.54833E+01	.13995E+01	.12776E+01	.13122E+01	.99002E+00
4	.55782E+01	.13311E+01	.13324E+01	.13142E+01	.98415E+00
5	.56244E+01	.12985E+01	.13808E+01	.13143E+01	.98058E+00
6	.56700E+01	.12479E+01	.14461E+01	.13138E+01	.97808E+00
7	.57143E+01	.11990E+01	.15344E+01	.13127E+01	.97780E+00
8	.57646E+01	.11405E+01	.16750E+01	.13106E+01	.98314E+00
9	.58230E+01	.10744E+01	.19153E+01	.13078E+01	.10018E+01
10	.58985E+01	.10129E+01	.23236E+01	.13033E+01	.10449E+01
11	.59474E+01	.98641E+00	.29604E+01	.12982E+01	.11107E+01
12	.59988E+01	.96620E+00	.33260E+01	.12926E+01	.11980E+01
13	.60481E+01	.96125E+00	.34141E+01	.12883E+01	.13173E+01
14	.60951E+01	.95939E+00	.32571E+01	.12842E+01	.15130E+01
15	.61464E+01	.96774E+00	.24233E+01	.12732E+01	.18551E+01
16	.61987E+01	.98760E+00	.13527E+01	.12636E+01	.25408E+01
17	.62674E+01	.99276E+00	.10145E+01	.10505E+01	.29661E+01
18	.72024E+01	.99939E+00	.10046E+01	.10178E+01	.29876E+01
19	.77006E+01	.10004E+01	.10015E+01	.10054E+01	.29953E+01
20	.82001E+01	.10007E+01	.10004E+01	.10014E+01	.29979E+01
21	.87006E+01	.10008E+01	.10001E+01	.10003E+01	.29986E+01
22	.92000E+01	.10008E+01	.10000E+01	.10000E+01	.29987E+01
23	.97006E+01	.10008E+01	.10000E+01	.10000E+01	.29987E+01

KOUNT= 385

X = .22033E+01

VISCOSITY = .75275E-03 (LB*SEC/FT**2)

PT.	Y	G	T	P
1	.49993E+01	.14411E+01	.12261E+01	.11912E+01
2	.52410E+01	.14403E+01	.12455E+01	.12604E+01
3	.54822E+01	.13328E+01	.12665E+01	.13052E+01
4	.55768E+01	.13163E+01	.13419E+01	.13230E+01
5	.56231E+01	.12765E+01	.13419E+01	.13286E+01
6	.56683E+01	.12297E+01	.14583E+01	.13333E+01
7	.57125E+01	.11794E+01	.15462E+01	.13373E+01
8	.57627E+01	.11214E+01	.16835E+01	.13411E+01
9	.58212E+01	.10563E+01	.19135E+01	.13444E+01
10	.58864E+01	.99560E+00	.22965E+01	.13466E+01
11	.59454E+01	.93574E+00	.27873E+01	.13474E+01
12	.59974E+01	.94301E+00	.32701E+01	.13471E+01
13	.60472E+01	.94166E+00	.36073E+01	.13459E+01
14	.60946E+01	.94986E+00	.33670E+01	.13429E+01
15	.61447E+01	.96608E+00	.29994E+01	.13344E+01
16	.61994E+01	.97575E+00	.13946E+01	.13018E+01
17	.67068E+01	.99417E+00	.10167E+01	.10578E+01
18	.72029E+01	.99917E+00	.10055E+01	.10205E+01
19	.77065E+01	.10063E+01	.10017E+01	.10065E+01
20	.82062E+01	.10007E+01	.10005E+01	.10017E+01
21	.87000E+01	.10004E+01	.10001E+01	.10004E+01
22	.92000E+01	.10006E+01	.10000E+01	.10000E+01
23	.97000E+01	.10006E+01	.10000E+01	.10000E+01

TH	EM	RHO	GAM	XMASS
-.21235E-01	.10593E+01	.67833E-01	.13912E+01	0.
-.13495E-01	.10180E+01	.71014E-01	.13907E+01	.12639E+00
-.10567E-01	.99174E+00	.75910E-01	.13893E+01	.26036E+00
-.10962E-01	.97814E+00	.81891E-01	.13865E+01	.31605E+00
-.11370E-01	.97120E+00	.86321E-01	.13840E+01	.34430E+00
-.11851E-01	.96556E+00	.92049E-01	.13807E+01	.37281E+00
-.12126E-01	.96236E+00	.99285E-01	.13762E+01	.40176E+00
-.12090E-01	.96433E+00	.10999E+00	.13677E+01	.43642E+00
-.11134E-01	.97862E+00	.12657E+00	.13524E+01	.47993E+00
-.98044E-02	.10166E+01	.15129E+00	.13288E+01	.53424E+00
-.11814E-01	.10776E+01	.17989E+00	.13031E+01	.59079E+00
-.32427E-02	.11592E+01	.21153E+00	.12815E+01	.64827E+00
-.58919E-02	.12719E+01	.25236E+00	.12674E+01	.71383E+00
-.91655E-03	.14598E+01	.32685E+00	.12705E+01	.79279E+00
.30180E-02	.18066E+01	.48830E+00	.12947E+01	.91238E+00
.42923E-02	.24946E+01	.92523E+00	.13436E+01	.11446E+01
.13027E-01	.29614E+01	.10385E+01	.13698E+01	.43369E+01
.47614E-02	.29860E+01	.10130E+01	.13706E+01	.78474E+01
.15107E-02	.29947E+01	.10029E+01	.13709E+01	.11586E+02
.41615E-03	.29976E+01	.99943E+00	.13710E+01	.15563E+02
.10372E-03	.29985E+01	.99844E+00	.13710E+01	.19785E+02
.31357E-04	.29987E+01	.99819E+00	.13710E+01	.24256E+02
.34577E-05	.29987E+01	.99816E+00	.13710E+01	.28977E+02

X = .22547E+01

VISCOSITY = .77054E-03 (LB*SEC/FT**2)

PT.	Y	Q	T	P	EM
1	.49974E+01	.14741E+01	.12403E+01	.12059E+01	.10482E+01
2	.52409E+01	.14437E+01	.12445E+01	.12558E+01	.10212E+01
3	.54414E+01	.13999E+01	.12796E+01	.12979E+01	.99902E+00
4	.55763E+01	.13234E+01	.13419E+01	.13125E+01	.98493E+00
5	.56225E+01	.12410E+01	.13922E+01	.13192E+01	.97741E+00
6	.56676E+01	.12336E+01	.14567E+01	.13255E+01	.97100E+00
7	.57117E+01	.11933E+01	.15460E+01	.13314E+01	.96671E+00
8	.57619E+01	.11240E+01	.16816E+01	.13379E+01	.96707E+00
9	.58263E+01	.10576E+01	.18674E+01	.13450E+01	.97878E+00
10	.58857E+01	.99524E+00	.22826E+01	.13524E+01	.10129E+01
11	.59456E+01	.95629E+00	.27561E+01	.13587E+01	.10697E+01
12	.59969E+01	.93858E+00	.32407E+01	.13639E+01	.11468E+01
13	.60463E+01	.93582E+00	.35490E+01	.13675E+01	.12546E+01
14	.60947E+01	.94358E+00	.34058E+01	.13695E+01	.14357E+01
15	.61449E+01	.95916E+00	.28470E+01	.13523E+01	.17814E+01
16	.61997E+01	.97467E+00	.14162E+01	.13242E+01	.24708E+01
17	.67165E+01	.99566E+00	.10178E+01	.10618E+01	.29589E+01
18	.72032E+01	.99906E+00	.10059E+01	.10218E+01	.29851E+01
19	.77004E+01	.10003E+01	.10019E+01	.10070E+01	.29944E+01
20	.82002E+01	.10007E+01	.10005E+01	.10019E+01	.29975E+01
21	.87000E+01	.10004E+01	.10001E+01	.10004E+01	.29985E+01
22	.92000E+01	.10008E+01	.10000E+01	.10001E+01	.29987E+01
23	.97000E+01	.10006E+01	.10000E+01	.10000E+01	.29987E+01

KOUNT= 395

X = .23046E+01

VISCOSITY = .78617E-03 (LB*SEC/FT**2)

PT.	Y	Q	T	P	EM
1	.49954E+01	.14784E+01	.12305E+01	.12038E+01	.10489E+01
2	.52404E+01	.14491E+01	.12393E+01	.12359E+01	.10347E+01
3	.54414E+01	.14054E+01	.12746E+01	.12724E+01	.10154E+01
4	.55757E+01	.13385E+01	.13379E+01	.12887E+01	.10005E+01
5	.56218E+01	.12550E+01	.13886E+01	.12958E+01	.99224E+00
6	.56668E+01	.12466E+01	.14550E+01	.13048E+01	.98487E+00
7	.57108E+01	.11953E+01	.15417E+01	.13129E+01	.97937E+00
8	.57609E+01	.11347E+01	.16755E+01	.13223E+01	.97790E+00
9	.58193E+01	.10683E+01	.18974E+01	.13335E+01	.98680E+00
10	.58848E+01	.10011E+01	.22530E+01	.13465E+01	.10168E+01
11	.59442E+01	.95515E+00	.27299E+01	.13586E+01	.10690E+01
12	.59964E+01	.93340E+00	.32077E+01	.13704E+01	.11408E+01
13	.60466E+01	.93294E+00	.35248E+01	.13809E+01	.12425E+01
14	.60947E+01	.93900E+00	.34412E+01	.13904E+01	.14151E+01
15	.61453E+01	.95454E+00	.25755E+01	.13786E+01	.17571E+01
16	.62001E+01	.97241E+00	.14387E+01	.13484E+01	.24464E+01
17	.67112E+01	.99552E+00	.10191E+01	.10661E+01	.29562E+01
18	.72034E+01	.99895E+00	.10063E+01	.10233E+01	.29842E+01
19	.77004E+01	.10002E+01	.10020E+01	.10075E+01	.29940E+01
20	.82002E+01	.10007E+01	.10006E+01	.10021E+01	.29974E+01
21	.87001E+01	.10005E+01	.10001E+01	.10005E+01	.29984E+01
22	.92000E+01	.10008E+01	.10000E+01	.10001E+01	.29987E+01
23	.97000E+01	.10006E+01	.10000E+01	.10000E+01	.29987E+01

KOUNT= 400

X = .23547E+01

VISCOSITY = .80622E-03 (LB*SEC/FT**2)

PT.	Y	U	T	P	EM	RHO	GAM
1	.49937E+01	.14490E+01	.12270E+01	.11907E+01	.10577E+01	.67788E-01	.13912E+01
2	.52392E+01	.14332E+01	.12308E+01	.12048E+01	.10557E+01	.68860E-01	.13911E+01
3	.54816E+01	.14179E+01	.12364E+01	.12368E+01	.10382E+01	.73517E-01	.13896E+01
4	.55747E+01	.13614E+01	.13307E+01	.12543E+01	.10232E+01	.79685E-01	.13867E+01
5	.56207E+01	.13167E+01	.13416E+01	.12638E+01	.10141E+01	.84166E-01	.13842E+01
6	.56657E+01	.12670E+01	.14479E+01	.12737E+01	.10057E+01	.89876E-01	.13809E+01
7	.57096E+01	.12143E+01	.15339E+01	.12841E+01	.99891E+00	.97007E-01	.13765E+01
8	.57597E+01	.11519E+01	.16559E+01	.12965E+01	.99547E+00	.10747E+00	.13685E+01
9	.59181E+01	.10911E+01	.18436E+01	.13121E+01	.10014E+01	.12363E+00	.13541E+01
10	.58836E+01	.10123E+01	.22401E+01	.13308E+01	.10270E+01	.14797E+00	.13320E+01
11	.59432E+01	.96656E+00	.26963E+01	.13489E+01	.10742E+01	.17665E+00	.13073E+01
12	.59956E+01	.94228E+00	.31703E+01	.13671E+01	.11408E+01	.20890E+00	.12855E+01
13	.60462E+01	.93350E+00	.35633E+01	.13846E+01	.12363E+01	.25000E+00	.12694E+01
14	.60948E+01	.93681E+00	.34715E+01	.14029E+01	.13991E+01	.32190E+00	.12684E+01
15	.61457E+01	.95695E+00	.26144E+01	.14007E+01	.17346E+01	.48823E+00	.12915E+01
16	.62006E+01	.97007E+00	.14622E+01	.13734E+01	.24214E+01	.92968E+00	.13397E+01
17	.67119E+01	.99913E+00	.10204E+01	.10709E+01	.29532E+01	.10475E+01	.13695E+01
18	.72037E+01	.99882E+00	.10067E+01	.10243E+01	.29833E+01	.10161E+01	.13705E+01
19	.77019E+01	.10002E+01	.10022E+01	.10081E+01	.29937E+01	.10040E+01	.13708E+01
20	.82003E+01	.10006E+01	.10006E+01	.10023E+01	.29973E+01	.99984E+00	.13709E+01
21	.87001E+01	.10006E+01	.10002E+01	.10006E+01	.29984E+01	.99856E+00	.13710E+01
22	.92000E+01	.10008E+01	.10000E+01	.10001E+01	.29987E+01	.99822E+00	.13710E+01
23	.97000E+01	.10008E+01	.10000E+01	.10000E+01	.29987E+01	.99816E+00	.13710E+01

KOUNT= 400

X = .23547E+01

VISCOSITY = .80622E-03 (LB*SEC/FT**2)

PT.	ALP(1)	ALP(2)	ALP(3)	ALP(4)	ALP(5)	ALP(6)	ALP(7)
1	.49487E-06	.11561E-09	.38906E-03	.99853E+00	.16863E-06	.99773E-09	.10940E-02
2	.37274E-05	.13255E-09	.23175E-02	.99084E+00	.12815E-05	.39485E-08	.68351E-02
3	.42725E-04	.21582E-09	.20099E-01	.92006E+00	.14519E-04	.22748E-07	.59780E-01
4	.13562E-03	.30273E-09	.47891E-01	.80924E+00	.43880E-04	.60774E-07	.14269E+00
5	.21304E-03	.13239E-09	.66206E-01	.73611E+00	.66595E-04	.63148E-07	.19740E+00
6	.31619E-03	.48347E-09	.86794E-01	.65382E+00	.94369E-04	.13635E-06	.25897E+00
7	.44926E-03	.20418E-08	.10866E+00	.56548E+00	.12617E-03	.53075E-06	.32508E+00
8	.64684E-03	.14704E-07	.13526E+00	.45956E+00	.16555E-03	.26228E-05	.40427E+00
9	.95057E-03	.15518E-06	.16576E+00	.33700E+00	.20923E-03	.15531E-04	.49606E+00
10	.14026E-02	.23224E-05	.19851E+00	.21286E+00	.24584E-03	.99819E-04	.58889E+00
11	.19243E-02	.26527E-04	.21860E+00	.12190E+00	.31611E-03	.51559E-03	.65672E+00
12	.24244E-02	.22774E-03	.23115E+00	.62524E-01	.78600E-03	.20618E-02	.70082E+00
13	.26725E-02	.17593E-02	.22993E+00	.23421E-01	.46690E-02	.72252E-02	.73033E+00
14	.15470E-02	.53537E-02	.16329E+00	.48766E-02	.39360E-01	.13902E-01	.74865E+00
15	.44263E-03	.75482E-02	.92750E-01	.63626E-03	.13353E+00	.43723E-02	.76018E+00
16	.21253E-04	.44260E-03	.10192E-01	.26170E-04	.22190E+00	.13996E-03	.76728E+00
17	.38635E-07	.93494E-06	.69712E-04	.54998E-07	.23189E+00	.45164E-06	.76802E+00
18	.16934E-09	.17436E-06	.50555E-04	.20696E-09	.23200E+00	.12054E-08	.76795E+00
19	.11004E-09	.11247E-09	.50450E-04	.11018E-09	.23200E+00	.11200E-09	.76795E+00
20	.11000E-09	.11000E-09	.50450E-04	.11000E-09	.23200E+00	.11000E-09	.76795E+00
21	.11000E-09	.11000E-09	.50450E-04	.11000E-09	.23200E+00	.11000E-09	.76795E+00
22	.11000E-09	.11000E-09	.50450E-04	.11000E-09	.23200E+00	.11000E-09	.76795E+00
23	.11000E-09	.11000E-09	.50450E-04	.11000E-09	.23200E+00	.11000E-09	.76795E+00

KOUNT= 405

X = .24064E+01

VISCOSITY = .82520E-03 (LB*SEC/FT**2)

PT.	Y	U	T	P
1	.44915E+01	.15046E+01	.12199E+01	.11663E+01
2	.52360E+01	.15167E+01	.12188E+01	.11616E+01
3	.54761E+01	.14679E+01	.12956E+01	.11888E+01
4	.55725E+01	.13928E+01	.13148E+01	.12081E+01
5	.56196E+01	.13466E+01	.13709E+01	.12492E+01
6	.56636E+01	.12953E+01	.14370E+01	.12313E+01
7	.57076E+01	.12405E+01	.15226E+01	.12440E+01
8	.57577E+01	.11762E+01	.16523E+01	.12599E+01
9	.58162E+01	.11022E+01	.18650E+01	.12801E+01
10	.58819E+01	.10290E+01	.22131E+01	.13050E+01
11	.59418E+01	.97464E+00	.26986E+01	.13297E+01
12	.59945E+01	.95024E+00	.31276E+01	.13544E+01
13	.60455E+01	.93761E+00	.35337E+01	.13785E+01
14	.60946E+01	.93748E+00	.34951E+01	.14055E+01
15	.61442E+01	.94463E+00	.26527E+01	.14156E+01
16	.62013E+01	.96763E+00	.14867E+01	.13970E+01
17	.67128E+01	.99470E+00	.10220E+01	.10764E+01
18	.72040E+01	.99369E+00	.10071E+01	.10265E+01
19	.77011E+01	.10001E+01	.10024E+01	.10087E+01
20	.82003E+01	.10006E+01	.10007E+01	.10025E+01
21	.87001E+01	.10005E+01	.10002E+01	.10006E+01
22	.92000E+01	.10008E+01	.10000E+01	.10001E+01
23	.97000E+01	.10008E+01	.10000E+01	.10000E+01

TH	EM	RHO	GAM	XMASS
-.34384E-01	.10748E+01	.66800E-01	.13914E+01	0.
-.33962E-01	.10853E+01	.67111E-01	.13914E+01	.12639E+00
-.29546E-01	.10714E+01	.71672E-01	.13899E+01	.26037E+00
-.33092E-01	.10541E+01	.77840E-01	.13870E+01	.31605E+00
-.35793E-01	.10440E+01	.82298E-01	.13846E+01	.34430E+00
-.38729E-01	.10344E+01	.87955E-01	.13812E+01	.37281E+00
-.42090E-01	.10261E+01	.94997E-01	.13769E+01	.40177E+00
-.45718E-01	.10204E+01	.10529E+00	.13692E+01	.43642E+00
-.46655E-01	.10230E+01	.12119E+00	.13550E+01	.47994E+00
-.45073E-01	.10438E+01	.14520E+00	.13333E+01	.53425E+00
-.32423E-01	.10855E+01	.17365E+00	.13089E+01	.59080E+00
-.25887E-01	.11465E+01	.20579E+00	.12871E+01	.64821E+00
-.17334E-01	.12356E+01	.24666E+00	.12704E+01	.71371E+00
-.49522E-02	.13883E+01	.31696E+00	.12680E+01	.79253E+00
.86779E-02	.17151E+01	.48426E+00	.12904E+01	.91191E+00
.13924E-01	.23964E+01	.92957E+00	.13383E+01	.11431E+01
.17021E-01	.29497E+01	.10512E+01	.13694E+01	.43551E+01
.61523E-02	.29822E+01	.10174E+01	.13705E+01	.78785E+01
.20313E-02	.29933E+01	.10045E+01	.13708E+01	.11621E+02
.59778E-03	.29972E+01	.99999E+00	.13709E+01	.15600E+02
.15405E-03	.29984E+01	.99860E+00	.13710E+01	.19824E+02
.42172E-04	.29987E+01	.99824E+00	.13710E+01	.24295E+02
.68661E-05	.29987E+01	.99816E+00	.13710E+01	.29015E+02

VIII. CONCLUSIONS

The "viscous-characteristics" method for the analysis of supersonic viscous combusting flow fields has been extended to analyze local embedded subsonic regions as well as to analyze shocks produced by combustion and/or pressure mismatch between the injected gas and air stream. The numerical technique developed for analyzing subsonic zones requires that the subsonic region be bounded by a lower wall and an upper boundary that is slightly supersonic. The shape of the upper boundary is fixed by the flow conditions by requiring that y, θ, θ_s and θ_{ss} be continuous, but higher order terms may be specified to shape the streamline arbitrarily. The shape of the lower wall is a function of the upper wall shape specified. The program developed can be used in its current form to design centerbody shapes for a specified streamline shape in the combustion zone. Note that the program can be modified to make the upper boundary a specified pressure boundary and hence a lower wall shape can be obtained for a specified pressure distribution in the combustion zone. The program can also be extended to analyze embedded subsonic zones surrounded by supersonic flow on both sides provided that the flow can be assumed inviscid on one side. Referring to Figure (7), where the flow beneath the embedded region is inviscid, a marching scheme can be developed wherein the flow in the subsonic zone and above is analyzed by a mixing type grid, while C_+ characteristics are followed in the inviscid region. It is felt that these program modifications would be realistic extensions of the current effort and should be considered in plans for future research in this area. The extension of this program to embedded zones with viscous supersonic regions on both sides appears to require a more significant effort.

While the "viscous-characteristic" program developed for supersonic flow fields can be readily run by one with only a limited background in gas-dynamics, it is felt that the subsonic version be run by an analyst who is thoroughly familiar with the physics of the problem as well as the details of the analysis included in this report.

APPENDIX I

MARCHING SCHEME - FINITE DIFFERENCE METHOD

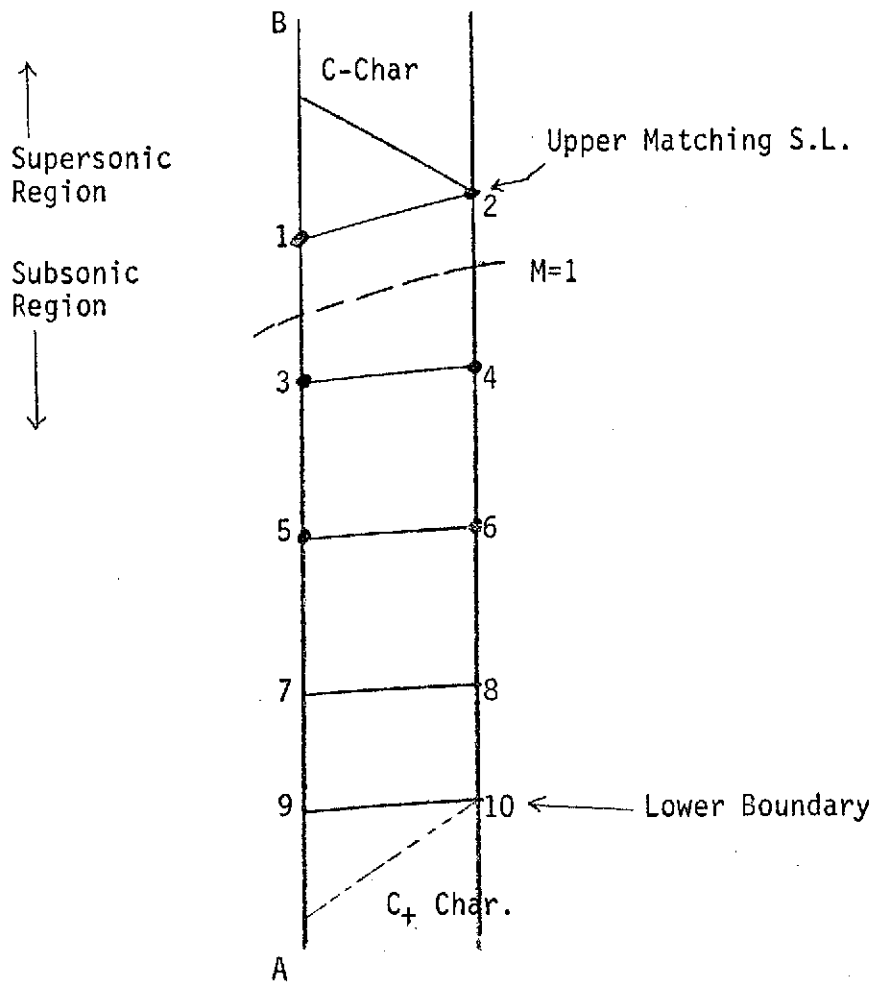

FIGURE I-1.

Referring to Figure (I-1), all properties are known at the initial station I and hence all derivatives $\partial/\partial y$ may be calculated at the mesh points 1, 3, 5 etc. The derivatives p_y and θ_y are related to the streamwise derivatives p_s and θ_s by the relations

$$p_s = \frac{\cos^2\theta\ [A]\ \gamma PM^2\cos^2\theta\ \theta_y - \sin\theta\ p_y}{M^2\cos^2\theta - 1} \qquad \text{(AI-1)}$$

$$\theta_s = \frac{\sin\theta\cos\theta\ [A] - (M^2-1)\cos\theta\ P_y - \sin\theta\gamma PM^2\theta_y}{\gamma PM^2(M^2\cos^2\theta - 1)} \tag{AI-2}$$

where

$$A = -\gamma PM^2\frac{J\sin\theta}{y} + \frac{S_1}{\gamma PM^2} - \frac{(\gamma-1)S_2}{\gamma Pq} - \frac{w}{\rho q}\Sigma\frac{S_{3_i}}{m_i} \tag{AI-3}$$

$$+ \frac{(\gamma-1)\ h_i\dot{w}_i}{(\gamma_\infty-1)M_\infty^2\gamma Pq} - \frac{w}{\rho q}\Sigma\frac{\dot{w}_i}{m_i}$$

Assuming a value of θ_{s_2} (or prescribing this value as a function of x in the inverse problem), all properties at 2 may be obtained by the boundary characteristic relation along 2-B and the s-momentum, energy and species diffusion equations applied along the streamline 1-2.

Knowing P_{2_2} and θ_{s_2}, we may obtain P_{y_2} and θ_{y_2} by inverting Equations (1) and (2).

Combining the s-momentum, energy and species continuity equation, the relation

$$(M^2-1)\ P_s + \gamma PM^2\theta_n = [A] \tag{AI-4}$$

is obtained, while the normal momentum equation is written

$$P_n + \gamma PM^2\theta_s = 0 \tag{AI-5}$$

Between points (2) and(4)

$$P_4 = P_2 + [P_{y_4} + P_{y_2}]\ \frac{\Delta y_{24}}{2} \tag{AI-6}$$

$$\theta_4 = \theta_2 + [\theta_{y_4} + \theta_{y_2}]\ \frac{\Delta y_{24}}{2} \tag{AI-7}$$

Between points (3) and (4)

$$P_4 = P_3 + [P_{s_3} + P_{s_4}] \frac{\Delta s_{34}}{2} \tag{AI-8}$$

$$\theta_4 = \theta_3 + [\theta_{s_3} + \theta_{s_4}] \frac{\Delta s_{34}}{2} \tag{AI-9}$$

The system of Equations (4) to (9) (with Equations 4 and 5 applied at point (4)) along with the transformations

$$\frac{\partial}{\partial s} = \cos\theta \frac{\partial}{\partial x} + \sin\theta \frac{\partial}{\partial y}$$

and

$$\frac{\partial}{\partial n} = \cos\theta \frac{\partial}{\partial y} - \sin\theta \frac{\partial}{\partial x}$$

can be combined to yield the relations

$$P_4 * \left(\frac{2(\theta_4-\theta_3)}{\Delta s_{34}} \gamma_4 M_4^2 (M_4^2\cos^2\theta_4 - 1) - \gamma_4 M_4^2 s_3 (M_4^2\cos^2\theta_4 - 1) \right.$$

$$\left. + \frac{2\gamma_4 M_4^2 (\theta_4-\theta_2)\sin\theta_4}{\Delta y_{24}} - \gamma_4 M_4^2 \theta_{y_2} \sin\theta_4 + \frac{2(M_4^2-1)\cos\theta_4}{\Delta y_{24}} \right) \tag{AI-10}$$

$$- \frac{2(M_4^2-1)P_2\cos\theta_4}{\Delta y_{24}} - (M_4^2-1)\, P_{y_2} \cos\theta_4 - \sin\theta_4 \cos\theta_4 [A] = 0$$

and

$$P_4 * \left(2(M_4^2\cos^2\theta_4 - 1) + \frac{2\gamma_4 M_4^2 (\theta_4-\theta_2)\cos\theta_4}{\Delta y_{24}} - \gamma_4 M_4^2 \cos\theta_4\, y_2 \right.$$

$$\left. + \frac{2\sin\theta_4}{\Delta y_{24}} \right) - \left(P_{s_3} + \frac{2P_3}{\Delta s_{23}}\right) (M_4^2\cos^2\theta_4 - 1) - \frac{2P_2\sin\theta_4}{\Delta y_{24}} \tag{AI-11}$$

$$- P_{y_2} \sin\theta_4 - [A] \cos^2\theta_4 = 0$$

Equations (AI-10) and (AI-11) both are of the form

$$P_* f(\theta, M) + g(\theta, M, [A]) = 0 \qquad \text{(AI-12)}$$

An iterative procedure for the solution of the above system proceeds as follows:

(a) A value for P_4 is assumed (i.e., $P_4 = P_3 + P_{s_3} \Delta s_{34}$).

(b) Application of the s-momentum, energy and species equation along 3-4 $\rightarrow q_4$, T_4, $\alpha_{i_4} \rightarrow M_4$.

(c) Equation (AI-10) $\rightarrow \theta_4$ by an iterative procedure.

(d) Equation (AI-11) $\rightarrow P_4^*$ which is compared to the value of P_4 assumed.

If $|P_4^* - P_4| > \Sigma$, where Σ is some specified tolerance, a new value of P_4 is assumed and steps (b), (c) and (d) are repeated until convergence is obtained.

The calculation y points 6, 8 and 10 are performed in an analogous fashion, until the lower boundary 9-10 is reached. In the direct problem 9-10 may be a wall, axis or lower matching streamline (in which case a P-θ relation exists along the C_+ characteristic 10-A), while in the inverse problem 9-10 must be a wall. The direct problem requires that the deflection angle θ_{10} obtained by the subsonic solution match the wall angle $\theta_{w_{10}}$, = 0 if 9-10 is an axis, or satisfy the compatibility relation along A-10. If it does not, the value of θ_{s_2} must be iterated upon and the entire system solved repeatedly until the value of θ_{s_2} that satisfies the lower boundary conditions is obtained. In the inverse problem, the value of θ_{10} determined by the subsonic solution yields the shape of the lower boundary and no iteration is required.

APPENDIX II

MARCHING SCHEME - POLYNOMIAL METHOD

In the subsonic region, the pressure distribution and flow inclination are expressed by the following power series in y:

$$p(x,y) = P_0(x) + P_1(x)\,\bar{y} + P_2(x)\,\bar{y}^2 + P_3(x)\,\bar{y}^{3*} \qquad \text{(AII-1)}$$

$$\theta(x,y) = \theta_0(x) + \theta_1(x)\,\bar{y} + \theta_2(x)\,\bar{y}^{2*} \qquad \text{(AII-2)}$$

Referring to Figure (II-1), the subsonic region is bounded by the two streamlines D_1C_1 and D_2C_2 along which the Mach number has low supersonic values. The subsonic region is matched to the supersonic regions employing the viscous characteristic compatibility relations along the characteristics BC_2 and AC_1. The analysis developed also considers the possibility that the subsonic region extends to an axis or lower wall.

The derivatives P_s and θ_s at points D_1 and D_2 are calculated employing Equations (AI-1) and (AI-2). The following procedure is used to calculate the subsonic region.

Step 1. A value for $p_{s_{C_1}}$ is assumed (or prescribed for inverse problem).

Step 2. $P_{C_1} = P_{D_1} + \frac{1}{2}\left(P_{s_{D_1}} + P_{s_{C_1}}\right)\Delta s.$

Step 3. The compatibility relation applied along the C+ characteristic AC_1 yields θ_{C_1}.

Step 4. $\theta_{s_{C_1}} = \frac{2}{\Delta s}\left(\theta_{C_1} - \theta_{D_1}\right) - \theta_{s_{D_1}}.$

---

* $\bar{y} = y - y_L$ where L denotes the lower subsonic boundary. If the lower boundary is an axis of symmetry, $y_L = 0$ and the polynomials take the form $P_{(y)} = P_0 + P_2y^2 + P_4y^4$ and $\theta_{(y)} = \theta_1 y + \theta_3 y^3$.

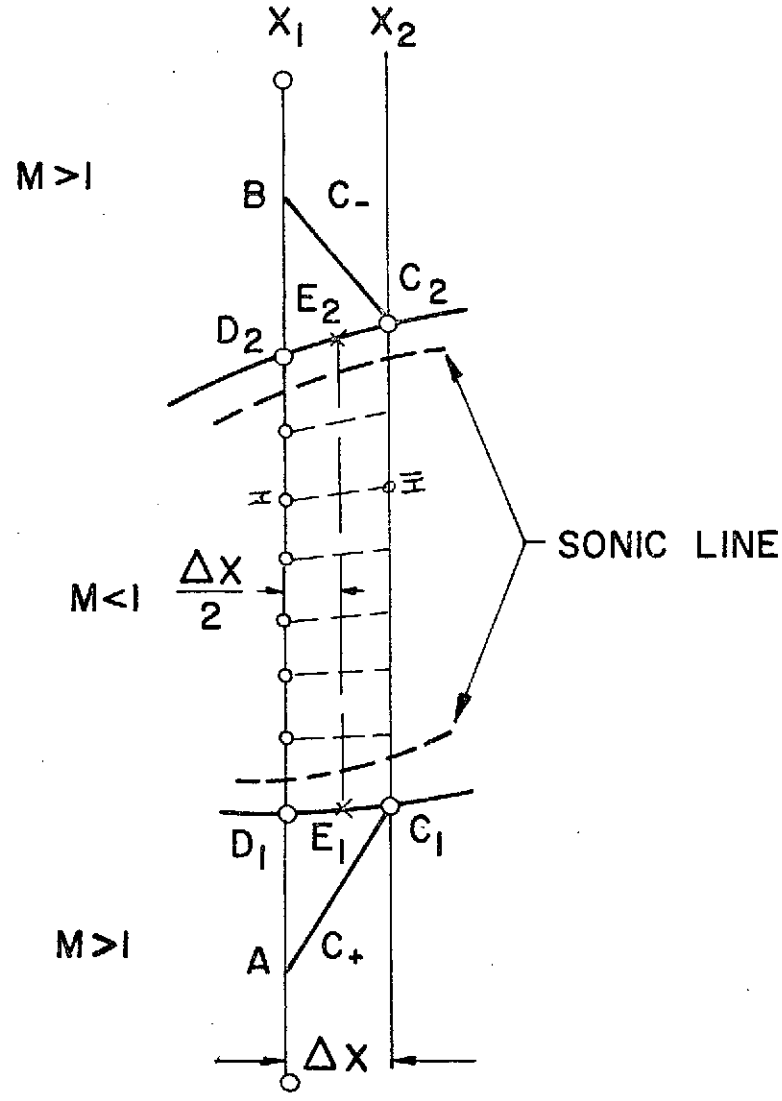

FIGURE II-I

Note, that if the lower subsonic boundary is a wall or axis, the flow deflection θ_{C_1} is known and no compatibility relation is required.

Step 5. With the pressure gradient and streamline location known, the velocity, temperature and species mass fraction may be obtained at C_1 (or any mesh point $\bar{I}$) by using the explicit finite difference formulation of Equations (5), (7) and (8).

Step 6. Knowing P_s and θ_s at point C_1, Equations (AI-1) and AI-2) may be inverted to yield $(P_y)_{C_1}$ and $(\theta_y)_{C_1}$.

Step 7. Since the $\theta_{(y)}$ polynomial contains three unknowns, and two boundary conditions are already known at C_1 (θ and θ_y), only one value of θ at the upper boundary C_2 will be consistent with both the θ polynomial and the modified continuity equation**. A local iteration to find this value of θ proceeds as follows:

Step 7a. A value of θ_{C_2} is assumed.

Step 7b. The coefficients θ_0, θ_1 and θ_2 at y_{C_1}, $\theta=\theta_{C_1}$ and $\theta=\theta_{y_{C_1}}$ and at y_{C_2}, $\theta=\theta_{C_2}$. The θ polynomial is then

$$\theta_{(y)} = \theta_0 + \theta_1 + \theta_2 \bar{y}^2$$

Step 7c. $$\theta_{s_{C_2}} = \frac{2}{\Delta s} (\theta_{C_2} - \theta_{D_2}) - \theta_{s_{D_2}}.$$

**$(M^2-1)\, P_s + \gamma P M^2 \theta_n = A$ (AII-3)

where A is described by Equation (AI-3).

Step 7d. The compatibility relation along characteristic BC_2 yields P_{C_2}.

Step 7e. $P_{s_{C_2}} = \frac{2}{\Delta s}(P_{C_2} - P_{D_2}) - P_{s_{D_2}}$.

Step 7f. Using the modified continuity equation

$$\theta_{n_{C_2}} = \left[\frac{A - (M^2-1)\,P_s}{\gamma P M^2}\right]_{C_2}.$$

Step 7g. Since $\frac{\partial}{\partial y} = \cos\theta \frac{\partial}{\partial n} + \sin\theta \frac{\partial}{\partial s}$ $\theta_{y_{C_2}} = \cos\theta_{C_2}$

$$\theta_{n_{C_2}} + \sin\theta_{C_2}\,\theta_{s_{C_2}}.$$

Step 7h. But using the polynomial $\theta_{(y)}$

$$\theta^*_{y_{C_2}} = \theta_1 + 2\theta_2\bar{y}$$

Step 7i. The values of $\theta_{y_{C_2}}$ and $\theta^*_{y_{C_2}}$ must be identical to within a specified tolerance. If they do not agree, a new value of θ_{C_2} is assumed and Steps (7b) - (7h) are repeated. Convergence is obtained by use of a linear error extrapolation procedure.

Step 8. Flow properties are computed at C_2.

Step 9. $P_{n_{C_2}}$ is computed using the normal momentum equation

$$P_{n_{C_2}} = -(\gamma P M^2)_{C_2}\,\theta_{s_{C_2}}.$$

Step 10. $P_{y_{C_2}}$ is computed $P_{y_{C_2}} = \cos\theta_{C_2}\,P_{n_{C_2}} + \sin\theta_{C_2}\,P_{s_{C_2}}$.

Step 11. The coefficients of the pressure polynomial $P_{(y)}$ between C_1 and C_2 can now be evaluated using the conditions

$$\text{at } y_{C_1},\ P=P_{C_1} \text{ and } P_y=P_{y_{C_1}}$$

$$\text{at } y_{C_2},\ P=P_{C_2} \text{ and } P_y=P_{y_{C_2}}$$

yielding $P_{(y)} = P_0 + P_1\bar{y} + P_2\bar{y}^2 + P_3\bar{y}^3$.

Step 12. The interior mesh points $\bar{I}$ between C_1 and C_2 are evaluated as follows.

Step 12a. A value of $y_{\bar{I}}$ is assumed.

Step 12b. Using the polynomial $P_{(y)}$ and $\theta_{(y)}$, $P_{\bar{I}}$ and $\theta_{\bar{I}}$ are obtained.

Step 12c. Flow properties are obtained using the streamline relations.

Step 12d. The mass flow at $\bar{I}$ is evaluated by

$$\psi_{\bar{I}} = \psi_{\bar{I}-1} + [(\rho q \cos\theta)_{\bar{I}-1} + (\rho q \cos\theta)_{\bar{I}}]$$

$$\frac{(y_{\bar{I}}^{1+j} - y_{\bar{I}-1}^{1+j})}{1+j}.$$

Step 12e. Since $I\bar{I}$ is a streamline, ψ_I should equal $\psi_{\bar{I}}$. If it does not agree to within a specified tolerance, a new value of $y_{\bar{I}}$ is assumed and the process is iterated until convergence.

Step 13. The overall mass flow between C_1C_2 is compared to that between D_1D_2. If the mass flow is not correct the entire process (Steps (1) - (13)) must then be repeated with a new value of $P_{s_{C_1}}$ for the direct problem.

Generally, convergence was obtained with under five iterations, except when the subsonic flow field is close to sonic in a mass averaged sense. This situation occurs in the vicinity of the supersonic to subsonic transition and again in the vicinity of the subsonic to supersonic transition. In these critical regions, the error curve may yield two solutions (supersonic and subsonic branch) in which case knowledge of downstream conditions indicates which branch is physically correct. For arbitrary initial conditions, the flow does not necessarily undergo a smooth super to subsonic transition and the matching Mach number tends to be an important factor in effecting this transition. The transition from sub to supersonic flow (i.e., closing the sonic line) poses an even greater problem.

In this region, the flow may choke, indicating that a shock is required in the initial super to sub transition to allow the mass flow to pass. If the subsonic region is bounded by a wall on one side, when choking occurs, the wall may be opened to allow passage of the correct mass flow. If the subsonic region is embedded in the flow field, then the wall would have to be modified upstream of the choked station to allow passage of the proper mass flow. In the inverse case, one of the subsonic boundaries would have to be a wall and P_s prescribed at one boundary would yield the wall shape at the other boundary.

APPENDIX III

STEP SIZE AND GRID SPACING CRITERION

A. Step Size Criterion - Limitations on the marching step Δx result from characteristic criterion, parabolic stability criterion associated with an explicit difference scheme and criterion associated with the solution of the finite rate chemistry. The criterion associated with characteristics is the Courant-Friedrichs-Lewy condition which states that "the numerical domain of dependence of a difference scheme should include the domain of dependence of the differential equation or else, convergence is not always possible" (Reference 9). This criterion is numerically satisfied by intersecting all free running characteristics emanating from grid points of the supersonic portions of the initial profile and obtaining the intersection yielding the minimum forward marching step Δx_{char} as shown in Figure (III-1).

The stability criterion associated with an explicit parabolic marching scheme has been discussed extensively in the literature (Reference 10), based upon equations with constant coefficients. The solution of the s-momentum, energy and species diffusion equation are all solved by an explicit scheme using the grid depicted in Figure (III-2) where the spacing Δy between grid points is not necessarily uniform. Linearized stability criterion imposes the condition:

$$\frac{2\mu L_e \Delta x}{\rho q \, Pr \, Re \, \Delta y^2} \leq 1 \qquad \text{(AIII-1)}$$

Then the parabolic step size is determined by applying Equation (AIII-1) at each grid point I and selecting the minimum Δx_{vis}. The Δy employed in the equation is the average Δy of the interval I-1 to I+1; i.e., $\Delta y_I = \frac{1}{2^*} (\Delta y_1 + \Delta y_2)$. Then

$$\Delta x_{vis} = \frac{P_r \, Re}{2 \, L_e \, \mu} \left[\rho_I \, q_I \, \Delta y^2\right]_{min} \qquad \text{(AIII-2)}$$

It should be noted that the hyperbolic (characteristic) stability criterion is determined with the diffusive terms neglected and the parabolic (diffusive) stability limit is determined with the convective terms neglected. It had

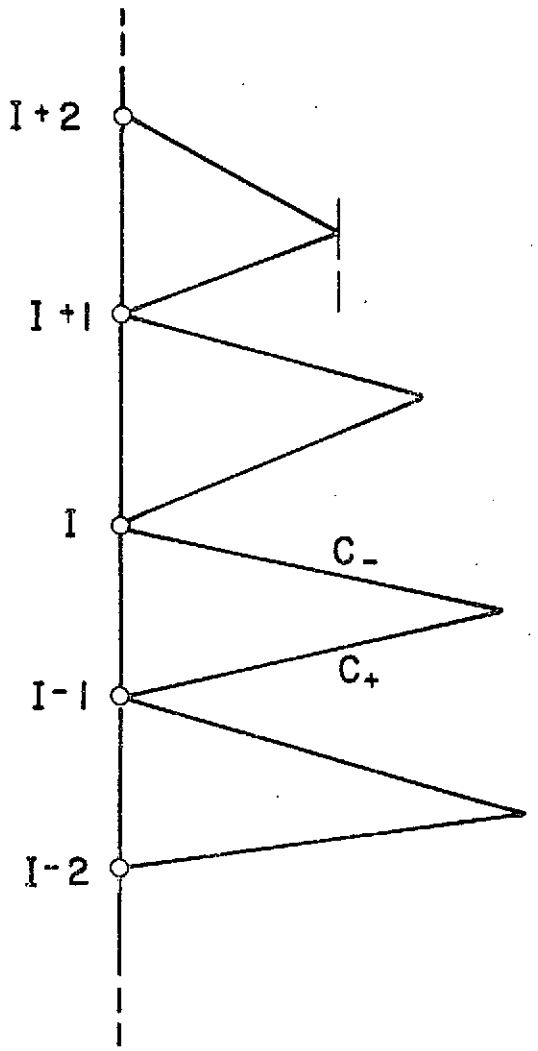

FIGURE (III-1)

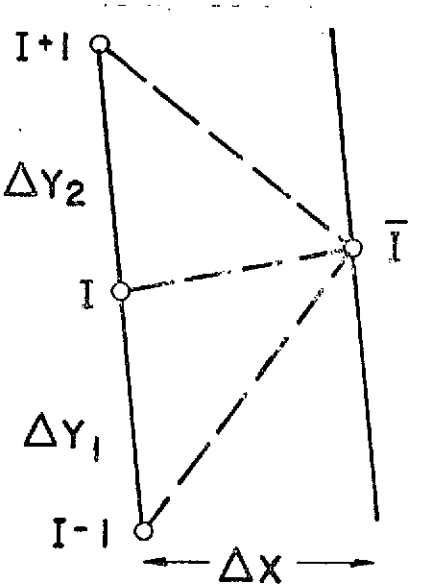

FIGURE (III-2)

been thought that the smaller of these two step sizes should be taken as the stability limit of the system as noted in Reference (2), but it was also pointed out in this reference that use of this criterion still led to instabilities in some cases. A superposition of the diffusive and convective terms may yield more restrictive stability limits than choosing the smaller of the step sizes. As pointed out by Cheng in Reference (11), the appropriate combined "hyperbolic-parabolic" criterion is

$$\Delta x \leq \frac{1}{2} \frac{1}{\frac{1}{\Delta x_{char}} + \frac{1}{\Delta x_{vis}}}$$

The finite rate hydrogen-air chemistry employed in this analysis is described in References (12) and (13) and uses a fixed time interval $\Delta t = 4.*10^{-7}$ seconds. Hence, the chemical step size is

$$\Delta x_{chem} = \frac{q_I * U_\infty}{r_{jet}} \Delta t$$

Since the chemistry is uncoupled based on the procedure developed in Reference (14) and described for viscous-characteristics in Reference (2), several chemical steps may be taken in one overall marching step. The number of chemical steps to be allowed in a marching step is left as a user option and is dependent on the grid spacing in the transverse direction (Δy spacing). Note that when mixing is initiated, a very small grid spacing Δy is required, hence the overall marching step may be significantly smaller than a chemical step, while far downstream, when the Δy is substantially larger, the chemistry criterion may dominate the overall step size.

B. Grid Spacing In The Transverse Direction - The program developed can analyze a wide variety of flow situations. The lower boundary may be a wall or an axis, while the upper boundary may be a wall or constant pressure surface. The initial profile may be entirely nonuniform, in which case all grid points must be input initially or may have: (a) uniform jet, uniform air (b) uniform jet, nonuniform air (c) nonuniform jet, uniform air. In each

of these cases, the jet-air pressure may be balanced or unbalanced. If the pressure is unbalanced, the jet underexpansion interaction is calculated. For flow with an axis or straight centerbody, only the jet properties, an initial Δy based on mixing considerations, and the maximum number of points on the jet side have to be input for a uniform jet (cases a or b). As mixing progresses, the program adds points at Δy on the jet side, until the maximum number of jet points is obtained at which point Δy is doubled, and alternate points on the jet side are dropped. This process is continued until the wall or axis is reached. Similarly, if the airstream is uniform (case a or c) and the upper boundary is such that it sends no waves into the flow field, the same procedure applies on the air side. For the unbalanced pressure case, jet points are added below the Prandtl-Meyer region and the free stream side of the shock serves as the upper boundary if the air is uniform. As the distance between the underexpansion shock and the mixing zone increases, mesh points are automatically added in this region.

APPENDIX IV
VISCOSITY MODEL

The turbulent eddy viscosity model referred to as the "Ferri-Kleinstein" model is described in References (18) and (19). This model has been incorporated as a subroutine in the developed program and assumes an eddy viscosity variation in the axial direction only. Incorporation of a different model employing only an axial variation simply involves changing the viscosity subroutine while incorporation of a model employing both an axial and radial variation can be easily accomplished by minor program modifications.

Defining x* as the length of the potential core,

$$\mu = K_1 \; X \; Re \left((\rho u)_{max} - (\rho U)_{min} \right) + K_3 \qquad \text{(AIV-1)}$$

for $x < x^*$

and

$$\mu = K_2 \; r_{\frac{1}{2}} \; Re \left((\rho u)_{Max} - (\rho u)_{min} \right) + K_4 \qquad \text{(AIV-2)}$$

for $x > x^*$

where $r_{\frac{1}{2}}$ is the radial distance to the point in the jet where $\rho u = \frac{1}{2} \left((\rho u)_{max} + (\rho u)_{min} \right)$.

For a uniform jet and external stream the term $(\rho u)_{max} - (\rho u)_{min}$ is replaced by the appropriate jet and external stream properties, as depicted in Figure (IV-1). For an underexpanded jet, the viscosity is computed on the basis of the region below the bounding shock. Due to burning the difference between $(\rho u)_{jet}$ and $(\rho u)_{exit}$ may be less than that in the combustion zone in which case the max difference is obtained as depicted in Figure (IV-2). The coefficients K_1, K_2, K_3 and K_4 and the potential core length X* are input items in the program.

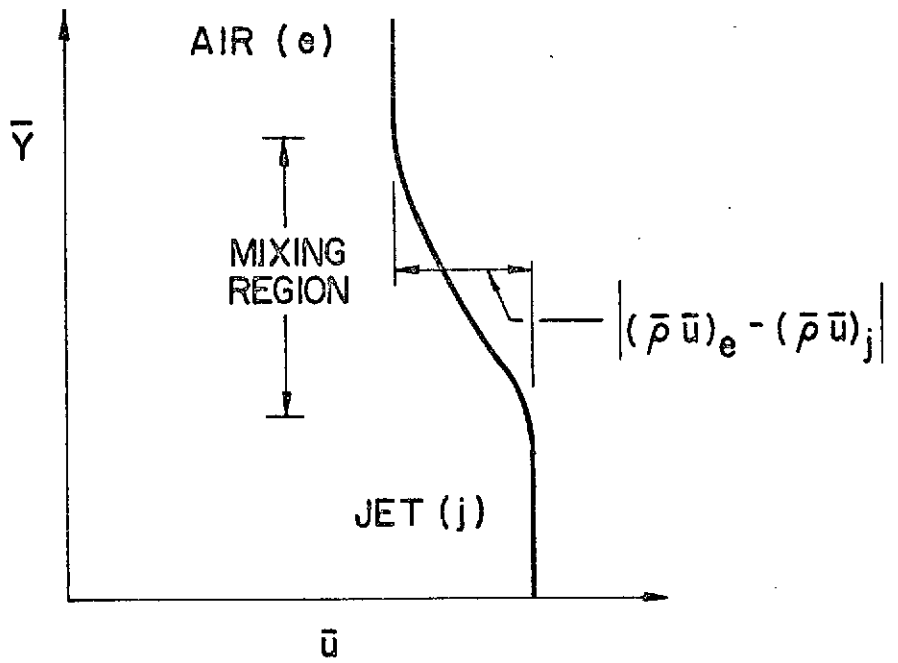

FIGURE (IV-1)

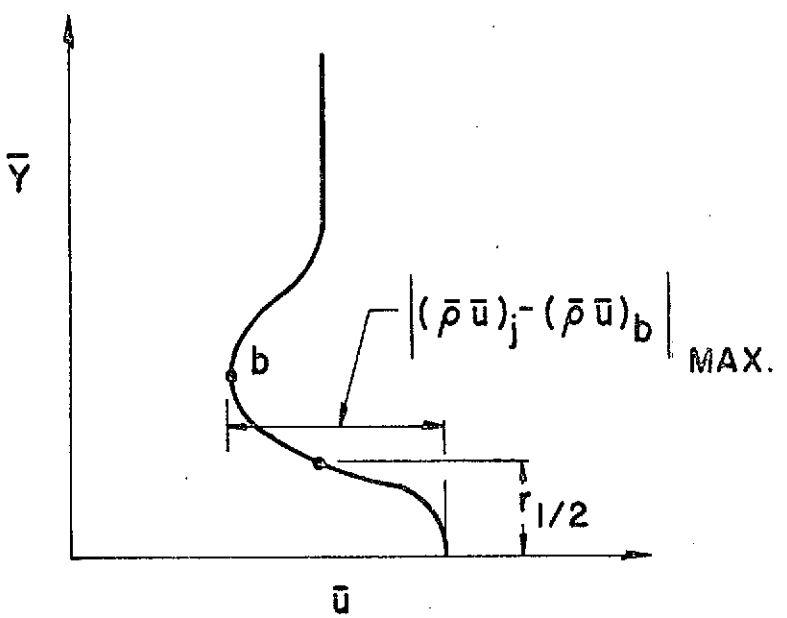

FIGURE (IV-2)

REFERENCES

1. Ferri, A., "Review of Problems in Application of Supersonic Combustion," Seventh Lanchester Memorial Lecture, Royal Aero. Soc. Journal, Vol. 68, No. 645, September 1964.

2. Dash, S., "An Analysis of Internal Supersonic Flows with Diffusion, Dissipation and Hydrogen-Air Combustion," NASA CR-111783 (Also see ATL TR 152), May 1970.

3. Ferri, A., "Axially Symmetric Heterogeneous Mixing," Polytechnic Institute of Brooklyn Report No. 787 (also AFOSR-5326), September 1963.

4. Moretti, G., "Analysis of Two Dimensional Problems of Supersonic Combustion Controlled by Mixing," AIAA Preprint No. 64-96, January 1964.

5. Davis, R. T. and Flugge-Lutz, I., "Second Order Boundary Layer Effects in Hypersonic Flow Past Axisymmetric Blunt Bodies," Journal of Fluid Mechanics, Vol. 20, Part V, pp. 593.623, 1964.

6. Ferri, A. and Dash, S., "Viscous Flow at High Mach Numbers with Pressure Gradients," Proceedings of the 1969 Symposium on Viscous Interaction Phenomena in Supersonic and Hypersonic Flow, University of Dayton Press, pp. 271-318, 1970.

7. Chow, W. L. and Addy, A. L., "Interaction between Primary and Secondary Streams of Supersonic Ejector Systems and Their Performance Characteristics," AIAA Journal, Vol. 2, No. 4, April 1964.

8. Hayes, W. and Probstein, R., Hypersonic Flow Theory, Academic Press, 1966.

9. Isaacson, I. and Kella, H., Analysis of Numerical Methods, John Wiley and Sons, 1966.

10. Richtmyer, R. and Morton, K., Difference Methods for Initial-Value Problems, Interscience Publishers, 1967.

11. Cheng, S. I., "Numerical Integration of Navier Stokes Equations," AIAA Journal, Vol. 8, No. 12, pp. 2115-2123, December 1970.

12. Abett, M., "Users Manual for the One Dimensional Fluid Flow, Finite Rate Chemical Kinetics Program with Specified Pressure or Area for the Hydrogen-Air System," General Applied Science Laboratories, Inc., TR 597, February 1966.

13. Moretti, G., "A New Technique for the Numerical Analysis of Nonequilibrium Flows," AIAA Journal, Vol. 3, No. 2, pp. 223-229, February 1965.

REFERENCES (Continued)

14. Ferri, A., Moretti, G. and Slutsky, S., "Mixing Processes in Supersonic Combustion," J. Soc. Indust. Appl. Math., Vol. 13, No. 1, March 1965.

15. McBride, B., Heimel, S., Ehlers, J. and Gordon, S., "Thermodynamic Properties to 6000°K for 210 Substances Involving the First 18 Elements," NASA SP-3001, 1963.

16. Chow, R. R. and Ting, L., "Higher Order Theory of Curved Shock," PIBAL Report No. 609, August 1960.

17. Chow, R. R., "High Speed Low Density Flow Near the Stagnation Point of a Blunt Body," PIBAL Report No. 765, February 1963.

18. Ferri, A., Libby, P.A. and Zakkay, V., "Theoretical and Experimental Investigation of Supersonic Combustion," PIBAL Report No. 713, ARL 62-467, September 1962.

19. Kleinstein, G., "On the Mixing of Laminar and Turbulent Axially Symmetric Compressible Flows," PIBAL Report No. 756, February 1963.